Breaching of sea dikes initiated from the seaside by breaking wave impacts

Dissertation

submitted to and approved by the

Faculty of Architecture, Civil Engineering and Environmental Sciences
University of Braunschweig – Institute of Technology

and the

Faculty of Engineering
University of Florence

in candidacy for the degree of a
Doktor-Ingenieur (Dr.-Ing.) /
Dottore di Ricerca in Risk Management on the Built Environment *)

by
Grzegorz Stanczak
Born 24.03.1980
from Szczecin, Poland

Submitted on	17 March 2008
Oral examination on	29 May 2008
Professorial advisors	Prof. Hocine Oumeraci
	Prof. Pierluigi Aminti

2008

*) Either the German or the Italian form of the title may be used.

The researches described in the following thesis were performed during my stay on two universities: Technische Universität Braunschweig (Germany) and Universita degli Studi di Firenze (Italy) in the frames of the International Graduate College GRK802.

First of all, I would like to thank my two tutors: prof. Hocine Oumeraci and prof. Pierluigi Aminti for their continuous support and inspiration. I am very grateful to my co-workers in the frames of the FloodSite project: Andreas Kortenhaus, Claudia D'Eliso and Peter Geisenhainer for the numerous discussions we had and for the time we spent together on conferences and meetings. I would also like to thank to the entire LWI staff for their continuous help: Gabi Fournier, Agnieszka Strusinska, Juan Recio, Rainer Kvapil and Markus Brühl as well as to the students who performed most of the laboratory experiments: Benjamin Rohloff, Christian Klein and Semeidi Husrin.

The support of the German Research Foundation in the frames of the GRK802 represented by prof. Udo Peil and prof. Claudio Borri as well as of the European Community in the frames of the FloodSite project is gratefully acknowledged.

Mojej żonie Kamili w podziękowaniu za nieustanne wsparcie, inspirację oraz motywację dedykuję niniejsza pracę.

Contents

List of Figures

List of Tables

List of symbols

$1:n$	-	tangent of the outer slope $[-]$
$1:m$	-	tangent of the inner slope $[-]$
a	-	depth of the crack $[m]$
A	-	Breach channel cross-section $[m^2]$
B	-	Breach width $[m]$
B_B	-	Breach width at the location of overflow $[m]$
$B_{B,ini}$	-	Width of the initial breach channel $[m]$
B_D	-	width of the dike crest $[m]$
c	-	undrained soil cohesion $[N/m^2]$
$c_{\%}$	-	clay percentage $[-]$
c_r	-	apparent root cohesion [N/m^2]
C_0	-	wave phase speed in deep water $[m/s]$
C_g	-	wave group celerity $[m/s]$
C_f	-	grass cover factor $[-]$
db	-	Change in the breach width $[m]$
d_b	-	depth at the wave breaking $[m]$
d_c	-	thickness of the clay cover $[m]$
$d_{c,max}$	-	Maximal depth of clay erosion for a single impact $[m]$
d_g	-	thickness of the grass cover $[m]$
$d_{g,max}$	-	Maximal depth of grass erosion for a single impact $[m]$
d_{max}	-	Maximal allowable distance between point of impact and i-th point on the dike $[m]$
dz	-	Change in the breach depth $[m]$
D	-	wave energy dissipation per unit water volume $[Nm/m^3/sec]$
D_{50}	-	median grain size $[mm]$
D_{eq}	-	equilibrium energy dissipation per unit water volume $[Nm/m^3/sec]$
e_b	-	Bed load efficiency coefficient $[m]$
e_s	-	Suspended load efficiency coefficient $[m]$
E	-	wave energy density $[Nm/m^2]$
E_c	-	Clay erodibility coefficient $[m^{-1} \cdot s^{-1}]$
E_g	-	Grass erodibility coefficient $[m^{-1} \cdot s^{-1}]$
E_k	-	kinetic energy of impact $[J]$
E_s	-	stable wave energy density $[N \cdot m/m^2]$
F	-	wave energy flux $[N \cdot m/m \cdot s]$
F_{crack}	-	force acting on the wall of the crack $[N]$
F_s	-	stable wave energy flux $[N \cdot m/m \cdot s]$
g	-	the gravity acceleration $[m/s^2]$
h	-	water depth or water layer thickness $[m]$
h_c	-	layer thickness on the crest $[m]$
h_b	-	air entry value $[cm]$
h_l	-	layer thickness on the inner slope $[m]$
h_s	-	layer thickness on the outer slope $[m]$
h_{of}	-	Overflow head$[m]$
h_p	-	Backwater level $[m]$
H	-	wave height at the dike toe $[m]$

H_b - breaker height $[m]$
H_d - dike height $[m]$
H_s - significant wave height $[m]$
J - Energy slope $[-]$
k_d - empirical detachability coefficient $[m^3/Pa]$
k_s - saturated hydraulic conductivity $[m/s]$
l_{crit} - critical length of the undermined clay cover $[m]$
L_0 - deep water wave length $[m]$
L_c - length of the crack $[m]$
L_s - stem length $[m]$
n - Manning roughness $[m^{-1/3} \cdot s]$
n_{tot} - total Manning roughness $[s \cdot m^{-1/3}]$
N - pore size distribution index $[-]$
p - Porosity of the soil $[-]$
$p_{max,i}$ - Impact pressure that is not exceeded for $i\%$ of the waves $[Pa]$
P - Wetted perimeter of the breach channel $[m]$
q_{sb} - Volumetric bed load sediment transport $[m^3 \cdot s \cdot m^{-1}]$
$q_{overtopping}$ - Averaged volume of overtopping $[l \cdot m^{-1} \cdot s^{-1}]$
Q - flow discharge$[m^3 \cdot s^{-1}]$
Q_{single} - Volume of sand eroded for a single impact $[m^3]$
Q_{st} - Total volumetric sediment transport $[m]$
r_h - length of the initial breach channel $[m]$
R - Hydraulic radius $[m]$
R_d - volume of soil eroded after a single impact event $[m^3]$
R_c - Freeboard $[m]$
S - shear stress on the shear failure plane $[N/m^2]$
S_p - sand percentage $[-]$
S_Q - backwater level coefficient $[-]$
S_{xx} - radiation stress component directed onshore $[m/s]$
t_c - core wash out time $[h]$
t_{cf} - clay erosion time $[h]$
t_d - breach development time $[h]$
t_f - breach formation time $[h]$
t_{gf} - grass erosion time $[h]$
t_i - breach initiation time $[h]$
t_{sf} - sand erosion time $[h]$
t_t - total breaching time $[h]$
T_p - peak period $[s]$
T_R - root tensile strength [N/m^2]
T_w - water temperature $[^0C]$
v - depth averaged flow velocity $[m \cdot s^{-1}]$
v_c - flow velocity on the crest $[m/s]$
v_l - flow velocity on the inner slope $[m/s]$
v_s - flow velocity on the outer slope $[m/s]$
V - total volume of soil including the roots $[m^3]$
V_R - volume of roots in soil $[m^3]$

w - damping effectiveness coefficient $[-]$
w_s - Settling velocity $[m \cdot s^{-1}]$
W - resistance force on the shear failure plane $[N]$
W_A - resistance force on side walls of crack $[N]$
x_{single} - Progress of sand core erosion in x direction for a single impact
$x_{total,n}$ - Progress of sand erosion in the direction of waves after n impacts $[m]$
z_0 - Roughness height $[m]$
z_{impact} - z-coordinate of the impact point on the dike $[m]$
z_h - elevation of the breach bottom at the breach entrance $[m]$
z_r - wave run-up $[m]$
z_{single} - Height of the vertical cliff $[m]$
α - outer slope $[rad]$
α_{breach} - Angle of initial breach channel $[deg]$
α_{ce} - breach section contraction-expansion coefficient $[-]$
α_{impact} - Angle of impact $[deg]$
β - inner slope $[rad]$
Γ - stable wave height coefficient $[-]$
Δ - Relative density of soil particles $[-]$
Δx - numerical time step $[s]$
Δt - numerical grid $[m]$
λ_i - spatial decay coefficient $[l/m]$
κ - empirical wave decay coefficient $[-]$
κ_i - wave steepness function $[-]$
ϕ - Internal friction angle $[deg]$
ρ_w - water density $[kg/m^3]$
ρ_g - number of stems per square meter $[-]$
ρ_{cw} - density of water-soil mixture $[kg/m^3]$
θ - Shields parameter $[-]$
θ_w - wave angle with respect to the bottom contours
θ_r - root angle of shear rotation [deg]
τ_0 - bottom shear stress $[N/m^2]$
$\tau_{0,cr}$ - critical bottom shear stress $[N/m^2]$
$\tau_{0,e}$ - effective shear stress $[N/m^2]$
τ_{ij} - viscous stress $[N/m^2]$
ξ - Surf similarity parameter $[-]$

1 Introduction

1.1 Problem definition and motivations

Sea dikes are of crucial importance in the defence systems of low-lying coastal areas in countries such as Germany, The Netherlands, Denmark, etc. As the sea dikes breaching induced by storm surges is regarded as one of the main causes of coastal flood disasters, a reliable predictions of both initial conditions for the breach occurrence and the breach development itself are urgently needed.

Until the 19th century the empirical approaches were primarily used for the design of sea dikes. The highest known water level was used as the basis for the estimation of the design water level, which results in an inadequate protection level (Pilarczyk, 1998, Oumeraci, 2004). After the disastrous flood event in The Netherlands in 1953 the overload-based approach was introduced. In this approach, the design water level is described by extreme storm surge levels with a given probability of exceedance with other structural requirements prescribed by the standards, which are in fact different for different countries (D'Eliso, 2007). The probability of failure for the entire defence line, which is in fact the most important term of flood risk assessment and management is however still unknown (Oumeraci and Kortenhaus, 2002). The European Community supports currently the research efforts aiming to develop a risk-based approach for flood defence systems (Oumeraci, 2004). This approach is based on the analysis of predicted and tolerable risk, where the dike failure represents both (i) the vulnerability of the flood defence and (ii) the risk pathways, i.e. the way risk sources are transferred to the risk receptors (see Fig. 1.1)

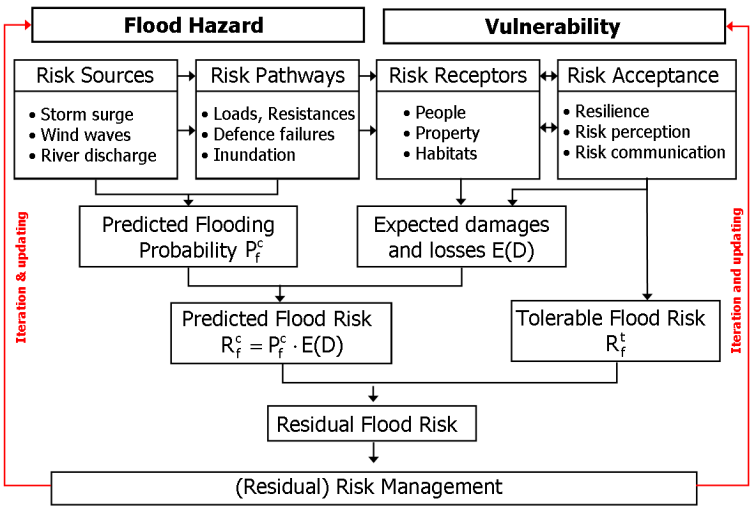

Figure 1.1: Risk-based approach for the design of flood defence structures (Modified from Oumeraci, 2004)

The knowledge on the processes of breach initiation and development is crucial for the prediction of the initial conditions at the defence line which are needed to model the flood wave propagation. Depending on the hydraulic and morphological boundary conditions, one may distinguish several causes for the initiation and formation of a dike breach. Among the failure mechanisms, the most important are (TAW,1999a):

- wave overtopping and overflow, which may lead to the erosion of the shoreward slope and finally to breach initiation from the landward side
- breaking wave impact, including wave run-up and run-down processes which may lead to the erosion of the seaward slope and finally to breaching from the seaward side

For the prediction of a dike breach initiated by wave overtopping, a PhD research work was completed very recently (D'Eliso, 2007). However, as the processes associated with the initiation of a dike breach from the seaside as well as the breach growth itself are completely different from those related to wave overtopping, there is also an urgent need for a model to predict the breach growth initiated from the seaside by breaking wave impact on the outer slope. The main differences in the processes of breaching initiated from the seaside and from the landside refer to the loading conditions and the characteristic of the erosion processes. The loading on the outer slope (breaking wave impact) acts on a very limited area and during very short, intermittent periods, while the shear stress related to the wave overtopping acts on the entire inner slope and during longer periods of time. Consequently, the erosion processes and resulting breaching progress on the seaside is concentrated at the location of the highest impact pressures while the erosion due to wave overtopping occurs on the entire inner slope.

1.2 Objectives

The primary goal of this research is to develop a computational model for the sea dike breaching initiated by the breaking wave impact on the outer slope. The dike selected for this study is a typical sea dike made of a sand core protected by a grass-reinforced clay cover. All the considerations refer to the same cross-section of the dike along the defence line. The description of the dike breaching should account for the most relevant processes, from the breach initiation until the final breach providing a step towards a complete process-oriented simulation of dike breaching. The model outcomes should include the predicted times of breach initiation, formation and development, the final breach width and the outflow hydrograph. The model should be generally based on a deterministic approach, but uncertainty and sensitivity analyses should also be provided.

1.3 Methodology

The following methodology and the chapters related to the particular parts are pursued:

Based on a detailed review and analysis of the available knowledge on dike breaching, including the hydrodynamics, erosion and sediment transport processes (Chapter 2) the detailed objectives and methodology of the study as shown in Fig. 1.2 will be specified more precisely.

Chapter 3 describes the development of the preliminary model, including the hydrodynamic and morphodynamic modules. The first results and a tentative validation are also provided.

Chapter 4 provides the description and the results of laboratory experiments that are conducted in order to verify a number of conceptual models to be implemented in the detailed model.

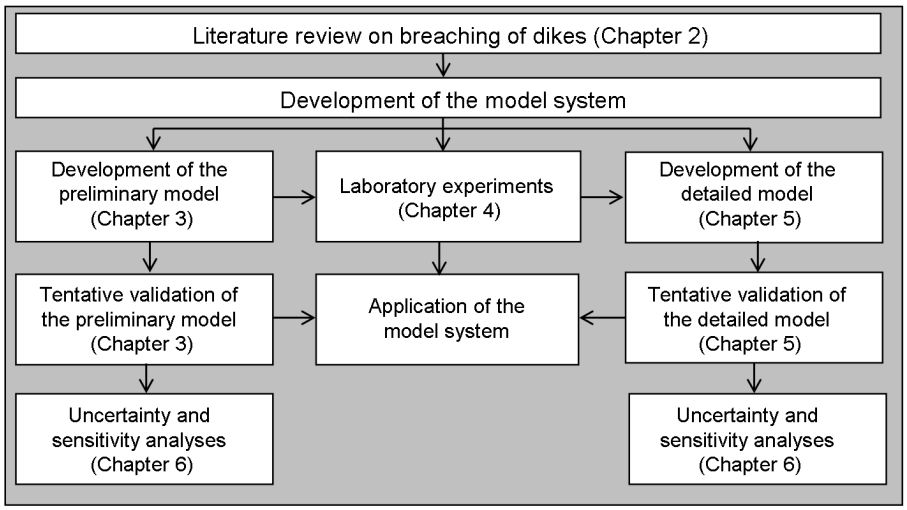

Figure 1.2: Overall methodology of the present study

Chapter 5 addresses the assumptions, mathematical formulations and computer implementation of the detailed model including the first results and a tentative validation.

Chapter 6 provides the information on the uncertainties associated with the model and the results of the sensitivity analysis.

The summary of the key results and the conclusions including some recommendations for the future research are given in Chapter 7.

2 Dike breaching processes and modeling: state of the art and study specification

The breaching of sea dikes occurs as a result of a complex interaction between fluid and soil structure. In the case of breaching initiated from the seaside usually the breaching process begins with the erosion of the grass cover and the underlaying clay layer, followed by the erosion of the uncovered sand core which leads to the overflow and the final breach. In order to better understand and predict the processes mentioned above, it is necessary to review the available knowledge on:

- the processes related to the dike breaching initiated from the seaside (Section 2.1);
- the erosion and instability processes of grass, clay cover and sand core (Section 2.2);
- the sediment transport models which are most appropriate to be implemented in the dike breaching model (Section 2.3);
- the limitations of the existing breach models (Section 2.4).

The main goal of this review is to define more precisely the objectives, methodology and procedure of the present study as tentatively formulated in the introducing chapter.

2.1 Causes of breach initiation and loading case considered

Depending on the structure of the sea dike and on the hydraulic and morphological boundary conditions, one may distinguish several causes for the initiation and formation of a breach (Fig. 2.1).

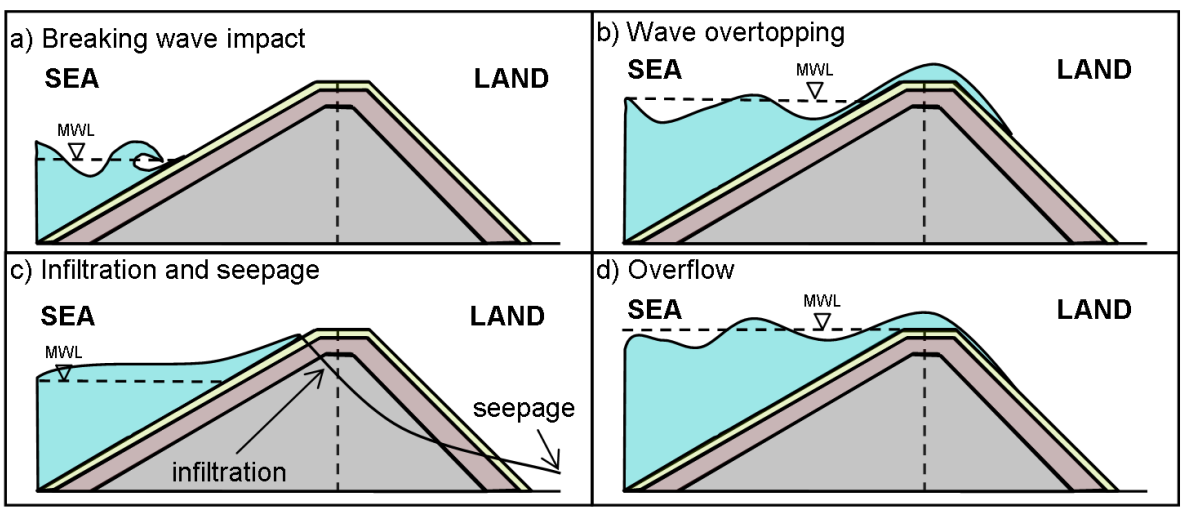

Figure 2.1: Causes of breach initiation in sea dikes

The main failure mechanisms which may lead to the breaching of sea dikes are (TAW,1999a):

- erosion and sliding initiated from the landside by wave overtopping and overflow. This is the subject of the completed PhD - Thesis process by D'Eliso (2007);
- the erosion of seaward slope resulting from breaking wave impacts and the flow induced by wave run-up and run-down;

2.1.1 Morphological and hydraulic boundary conditions

A typical North-Sea dike to which the current study applies is made of a sand core protected by the vegetated clay cover. A typical cross-section is schematically drawn in Fig. 2.2.

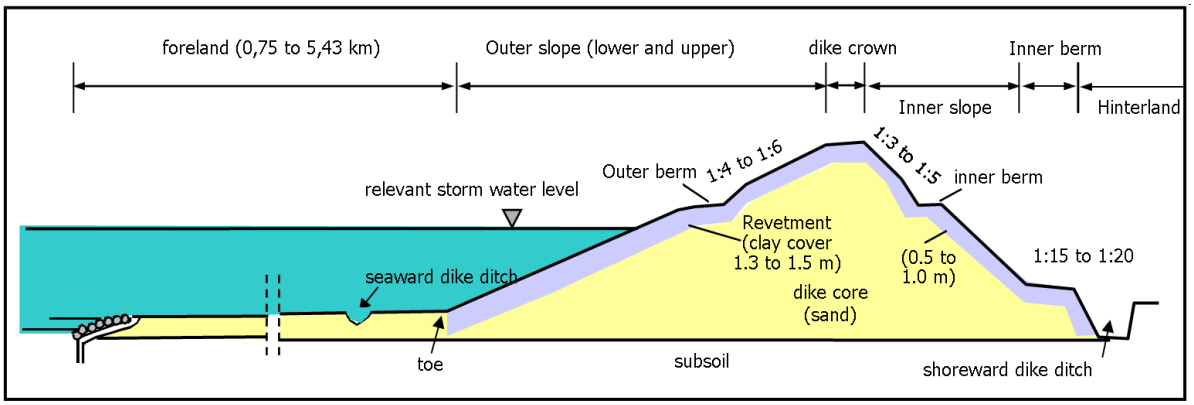

Figure 2.2: Simplified example of typical sea dike in Germany (Kortenhaus, 2003)

The materials used for the construction of sea dikes can be briefly characterised as follows:

Sand represents the main construction material (dike body) and is characterised by a loose, non-cohesive grain structure with a high hydraulic permeability and a relatively high mass density. The percentage of fine particles should be lower than 5% and the compaction of the sand should be between 90% and 98% of maximum Proctor density. This high compaction level provides good settlement and stability properties.

Clay is a cohesive, natural soil consisting of erosion and breakdown products of natural rocks, that were brought together again by natural processes. The most important properties of the clay refer to its good erosion resistance and high cohesion. The composition of the clay is based on the mass percentages of :

- **sand**: equivalent grain diameter greater than or equal to $63\mu m$ and less than 2 mm,
- **silt**: equivalent grain diameter greater than or equal to $2\mu m$ and less than $63\mu m$,
- **lutum** (argil) – equivalent grain diameter less than $2\mu m$.

Grass - although clay has relatively good erosion resistance, it generally reinforced by a protective layer made of grass. As shown in Fig. 2.3 a grass cover is composed of clay layer and herbage being the grass rooted in soil.

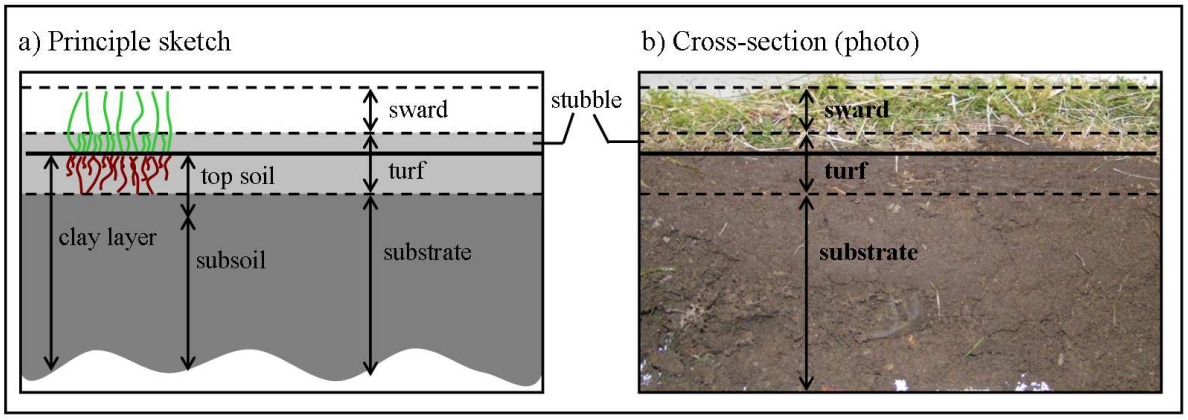

Figure 2.3: Structure of a grass cover - principle sketch and a picture of a cross-section

The very fine hair roots and symbiotic fungal threads due to connections with the finest particles bonds the soil particles, while the coarser plant roots keep large and smaller aggregates together in a sort of a network. This network of fine and coarse roots is the main reason, why the grass cover of a dike is a strong, springy and flexible layer that can deform without tearing. Both effects, i.e. keeping the soil together by the reinforcement made of roots and the structure of the soil between the roots, contribute to the good erosion resistance of the grass cover.

More detailed information on the morphological boundary conditions can be found in the State of the Art Report (Stanczak et al., 2007d)

For the prediction of the dike breaching, the assessment of the **hydraulic boundary conditions** is also required. The main hydraulic boundary conditions are (i) extreme water levels and (ii) wave action. Those two conditions are directly related - as the mean water level rises, larger waves occur and the dike is subject to stronger wave impact. The water level is subject to several types of fluctuations that are classified according to their period as follows:

- short-term fluctuations – storm surges, tides, barometric surges, seiches etc.;
- seasonal fluctuations – precipitations, evaporations;
- long-term fluctuations – eustatic sea level variations, isostatic land level emergence and subsidence, global climate changes

For the dike breaching modelling considered in this study, only the short-term fluctuations are taken into account. Although some ship-induced waves may occur in navigable areas they are negligibly small, and the main loading on the sea dikes is represented by the wind-induced waves. For the conditions at the sea dike toe, a double peaked wave energy spectrum typically reproduces the natural sea state, but in case when no recorded spectrum is available, the TMA spectrum is recommended (D'Eliso, 2007).

2.1.2 Breaking wave impact and flow of wave run-up and run-down

The loading on the outer dike slope due to breaking wave impact is essentially described by (i) the impact pressure and (ii) the flow velocity field associated with the wave run-up and run-down. A number of possibilities to calculate the impact pressures and flow velocities are available (see Stanczak et al, 2007d for more detailed description of the selected models):

1. **Empirical formulae:**
    - a selection of formulae derived from (i) field measurements (Grüne, 1988), (ii) near prototype scale model tests (Führböter and Sparboom, 1988; Führböter and Sparboom, 1988a) and (iii) small-scale model tests (Stive, 1983) are available for the calculation of the maximal impact pressures;
    - the maximal run-up and run-down velocities as well as the water layer thickness on the slope can be calculated with the formulae derived after (i) large-scale (Führböter, 1991) and (ii) small-scale tests (Schüttrumpf and Oumeraci, 2005; Neelamani 2003)
2. **Numerical models:**

- both impact pressures and flow field on the outer slope may be calculated with one of the available models solving the Reynolds-averaged Navier-Stokes equation with the Volume-of-Fluid method (RANS-VOF). The models of Doorn and van Gent (2003), Troch et al (2003), Thao and Shibayama (2006) or Liu and Lin (1997) can be referred to.

The above listed empirical models for the calculation of impact pressures and the flow velocity fields on the outer are significantly simpler than the available numerical models, but the latter are more generic. However, the numerical models, which provide a detailed description of the involved processes, are subject to very high computational effort. Nevertheless, currently the **RANS-VOF** models are considered to be the most efficient tool for the calculation of the loading on the dike slope.

During the breaching initiated from the seaside also the overflow may occur. For the calculation of the flow discharge and velocity during overflow either broad-crest weir formulae (D'Eliso, 2007) or Saint-Venant equations (Tuan, 2007) can be applied.

2.1.3 Infiltration

The erosion properties of the grass and clay revetment strongly depend on the water content in the soil, which in turn is a function of the water infiltration. Three main factors influence the water infiltration into the dike:

- mean water level;
- wave action (wave set-up, run-up and overtopping);
- rain.

For the dike breaching initiated from the seaside the water infiltration resulting from the high mean water level plays the crucial role. The progress of infiltration is usually horizontal and is strongly influenced by the presence of cracks and fissures in the clay revetment. The influence of the rain as well as infiltration due to wave overtopping are of a negligible importance for dike breaching initiated from the seaside and will therefore not be addressed in the present study. The infiltration due to rain can however be indirectly incorporated in the calculation during the estimation of the initial water content.

Two methods for the calculation of water infiltration are available:

- **numerical solution** of Richards equations (Richards, 1931) with the means of Finite Element Models (FEM). The available models combine the Darcy's law with the equations of water conservation in porous media. They provide a complete description of the infiltration processes, but are very expensive in the terms of numerical effort.
- **simplified models** are usually based on the laboratory tests and enable one to calculate the saturated and infiltration water fronts in the dike (Wang, 2000; Wang et al, 2003)

2.1.4 Implications for the present study

Both empirical and numerical models for the calculation of breaking wave impacts and the flow fields associated with run-up and run-down on the seaward slope of the dike referred to in Section 2.1.2 are only two-dimensional thus resulting in the limitation of erosion simulation for the two-dimensional domain. As a consequence, a reliable method to apply the

obtained two-dimensional results in a possibly three-dimensional dike breaching model has to be found. The same concerns the water infiltration models which are either one- or two-dimensional. Empirically based models are recommended for the preliminary model, as the computational effort should be kept low. On the other hand, the application of numerical models is recommended for the detailed model.

2.2 Erosion and mass instability processes and models

Erosion and instability processes occurring simultaneously or subsequently may result in a dike breaching. For a dike breaching initiated from the seaside, one may distinguish the following processes:

- grass erosion (Fig.2.4a and Section 2.2.2);
- clay erosion, including the shear failure in water-filled cracks and clay undermining (Figs. 2.4b and 2.4c and Section 2.2.3);
- erosion and washing-out of the sand core, including the mass instability (Figs. 2.4d, 2.4e and 2.4f and Section 2.2.5).

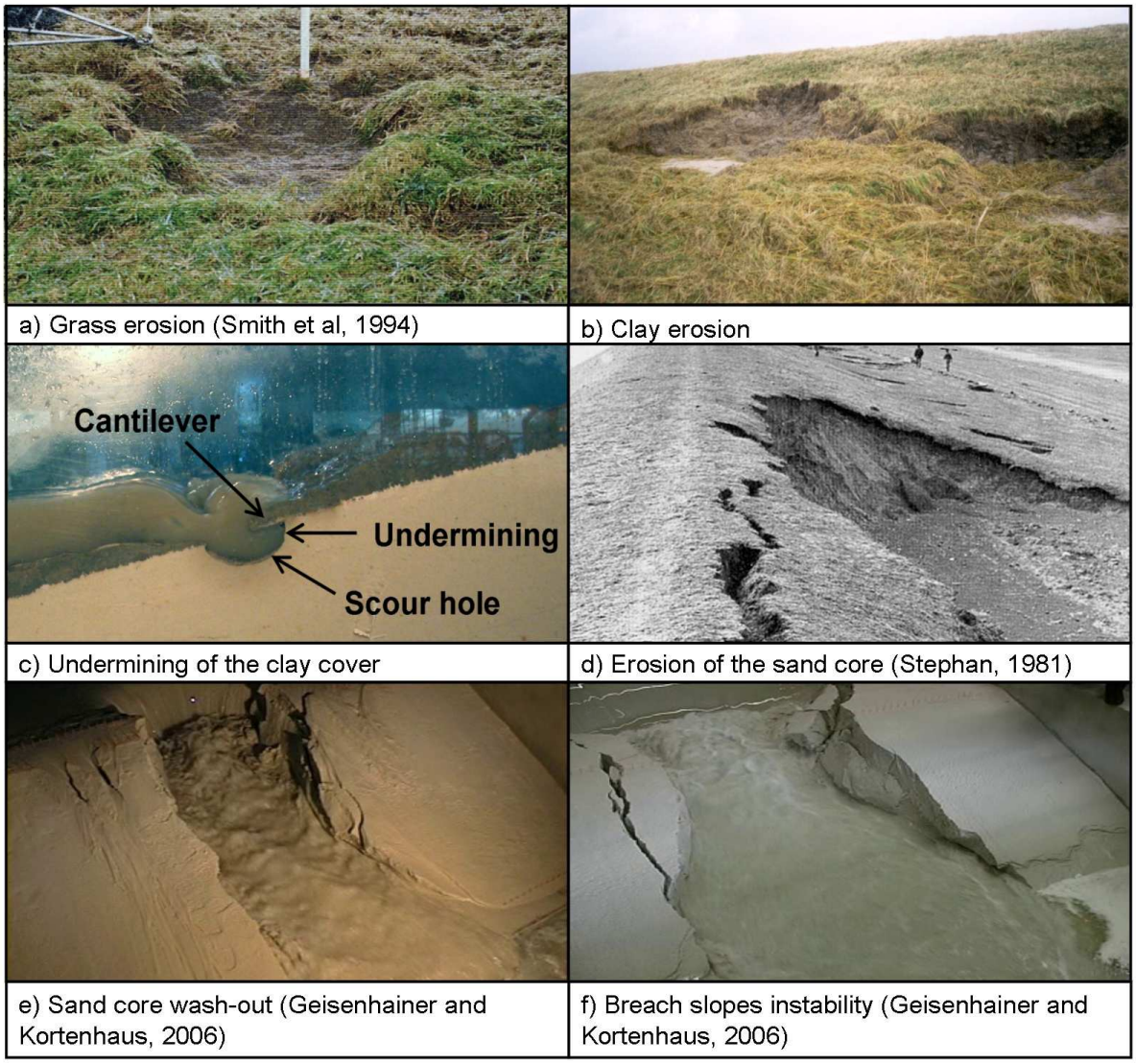

Figure 2.4: Dike breaching processes and phases

The total time of dike breaching can be given as a sum of the following phases (Fig. 2.5):

- *Time of grass failure* t_{gf} - time between the incipient erosion end the time of grass failure expressed in terms of erosion depth;
- *Time of cover failure* t_{cf} - time between the incipient erosion end the time when the revetment fails and the sand core becomes unprotected;
- *Time of core failure* t_{sf} - time between the incipient erosion end the time when the erosion reaches the inner slope and the erosion progress becomes irreversible;
- *Total breaching time* t_{tb} - time between the incipient erosion end the time when the water level on the landside becomes equal to the one on the seaside;
- *Breach initiation time* t_i - time between the incipient erosion and the initiation of the breach described in terms of erosion depth on the seaside;
- *Breach formation time* t_f - time between end of the breach initiation and the end of the breach formation;
- *Breach development time* t_d - time between the end of the breach formation and the start of the erosion of the inner slope;
- *Core wash-out time* t_c - time between the end of the breach development and the time when the water level on the landside becomes equal to the one on the seaside (final breach)

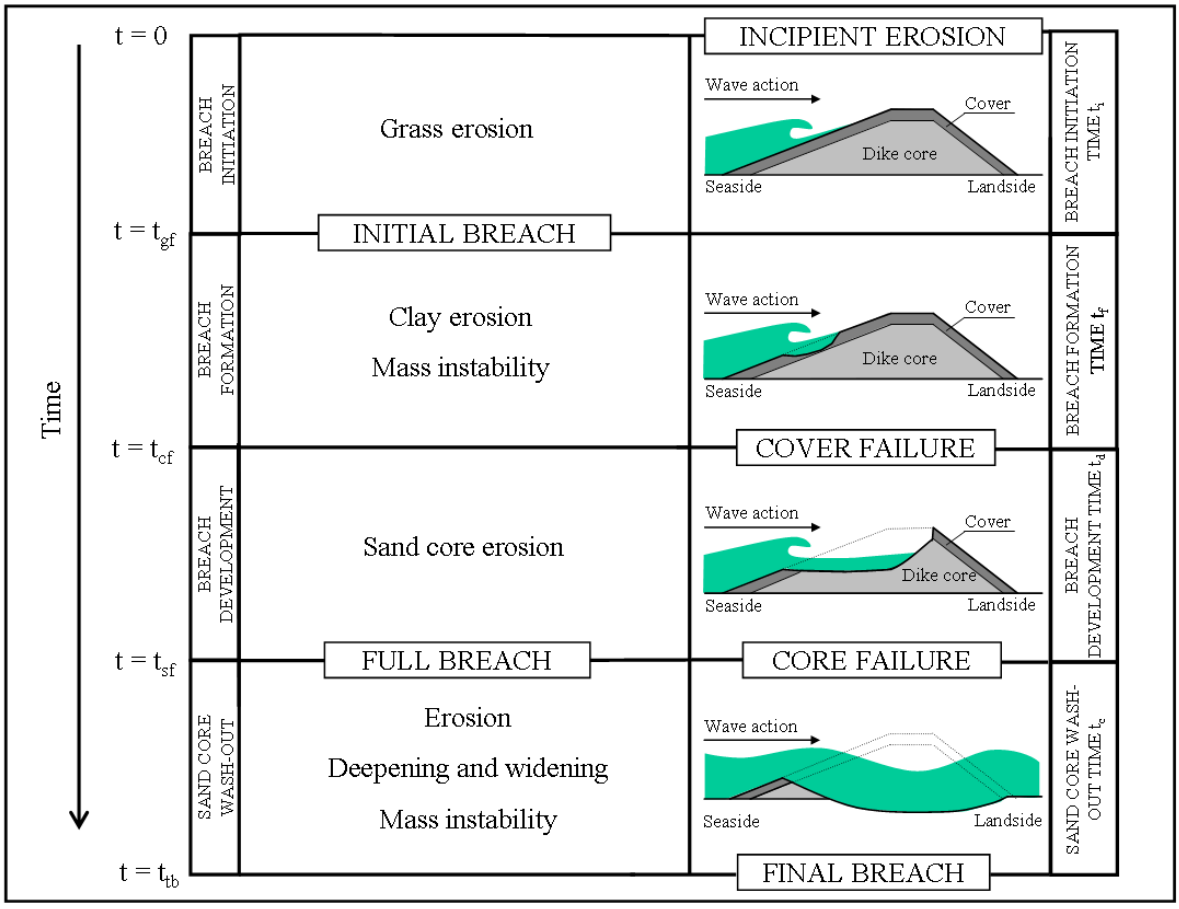

Figure 2.5: Phases of a dike breaching to be considered in simulation

2.2.1 Breach location along the dike route

Coastal dikes generally have a considerable length, so the breaches are difficult to localize. The prediction of the location that might be subject to a dike breaching is an important information in risk assessment related to dike failures. From the quantitative point of view, weaker points at a given location in the dike increase the probability of breach initiation at that location. The most important aspects that influence the probability of breach occurrence are:

- non-uniform grass cover, spots and holes due to burrowing animal activities
- weathered soil with strongly developed soil structure and cracks
- steep bathymetry in the front of a dike
- strong exposure high water level and waves

However, the considerations concerning the breach location along the dike route, although very important for the risk assessment and management of an entire flood defence system, are not the subject of this thesis. Therefore, the cross-section and the same loading conditions are considered along the entire dike route.

2.2.2 Erosion of the grass cover

The erosion of the grass cover is strongly related to the physical properties of the grass. For typical grass cover that is used in sea-dikes (c.f. Figure 2.3), the vertical succession of the root network properties, and consequently of the erosion resistance, can briefly be summarised as follows (TAW, 1999):

- the uppermost layer (so-called *stubble*) is up to 35mm thick and consists of loose soil and plant remains; this layer is washed away within short time by the waves.
- immediately below is a layer (*top-soil*) where the sod is closely rooted; this layer is only slowly eroded away. This layer is 5 to 50 mm thick
- in the next layer (*sub-soil*) the number of roots is considerably smaller; this zone is only attacked after a very long period of wave loading and is between 5 and 10 cm thick, while further below, the number of roots decreases significantly and the reinforcement properties of roots become negligible.

The total grass erosion due to waves breaking on the dike slope is a sum of the erosion resulting from two factors: (i) impact pressures directly at the location where the wave hits the slope and (ii) shear stress induced by the flow associated with the wave run-up and run-down.

A significant amount of knowledge is available on the erosion caused by flow induced shear stress (Temple et al, 1987, for instance), but no detailed investigations on the process of grass erosion due to impact pressures were performed. There is therefore a need to investigate this problem in more details, possibly by means of laboratory experiments. Furthermore, only a limited amount of information on the total grass erosion due to breaking wave impact is available (Smith et al, 1994), who performed full-scale tests in order to gain quantitative information on the wave loading, erosion rate and residual strength of a grass - covered dike (see Stanczak et al., 2007d) for more detailed information.

2.2.3 Erosion of the clay cover

The damage of the clay revetment related to the direct action of waves breaking on the dike slope was investigated during large-scale tests conducted in the Delta Flume and described by Delft Hydraulics (1992) and in the small scale tests in the LWI wave flume (Geisenhainer and Kortenhaus, 2006). The former showed that the erosion due to impact pressure of breaking waves is the main cause of damage from waves of 1 m in clay that is erosion-resistant against the flow up to flow 8 m/s. Although the main goal of the latter was to investigate the erosion due to wave overtopping, during tests with less wave overtopping severe damages at the seaward side of the dike occurred. However, due to time technical difficulties additional tests could not be performed to further test these preliminary observations. A number of erosion tests (Temple et al, 2003, for instance) under overflow conditions were also performed, showing clear similarities of the erosion mechanisms. Mirstkhoulava (1991) provided the detailed description of the scouring process of cohesive beds. The initial stage is characterised by loosening and washing away of dispersed particles and aggregates (separates) which consequently leads to a rougher surface with increased drag and lift forces. Higher pulsating drag and lift forces increase the vibration and dynamic action on protruding aggregates so that the bonds between aggregates are destroyed step by step until the aggregate is instantaneously torn out of the surface and carried away by the flow.

2.2.3.1 Erosion due to impact pressure

For the estimation of the clay erosion due to the flow of wave run-up and run-down the excess shear approach can be used, similarly as in the case of grass cover erosion. The problem is more complex in the case of erosion due to a "pure" impact pressure. One may use here the similarities to the "splash erosion" applied for the calculation of erosion due to the impact of water mass with known kinetic energy. The empirical model proposed by Woolhiser et al. (1990) is referred to :

$$R_d = k_d \cdot E_k \cdot e^{-wh} \tag{2.1}$$

with:

- R_d - volume of soil eroded after a single impact event $[m^3]$
- k_d - empirical detachability coefficient $[m^3/J]$
- E_k - kinetic energy of an impact event $[J]$
- w - empirical coefficient representing the effectiveness of a water layer to damp impact pressures $[-]$
- h - water layer thickness $[m]$

It is however necessary to emphasize, that its applicability for the impacts larger than raindrops was never verified in laboratory experiments.

2.2.3.2 Shear failure due to impact pressure in water-filled cracks

As the clay in a sea dike cover is subject to drying and wetting, changes in water content occur. The resulting shrinking and expanding of the clay in the unsaturated zone generally lead to the formation of two types of cracks (TAW,1996):

- **pull-cracks**: usually occur when soil shrinks. These cracks are differently oriented according to their size - larger shrinkage cracks (up to one meter) are almost always vertical and begin directly at the dike surface, smaller cracks (up to 20cm) may occur in all directions and can be found in the entire clay layer;

- **shear cracks**: are generally smaller (up to 20cm) than the pull-cracks and usually occur in shear areas that are caused by the swelling of clay. Those cracks occur in all directions.

The impact pressure acting on those cracks, especially the large (0.5m to 1m) pull-cracks that begin directly at the slope surface, may result in a shear failure and consequently in significant damage of the clay cover. Moreover, according to the recent study of Berkenbrink et al (2007) who performed photo-elastic, small-scale tests on cracks in a dike subject to impact pressures the impact pressure is transmitted not only into the crack walls, but also, to some extent, inside the dike, through the crack (Fig. 2.6).

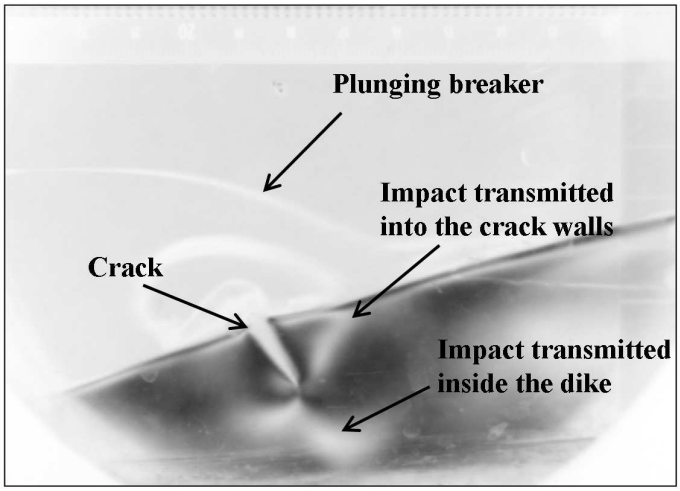

Figure 2.6: Impact of a plunging breaker on a crack in a dike - photo-elastic investigation (Berkenbrink et al, 2007)

The problem of shear failure in cracks subject to impact pressure was theoretically investigated by Führböter (1966) who proposed a conceptual model for the calculation of the shear failure angle and by Richwien (2002) who developed a simplified, graphical method for the estimation of shear failure occurrence possibility. More detailed these methods are given by Stanczak et al. (2007a). Although those conceptual models are widely referred to, they were never verified experimentally. However, since the model of Richwien (2002) provides only very general information on the possibility of shear failure, only the model of Führböter (1966) which provides more detailed information, including shear failure angle, will be referred to in the present study.

2.2.4 Erosion of the dike core

After the removal of the entire dike revetment, i.e grass and clay cover, the sand core of the dike becomes unprotected and the last phase of the dike breaching process - sand core erosion - begins. Due to variable flow conditions, this phase should be divided into two parts: (i) breach development , i.e. erosion of the front face of the breach due to the repeated action of breaking waves and (ii) sand wash-out, i.e. breach deepening and widening as a result of the overflow

and of the instability of the breach side slopes due to scouring erosion. Although currently no information on the erosion processes of the unprotected dike core is available,the extensive knowledge of the dune and beach erosion processes can be used to a certain extent. Generally, two approaches are available: (i) wave impact approach and (ii) beach profile approach.

2.2.4.1 Wave impact approach

The erosion phenomenon is a time-dependant process in which a series of successive waves attack the front face of the structure. As each individual wave erodes a finite volume of sand, the volume of soil eroded from a noncohesive dune for a single wave impact is a function of the impact force, so that the whole process of erosion in the direction of wave action can be described as a sum resulting from successive single impacts. Two models are referred to: Overton et al, (1994) and Larson et al, (2004). In both models the volume of soil eroded for a single wave impact Q_{single} is calculated as:

$$Q_{single} = C_E \cdot F_{impact} \tag{2.2}$$

with:

- F_{impact} - impact force $[kN]$
- C_E - empirical erosion coefficient $[m^3/kN]$

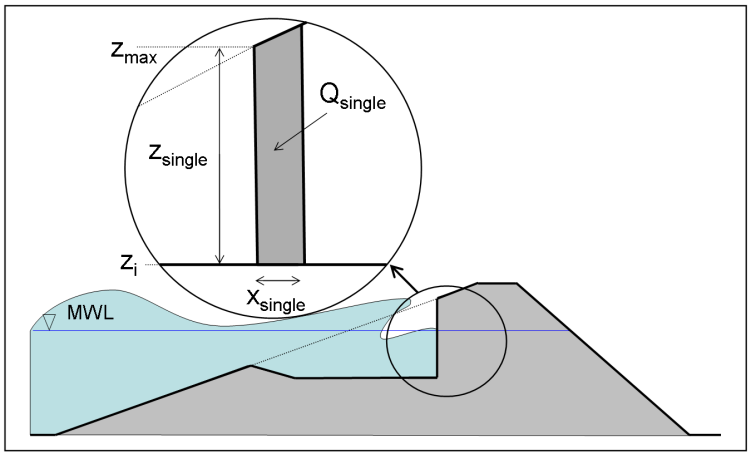

Figure 2.7: Wave impact approach - principle sketch

This *wave impact approach* (Fig. 2.7) is a simple, yet physically based and reliable method for the prediction of the erosion progress in sand dunes and it was verified against a number of small-scale wave tank experiments, large-scale tests and field measurements providing satisfactory results. More details on the models of Larson et al (2004) and Overton et al (1994) as well as on the erosion coefficients for sand are given by Stanczak et al (2007d).

2.2.4.2 Beach profile approach

The second available approach is based on the assumption, that if an earthen structure is subject to constant wave conditions for a sufficiently long time, it will attain an equilibrium profile, which dissipates incident wave energy without significant net change in shape. Two general types of equilibrium profiles - *berm profile* and *bar profile* - are observed, depending on the wave steepness and ratio of wave height to grain size - Fig. 2.8.

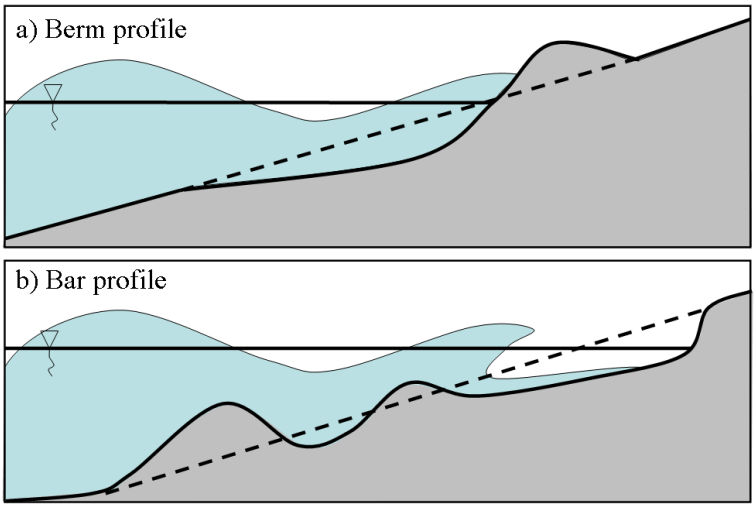

Figure 2.8: Equilibrium profiles

The net cross-shore sediment transport rate q and resulting profile evolution during a storm surge will then depend on the magnitude of deviation from this equilibrium state and can generally be calculated as (Larson and Kraus, 1989):

$$q = K \cdot (D - D_*) \tag{2.3}$$

where:

- K - transport rate coefficient K $[m^4/N]$
- D - wave-energy dissipation $[Nm/m^3/sec]$
- D_* - equilibrium wave-energy dissipation $[Nm/m^3/sec]$

The equilibrium wave-energy dissipation is a determined by sediment grain size, in which a coarser grain size gives a larger value and a steeper profile slope (Dean, 1977). This approach was confirmed in a large number of studies (e.g. Larson et al., 1999; Gonzalez et al., 1999).

2.2.5 Wash-out of the sand core

The last phase of the breaching process, i.e. sand core wash-out due to overflow was intensively investigated in the laboratory (Caan, 1996; Coleman et al, 2002; IMPACT, 2004; Pugh, 1985; Rozov, 2003; Verheij, 2003; Visser, 1998; Geisenhainer and Kortenhaus, 2006, Tuan, 2007). All laboratory experiments show similar erosion mechanisms, which can be summarised as follows (see also D'Eliso, 2007 and Stanczak et al, 2007d):

- after the overflow occurs, the breach proceeds vertically, and significantly slower also laterally. The initial breach channel is usually triangular, but soon after the begin of the overflow it becomes almost rectangular, with approximately vertical walls;
- when the breach progress reached the (non-erodible) dike base, the lateral erosion becomes dominant. The velocity of erosion progress decreases as the flow velocity and resulting sediment transport rate decrease due to increasing backwater level. The final breach channel is approximately trapezoidal, with the slopes angle equal to the angle of repose of the sand;

Based on the laboratory experiments and on the theoretical considerations, a number of conceptual models which can be used for the calculation of sand core erosion due to the overflow were developed (Visser, 1998; Hassan, 2002; Rozov, 2003, Tuan, 2007). These however do not include the superposed action of waves and have to be used with caution. In Stanczak et al, (2007d) more detailed description of those models is provided.

2.2.6 Implications for the present study

The following can be stated after the analysis of the available knowledge on the processes of erosion during dike breaching:

- there are no breach initiation models available;
- only very limited knowledge on the grass and clay erosion due to impact pressures is available, i.e. only one laboratory experiment on the grass erosion due to breaking wave impact was conducted (Smith et al, 1994), the laboratory experiments on clay erosion are also rare and poorly reported (Delft Hydraulics, 1992; Geisenheiner and Kortenhaus, 2006);
- despite its crucial importance for the process of dike breaching, shear failure in water filled cracks was investigated only theoretically, no laboratory experiments were performed to verify the proposed conceptual models;
- the entire process of dike breaching initiated from the seaside was never investigated experimentally from the breach initiation till the full breach, even in small-scale tests;
- in the case of breach initiated from the seaside, the erosion on the crest and on the landside can be generally neglected during the front face erosion, it becomes however dominant in the last phase, i.e. during the core wash-out;
- during transition phase between core erosion and core wash-out overtopping and resulting erosion of the landside slope may occur. This phenomenon has to be accounted for. The same concerns combined wave overtopping and overflow.
- influence of the infiltration and consequently of the water content in the soil on its erosion resistance and thus erosion processes is generally neglected;
- the grass cover on the outer slope is the most important reinforcement of the sand-clay dikes. Even if damaged locally, it still protects the remaining part of the dike. The investigations of the reinforcement properties of grass are lacking and therefore it is recommended to investigate this problem in more detailed manner.

2.3 Sediment transport processes and models

The eroded soil has to be removed by the flow. Although during the erosion of the outer slope it might be assumed that the eroded sediments are removed instantaneously , this assumption is not valid anymore during the wash-out of the sand core, where the sediment transport capacity of the flow in the breach governs the progress of erosion.

2.3.1 Sediment transport processes

The progress of erosion under overflow conditions which occurs during the core wash-out is determined by the sediment transport capacity of the flow. The following, general aspects play the most important role:

- the bed load determines the bottom evolution, while the suspended load is responsible for the erosion of breach sides;
- the flow is unsteady, usually super-critical;
- the water properties, especially viscosity, are strongly influenced by the high sediment concentration;
- combined action of waves and currents is observed;
- non-equilibrium sediment transport conditions prevail (Visser, 1998).

2.3.2 Sediment transport models

A number of sediment transport models are available (Bailard, 1981; Visser, 1998; Yang and Molinas, 1982; Smart, 1984) but none of them is capable to describe properly the process that occurs during dike breaching, as they are based on assumptions which are not strictly valid under breaching conditions (see Stanczak et al, 2007d and D'Eliso, 2007 for more detailed information):

- the available models are derived for steady sub-critical flows, equilibrium sediment transport and mild slopes, while during dike breaching the flow is generally super-critical, non-equilibrium transport conditions prevail, and the slopes are relatively steep;
- the bed transport is described with the median grain size, i.e. single grain size, although the extensions of single-grain size functions to multiple-grain size is possible, it might produce unreliable results ;
- most of the models neglect the influence of wave action on the sediment transport. In laboratory tests (Geisenhainer and Kortenhaus, 2006, for instance) it was however observed, that the erosion due to overflow can be strongly affected by the additional action of the waves;
- the available models are validated on open channels;

2.3.3 Implications for the present study

At the moment there are no sediment transport models that can be directly incorporated in the dike breaching model to be developed. Generally, depending on the specific situation, the most appropriate model should be selected among the available ones (Table 2.1)

Model	Model type	Transport type	reference
Yang	Equilibrium	Total	Yang (1979)
Bailard/Bagnold	Equilibrium	Bed and suspended	Bailard (1981)
Smart	Equilibrium	Bed	Smart (1984)
Visser	Equilibrium	Bed and suspended	Visser (1988)

Table 2.1: Selection of the available sediment transport models

2.4 Available breach models

The extensive literature review (Stanczak et al, 2007) has shown that no information was found on existing process-oriented model of sea dikes breaching initiated from the seaside by breaking wave impact. There are only a very limited number of simple empirical models that are used to gain basic information on failure modes in complex systems for the calculation of flooding probability or lifetime expectation of sea-dikes. All of them provide only a rough estimation of dike failure time assuming the shape of the scour hole or breach and using simple empirical equations. Among them, the most important ones are (i) module of dike erosion and breaching used in Dutch program PC-RING (INFRAM, 1999) and (ii) module of dike failure initiated from the seaside implemented in Danish model by Laustrup et al (1990). Considerable amount of information was found on erosion models for sand dunes (Bailard, 1981; Fisher and Overton, 1984; Kriebel and Dean, 1984; Vellinga, 1986; Overton et al, 1989; Steetzel, 1993; Bosboon et al, 2000; Koster, 2004; Larson et al, 2004; Wang and Kraus, 2005; Kobayashi et al, 2006, Tuan, 2007) , but only some of them may be used as the part of the dike breaching model to be developed (see Stanczak et al, 2007d for more details). Table 2.9 provides brief information on the existing models for the simulation of dike and dunes erosion and breaching, including their most important pro's and con's.

Model	Structure (part of structure)	Type of model	Pros	Cons	Reference
(no name)	Grass cover of a sea dike	Empirical model (wave impact)	The only model for grass erosion due to breaking wave impacts that is based on the results of large-scale laboratory experiments	Calibrated with very limited (only two!) number of tests, only one grass sample investigated	Smith et al (1994)
(no name)	Grass cover of a sea dike	Empirical model (wave impact)	Grass erosion model developed after tests with jets	Calibrated with limited number of tests, no influence of water flow included	Lautstrup et al (1990)
SITES	Vegetated earth spillways	Empirical model (excess shear stress)	Good theoretical basis, verified against large number of measurements	Developed only for steady, uniform flow	NRCS (1997)
PC-RING	Clay dikes	Empirical model (wave impact)	In fact only model for simulation of clay erosion due to breaking wave impact	No information on calibration and validation is provided, shape of erosion hole is assumed, not calculated	INFRAM (1999)
(no name)	Sand dune	Empirical model (wave impact)	Simple, robust model, similar to the model of Larson et al. (2004), provides almost the same results	Calibrated only with limited amount of data, shape of eroded hole is assumed, not calculated	Fisher and Overton (1984)
DUROSTA	Sand dune	Process-oriented numerical model (suspended sediment flux)	Good agreement with the field measurements, all relevant processes are simulated	Calibration and validation are still lacking	Steetzel (1993)
UNIBEST	Sand dune	Process-oriented numerical model (bedload and suspended sediment flux)	All relevant processes are simulated, good agreement with measurements	Very complicated, large computational effort needed, suitable rather for simulation of long-term profile changes	Bosboom et al (2000)
SBEACH	Sand dune	Process oriented numerical model (equilibrium profile approach)	Stable, relatively simple, provides very good results, grain size distribution is taken into account	Although the profile changes are good predicted, the transport rates needs to be verified	Larson and Kraus (1989)
EDUNE	Sand dune	Process oriented numerical model (equilibrium profile approach)	Stable, provides relatively good results, validated agains large number of field mesurements	No incipient motion criterion is included, when compared to SBEACH model	Kriebel and Dean (1984)
(no name)	Sand dune	Empirical model (wave impact)	Simple, robust model, verified against large amount of field and laboratory mesurements	Shape of eroded hole is assumed, not calculated	Larson et al (2004)
(no name)	Sand dune	Energetic model, efficiency of the water to transport sediment	Reasonable theoretical basis, the model is constantly being improved	Turbulence due to breaking waves ignored	Bailard (1981)
(no name)	Sand dune	Wave power approach	Both erosion and accretion are accounted for	Very complicated, large computational effort needed, validation lacking	Watanabe (1988)
(no name)	Clay dikes	Complete dike braching model	Model for the simulation of sea dikes breaching initiated by wave overflow.	Applicable only for clay dikes	Zhou (2006)
(no name)	Coastal barriers	Complete braching model	Model for the simulation of coastal barriers breaching. The volume-averaged approach for channel growth simulation can be applied in the present study	Only erosion due to overtopping and overflow is accounted for	Tuan (2007)
CDBS	Sea dikes	Complete braching model	Model for the simulation of dike breaching induced by wave overtopping. The core erosion module can be applied in the present study	Only erosion due to overtopping and overflow is accounted for	D'Eliso, 2007

Figure 2.9: Selected breaching models

2.4.1 Limitations of available breach models

The existing models for the breaching of sea dikes initiated from the seaside are not only rare but also based on strongly simplified assumptions and therefore subject to numerous limitations. The most important refer to:

- **Breach initiation** - none of the existing models takes the problem of breach initiation under consideration. In all cases, only the residual strength of the grass or clay cover is calculated with the means of simplified models;
- **Structure** - a number of models for homogenous sand dunes and coastal barriers are available (Fisher and Overton, 1984; Steetzel, 1993; Bosboom et al, 2000; Larson and Kraus, 1989; Kriebel and Dean, 1984; Watanabe, 1988; Tuan, 2007 , for instance). However, only two, very simplified models (PC-Ring (INFRAM, 1999) and Lautstrup et al,1990) might be applied for the composite dikes with vegetated clay revetment;
- **Reinforcing properties of grass roots** - are not investigated in terms of the involved basic processes, but only arbitrarily assumed based on simple laboratory experiments (Smith et al, 1994 or Lautstrup et al, 1990) or, more often, fully neglected;
- **The influence of soil parameters, including water content and infiltration** - in the existing models it is either included in a very simplified manner (INFRAM, 1999) or not included at all
- **Progress of erosion** - the existing models do not simulate the progress of erosion, but only the time that the revetment can withstand the prescribed loading.
- **Breach morphology** - is usually assumed based on a simplified geometry instead of being directly calculated;
- **Backwater effect** - is fully neglected
- **Basic understanding of the processes** including the erosion of grass, clay and sand as well as the formation of the breach is still lacking
- **Validation** - the models are validated only against the data for sand dunes or using a limited amount of small-laboratory experiments with grass and clay. No laboratory experiments or field experiments for real sea dikes are yet available.

Since all the relevant parameters, including sea state, material properties and model parameters are subject to large uncertainties, it is recommended to quantify the uncertainties, when deterministic models are applied.

2.4.2 Implications for the present study

After the extensive literature study (Stanczak et al, 2007) no existing model for dike breaching initiated from the seaside was found. However, a selection of models that are capable to partially simulate the processes that occur during dike breaching was made. Although none of the existing models can be directly applied, some parts of them could form the basis for further developments and consequently for the implementation in the model to be developed. This especially concerns the empirical models for grass erosion (Smith et al, 1994), clay erosion (INFRAM, 1999) and front-face sand core erosion (Larson et al, 2004). Furthermore, the

modules for the simulation of erosion due to overflow that are used in the existing models for dike breaching simulation initiated from the landside (D'Eliso, 2007, for instance) might be implemented in the model to be developed. Table 2.2 provides a brief overview on the existing models and indications of their applicability.

Reference	Structure investigated	Application area in new breaching model
Smith et al (1994)	Grass revetment of a sea dike	Grass erosion
SITES (NRCS, 1997)	Vegetated earth spillways	Grass and clay erosion
INFRAM (1999)	Clay dikes	Clay erosion
Larson et al (2004)	Sand dunes	Core erosion due to wave impact
D'Eliso (2007)	Sea dikes	Erosion due to overflow
Tuan (2007)	Coastal barriers	Erosion due to overflow

Table 2.2: Selection of the available breaching and erosion models and indications of their applicability

2.5 Specification of objectives and methodology

The tentative objectives and methodology formulated in the introducing chapter are specified below on the basis of the results of the review and analysis of the present knowledge.

2.5.1 Objectives

This work should contribute to the flood risk assessment by (i) improving the prediction of the warning time and of the initial conditions for the calculation of flood wave propagation in areas protected by sea dike and (ii) improving the capability of dike failure prediction. Those main objectives are supposed to be achieved by the means of a model system to be developed. The prospective model is expected to contribute to the risk-based design of sea-defence structures.
Based on the results of the literature survey presented in Chapter 2, the general requirements of the model to be developed are defined as follows:

- **Reproduced structure**: coastal dike made of a sandy core protected by clay revetment with grass cover;
- **Simulated processes**: initiation and development of breaching induced by breaking wave impact on the outer slope. A description of breach initiation, formation and development are included with focus on the processes leading to breach initiation;
- **Type of model**: process-oriented deterministic model that should serve as a practical tool for the prediction of breach initiation and development processes;
- **Model outcomes**: breach evolution in space and time, including information on final breach width and breaching times as well as outflow hydrograph
- **Model uncertainties**: sensitivity analysis, reliability analysis

Since the prospective model should primarily serve as a practical prediction tool, attention should be paid to the validation of the model in order to define the range of accuracy and applicability of the model.

2.5.2 Methodology and procedure

Similar to the PhD-Thesis of D'Eliso (2007) a tiered modular modelling approach will be adopted using a preliminary and a detailed computational model. The detail level of the description of breaking-wave impact pressures and erosion processes primarily constitutes the difference between the two models (see Fig. 2.10).
The preliminary model should be based on 2D+2D description of the process and is supposed to provide a rough, but fast estimation of the breach initiation and growth. The detailed model will be more demanding in terms of computational effort but it will allow a more reliable and complete description of the involved processes. Beside the differences associated with the computational effort and the accuracy of results the preliminary model will need less input data than the detailed model. Moreover, if both preliminary and detailed models have to be applied in practice, the former should provide more conservative results then the latter.

Both models are developed based on several modules that are applied sequently:

- **Input module:**
  - Sea state: water level and wave parameters;
  - Dike parameters: geometry and material parameters;
  - Model parameters - spatial and temporal discretisation.
- **Hydrodynamic module:**
  - Free surface flow: wave action on the outer slope, overflow;
  - Infiltration (detailed model only)
- **Morphodynamic module:**
  - Erosion of grass, clay and sand;
  - Instability (detailed model only);
  - Sediment transport processes.
- **Output module:**
  - Temporal breach progress: time of grass and clay erosion, time of core failure, total breaching time;
  - Geometrical breach parameters: final breach depth and width;
  - Outflow hydrograph, peak outflow discharge

The preliminary model is based on simple, mostly empirically based formulae. Therefore, less input data than for the detailed model will be required. Possibly, the results should be more conservative than those of the detailed model. Both requirements are important if the preliminary model has to be used in engineering practice. The model should: (i) provide a general view on the breach initiation, formation and development, (ii) help to identify the problems that might be expected in the development of the detailed model.

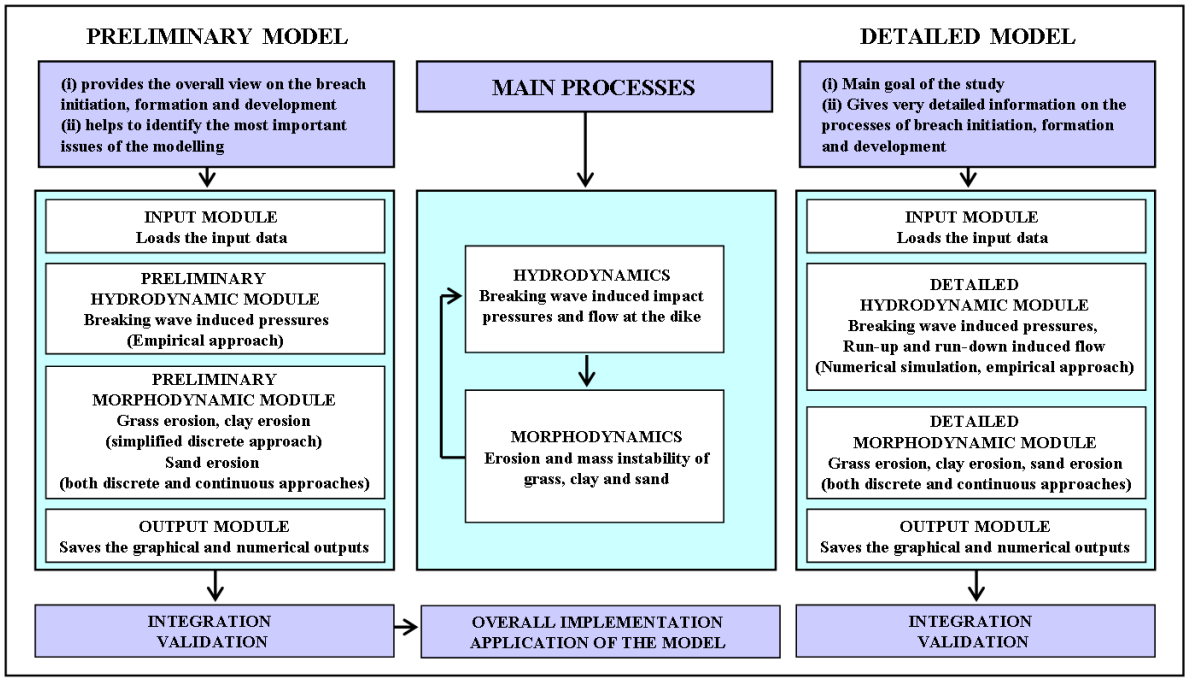

Figure 2.10: Overall approach

The detailed model represents the main goal of this study. This model should be a complete, but also still practically feasible modelling tool. Among the new aspects that are included, the most important is the focus on the breach initiation phase. The identification and modelling of the processes that lead to breach initiation and the breaching process itself are to be performed in order to obtain reliable results.

The following modelling and working steps are included in the present study:

1. **Preliminary hydrodynamic module** - only free surface flow will be included. This module calculates breaking-wave induced impact pressures on the outer slope during grass, clay and sand erosion. During the core wash-out the overflow in the breach channel is simulated with steady non-uniform free surface flow equations.

2. **Preliminary morphodynamic module** - the available grass, clay and sand erosion models will be combined and implemented. The breach initiates at the location where simultaneously the loading is the strongest and the grass is the weakest. The shape of the scour hole in the outer slope will be calculated as a function of the loading, while the growth of the breach channel will be calculated as a function of the sediment transport load and assumed constant relationship between breach widening and deepening.

3. **Laboratory tests** - a number of laboratory experiments on the grass and clay erosion will be performed by using a wave impact simulator. The focus of the tests should be on the processes that may lead to the breach initiation. The reinforcement properties of the grass cover will be quantified and empirical formulae for their estimation will be proposed. The existing conceptual model for shear failure in water-filled cracks will be verified and improved. Small-scale tests in the wave flume will also be performed on a

dike model in order to gain qualitative knowledge on the entire breaching process, from the breach initiation till the occurrence of the full breach.

4. **Detailed hydrodynamic module** - the flow during grass and clay erosion will be simulated with a RANS-VOF model (Cobras model). For the sand erosion simulation, the SBeach model and steady non-uniform free surface flow equations will be applied. Furthermore, the calculation of infiltration will be included by applying simplified infiltration models.

5. **Detailed morphodynamic module** - completely new formulae derived from the performed laboratory experiments will be used. The new aspects as compared to the preliminary model will include the separate calculation of erosion due to impact pressures and flow of run-up and run-down, the reinforcement model of grass, the calculation of shear failure in water-filled cracks, the stability of the revetment on the outer slope. The sand erosion module will be based on the beach profile model. Furthermore, the possible erosion of the inner slope due to overtopping and overflow will be accounted for by applying a model selected among the existing models for dike breaching initiated from the landside.

6. **Model uncertainties and validation** - a sensitivity analysis will be performed for the most uncertain input parameters. An uncertainty analysis will also be performed using a Monte Carlo simulation for both preliminary and detailed model. The complete model will tentatively be validated against the same data sets that were used for the validation of the preliminary model.

3 Preliminary model - development and implementation

The preliminary model for the simulation of dike breaching initiated from the seaside by breaking wave impact represents the first step of the tiered modelling approach. The main objective of the preliminary model is to rapidly provide an overview of the entire breaching process and to identify the most critical processes. The model is modular, primarily including hydrodynamic and morphodynamic modules. Figure 3.1 shows the structure and the most important components of the preliminary model.

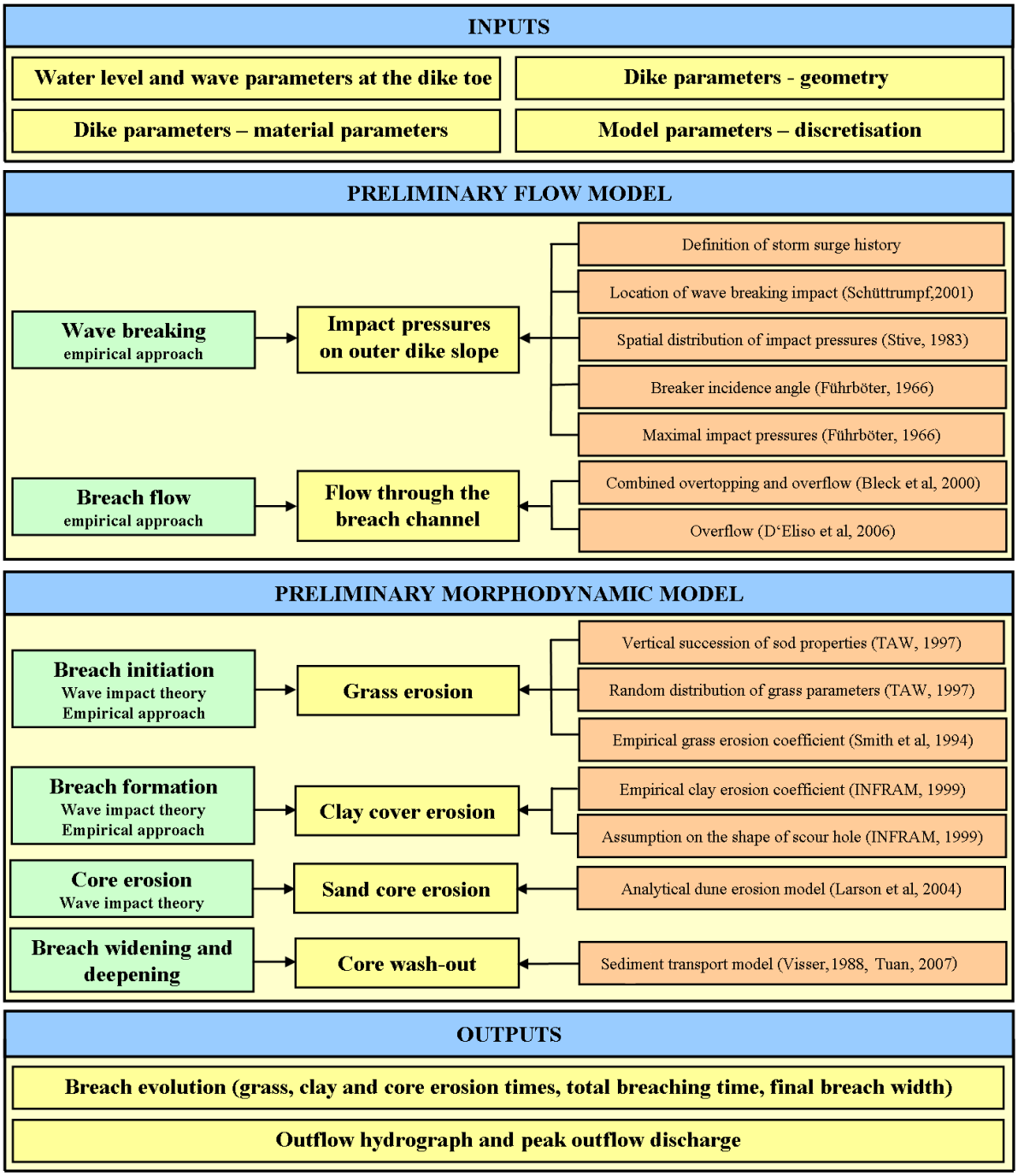

Figure 3.1: Structure and main components of the preliminary model

3.1 Mathematical formulation

The dike failures experienced in the past show that the dike breaching process represents a complex 3D fluid-structure interaction. However, in the preliminary model the simulation will be limited to 2D process during the first three phases, and to 2D+2D during the last phase, i.e. sand core wash-out. Further simplifications in the preliminary model may be summarised as follows:

- the wave run-up and run-down are not simulated;
- the overtopping that eventually might occur is not simulated;
- the infiltration is not accounted for;
- the grass and clay covers are assumed to fail instantaneously, as soon as they fail at one location;
- during the simulation of the front-face core erosion the shape of the breach is assumed, not calculated;
- no mixing of materials and consequently no interaction between them is assumed, during the entire simulation the soil parameters are kept constant;
- the hydrodynamic and morphodynamic modules are not coupled.

3.2 Input module

For the reliable prediction of the dike breaching process, a careful assessment of the hydraulic boundary conditions is necessary. The main hydraulic boundary conditions are (i) extreme water levels and (ii) wave loads. Those two conditions are directly related - as the mean water level rises, larger waves occur and the dike is subject to higher wave loads.

3.2.1 Hydrodynamic boundary conditions

The information on the mean water level and its variations can be loaded from an input file that contains the recorded history of a storm surge water level. Depending on the hypothetical location of the simulated dike, the data can be selected from the available input files that contain information on the typical storm surges that occur at different locations along the coast line. The mean water level can be also assumed to be constant during the entire breaching process. The preliminary model is capable to simulate either regular waves or irregular waves, in the case of irregular waves the water surface elevations are generated by the model according to the Rayleigh distribution of wave heights. For the proper simulation, the model needs the information on the wave height and water depth at the toe of the dike.

3.2.2 Dike geometry

The information on the geometry of the dike is needed for the proper reproduction of the morphological boundary conditions. Two types of input parameters are distinguished:

1. Dike geometry, which should contain information on: (i) dike height H_d, (ii) crest width B_D, (iii) outer $(1 : n)$ and inner $(1 : m)$ slope and (iv) thickness of the grass cover d_g and clay cover d_c.

2. Material properties, especially grass and clay erosion coefficient (E_g and E_c, respectively) and mean grain size D_{50} of the sand constituting the dike core

Additionally, the grid spacing Δx needs to be defined by the user. The time step during the front-face erosion is equal to the period of incident wave, but during the calculation of the overflow it is necessary to define the time step Δt. There is no allowable minimal grid space or minimal time step. The model was successfully tested with grid spaced in the range $\Delta x = 0.05m$ to $\Delta x = 2m$ and time step in the range $\Delta t = 0.1s$ to $\Delta t = 10s$.

3.3 Hydrodynamic module

The hydrodynamic module provides essentially the information on the wave loading of the dike which is then used as input for the morphodynamic module. The main load consists of the breaking wave impact on the outer slope, but the process of the overflow is also simulated after the breach has reached the inner slope. In the preliminary model, the simulation of wave run-up and run-down is not performed, as the effect of the flow related to the wave run-up and run-down is not explicitly included in the erosion models selected for the implementation in the preliminary model (see Section 3.4). The simulation of the infiltration is neglected since no changes in the soil properties resulting from the changes in the water content in the soil are accounted for.

The flow is simulated in two cases:

1. The flow conditions on the outer slope of the dike, from the toe of the dike up to the crest are simulated before and during the breach initiation, i.e. until the erosion has reached the inner slope (Fig. 3.2a and Fig. 3.2b)

2. The flow through the entire dike breach - from the outer up to the inner toe of the dike - is simulated in the last phase, i.e. after the erosion reached the inner slope, the breach channel formed and overflow occurred in the breach (Fig. 3.2c)

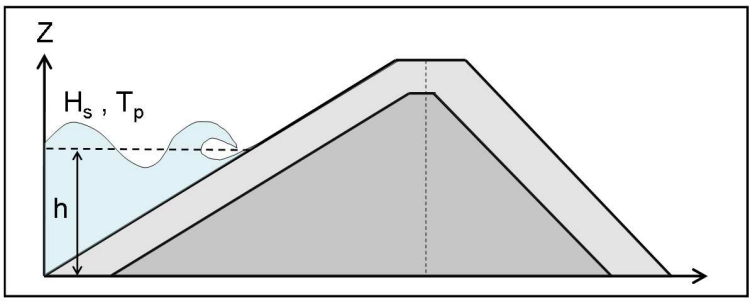

(a) Before breach initiation - erosion of grass and clay cover

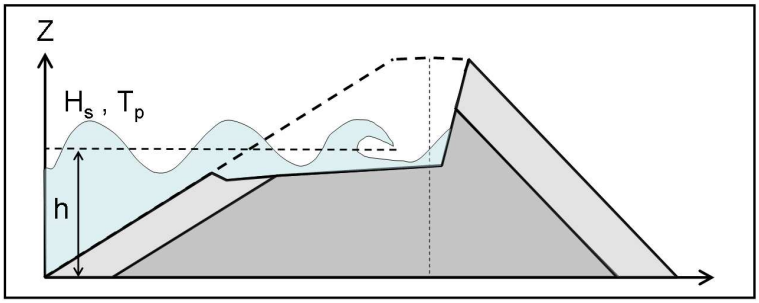

(b) During breach development - erosion of the sand core

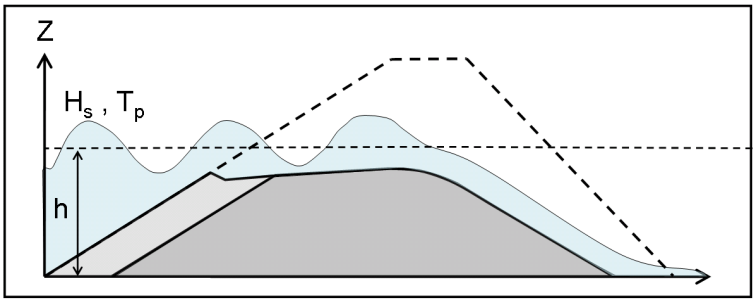

(c) Flow through the dike breach

Figure 3.2: Flow conditions dike breaching simulation

3.3.1 Breaking wave impact on the outer slope

The breaking wave impact on the outer slope represents the main loading on the dike during breach initiation and formation. The type of wave breaking is estimated using the non-dimensional surf similarity parameter ξ (e.g. Battjes, 1974):

$$\begin{aligned} \xi &= \frac{\tan\alpha}{\sqrt{\frac{H_s}{L_0}}} \quad \text{with} \quad L_0 = \frac{gT_m^2}{2\pi} \quad \text{for wave spectra} \\ \xi &= \frac{\tan\alpha}{\sqrt{\frac{H}{L_0}}} \quad \text{with} \quad L_0 = \frac{gT^2}{2\pi} \quad \text{for regular waves} \end{aligned} \tag{3.1}$$

where:

- α - outer dike slope $[deg]$
- H - wave height at the dike toe $[m]$
- H_s - significant wave height $[m]$
- L_0 - deep water wave length $[m]$
- T - wave period $[s]$
- T_m - mean wave period $[s]$

Table 3.1 provides the information on the types of wave breaking and the criteria of their occurrence.

Dike slope 1:n	Plunging breaker	Collapsing breaker	Surging breaker
1:6	$\xi < 2.1$	$2.1 < \xi < 2.8$	$\xi > 2.8$
1:4	$\xi < 2.4$	$2.4 < \xi < 3.1$	$\xi > 3.1$
1:3	$\xi < 2.6$	$2.6 < \xi < 3.3$	$\xi > 3.3$
mean	$\xi < 2.3$	$2.3 < \xi < 3.0$	$\xi > 3.0$

Table 3.1: Classificaton of breaking types on sea dikes (Schüttrumpf, 2001)

In terms of dike breaching caused by impact pressures on the outer slope, a plunging breaker (Fig. 3.3) represents the most crucial type of the wave breaking. The wave energy is dissipated over a short distance and within a short time, which results in relatively small surfaces exposed for a very short period of time (0.01 to 0.1 s) to very high impact pressures (up to 150 kPa). This impact load does not act continuously, but intermittently in time intervals of at least one wave period (usually longer with predominant impact on the water layer that results from the wave up and down rush process of the preceding wave). Therefore, the actual loading time (0.1 to 0.01 s) is small in comparison with the time period between the loads (5-12s). The wave breaking process is subject to strong variations due to the influence of the entrained air, so the parameters describing this process have to be described stochastically.

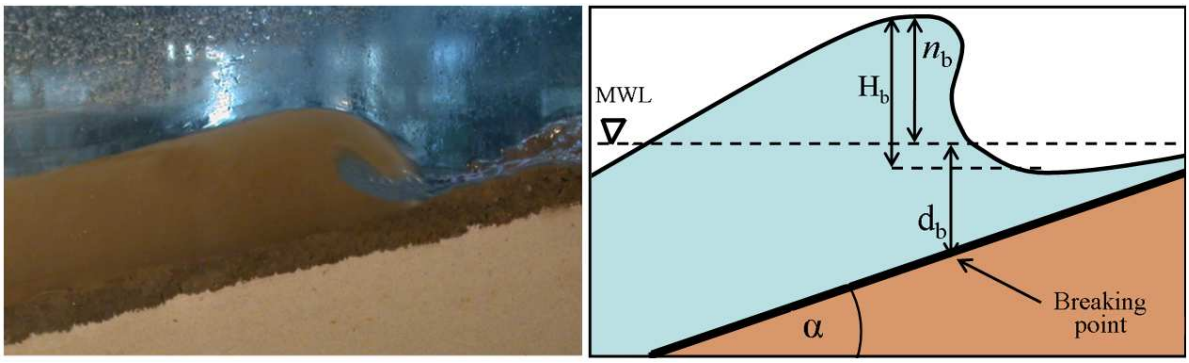

a) In the small LWI-flume b) principle sketch

Figure 3.3: Plunging breaker on a dike slope

The loading on the outer slope is defined by the following parameters:

1. **Maximal impact pressures** - since the maximum impact pressure represents a stochastic variable, the maximum impact pressure has to be defined more specifically. To indicate the maximum pressure that is not exceeded in i % of the cases, the notation $p_{max,i}$ is used. In practice $p_{max,99.9}$ is considered as the highest measured maximum impact pressure.

   In the preliminary model, for the calculation of the impact pressure induced by **plunging breakers** the approach proposed by Zhong (1985) is selected:

$$p_{max,i} = \kappa_i \cdot \rho_w \cdot g \cdot H \cdot \tan\alpha \tag{3.2}$$

   with:

   - g - acceleration due to gravity $[m/s^2]$
   - ρ_w - density of water $[kg/m^3]$

- κ_i - empirical parameter that depends on the deep water wave steepness $H/(gT^2/2\pi)$:

$$\kappa_{50} = -289 \cdot \frac{H}{g \cdot T_p^2} + 11.2 \tag{3.3}$$

and:

- $\kappa_{90} = 1.33 \cdot \kappa_{50}$
- $\kappa_{99} = 1.67 \cdot \kappa_{50}$
- $\kappa_{99.9} = 2.5 \cdot \kappa_{50}$

The decrease of the impact pressure on a flatter dike slope is the result of the damping effect of the water layer resulting from the run-down of the preceding wave. The thickness of this back-rush water layer increases with flatter slope so that the maximum pressures decreases proportionally. This was reported by Bölke and Relotius (1974) and Führböter et al (1976), who presented time series of impact pressures based on simultaneous measurements during a storm surge in 1973. The conclusion states that the number of waves generating impact pressures is much lower for a slope 1:6 than for a slope 1:4.

2. **Location of the impact on the dike slope** - is calculated as a function of the surf similarity parameter ξ using the following formula proposed by Schüttrumpf and Oumeraci (2005):

$$\frac{Z_{impact}}{H_s} = h_{MWL} - 0.8 + 0.6 \cdot tanh(\xi - 2.1) \tag{3.4}$$

where Z_{impact} is defined in Fig. 3.4

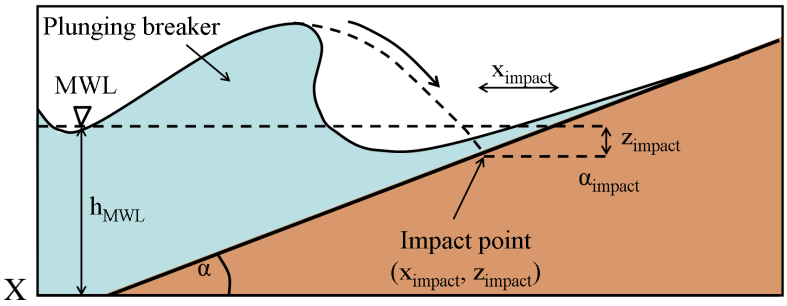

Figure 3.4: Location of the impact on a slope - definition sketch

This empirical formula is associated with a satisfying degree of uncertainty ($\sigma' = 20\%$) and can be applied for both regular waves and irregular waves.

3. **Distribution of the impact pressures on the slope** - For the preliminary model the following formula for the impact pressure on an i-th point with given coordinates x_i and z_i is used (after Stive, 1983) :

$$p_i = \left[-\frac{2.75}{H^2} \cdot \left((z_i - z_{impact})^2 + (x_i - x_{impact})^2 \right) + 1 \right] \cdot p_{max} \tag{3.5}$$

with:

- x_i and z_i - coordinates of the i-th point

- x_{impact} and z_{impact} - coordinates of the impact point calculated as (see Fig.3.5):
  - $z_{impact} = MWL - Z_{impact}$
  - $x_{impact} = z_{impact}/tan\alpha$

Eq. 3.5 provides a negative impact pressure for the distance d_i between the i-th point and the point of impact larger than the maximal distance d_{max} (Fig. 3.5):

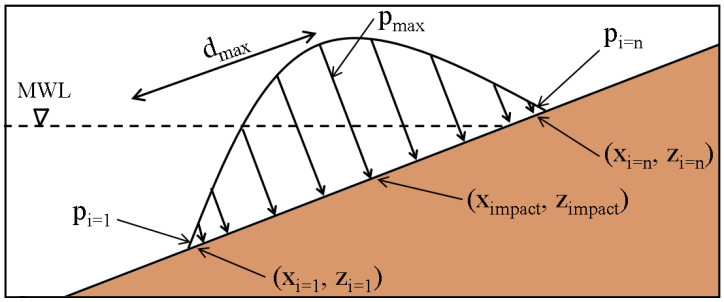

Figure 3.5: Impact pressure distribution on the dike slope

To avoid this problem, the following limits for the applicability of Eq.3.5 are introduced (Fig. 3.5):

$$\begin{aligned} d_i &= d_i \quad \text{for} \quad |d_i| < d_{max} \\ d_i &= 0 \quad \text{for} \quad |d_i| \geq d_{max} \end{aligned} \tag{3.6}$$

with d_{max} calculated as:

$$d_{max} = \frac{H}{\sqrt{2.75}} \tag{3.7}$$

Eqs. 3.5 - 3.7 were derived based on the results of large-scale tests reported by Stive (1983). This approach is however strongly simplified and gives a deterministic description of the spatial distribution of the impact pressures.

4. **Incidence angle of plunging wave impact** - the angle of incidence of the breaking wave plunging on the dike slope (Fig. 3.6) is calculated using the approach proposed by Führböter (1966). This theoretical formula yields the angle α_{impact} as a function of the seaward slope angle α and reads:

$$\alpha_{impact} = atan\left(\frac{1 + \cot\alpha \cdot f(\alpha)}{\cot\alpha - f(\alpha)}\right) \tag{3.8}$$

with:

$$f(\alpha) = \frac{\sqrt{1 + 2\cot^2\alpha} - 1}{\cot\alpha} \tag{3.9}$$

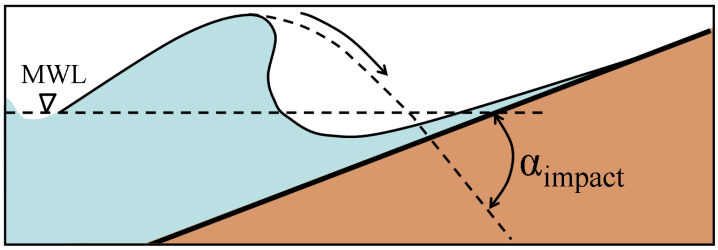

Figure 3.6: Incidence angle of plunging breaker on a dike slope (after Führböter, 1966)

3.3.2 Flow through the breach channel

After the erosion has reached the inner slope of the dike, the remained part of the dike starts to be also eroded due to overflow. The flow velocity and depth along the entire dike profile (see Fig. 3.7 for definitions) are calculated using the equations for steady, non-uniform free surface flows ($\partial v/\partial t = 0$ and $\partial v/\partial x \neq 0$) :

- Continuity equation:

$$Q = B \cdot h \cdot v = \text{const} \tag{3.10}$$

  where Q denotes the flow discharge $[m^3/s]$

- Total flow energy balance (Bernoulli equation):

$$H = z + h + \frac{v^2}{2g}; \qquad \frac{dH}{dx} = -J \tag{3.11}$$

  where H is the total hydraulic head and J its gradient in the flow direction.

The model calculates the discharge at the location of the highest node (x_{of}) either as a function of freeboard R_c for wave overtopping ($R_c > 0$) and combined wave overtopping and overflow ($R_c < 0$) or as a function of the overflow head (h_{of})

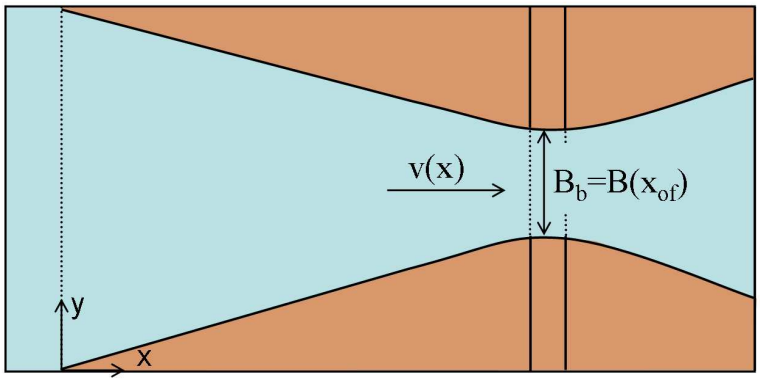

a) overflow - cross-section through the breach

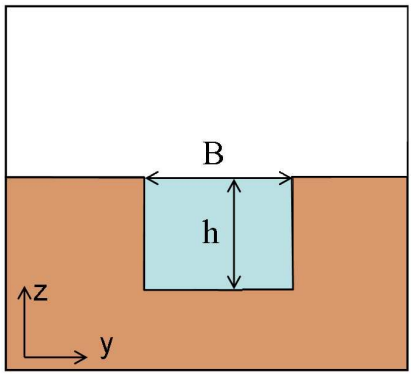

b) cross-section of breach at any location of the dike

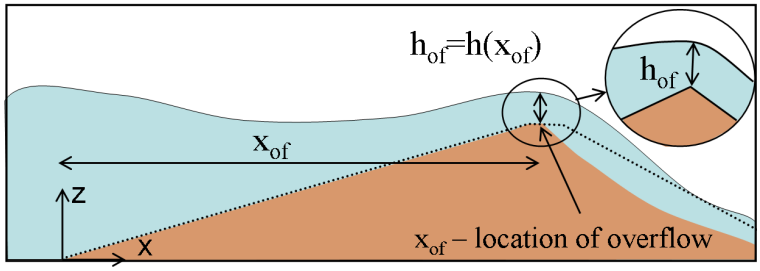

c) plan view of breach

h –flow depth [m]
B –breach width [m]
B_b–breach width at the overflow [m]
h_{of} – overflow head [m]
v – flow velocity [m/s]

Figure 3.7: Overflow - breach channel geometry

The flow depth and velocity are calculated for three loading cases:

a) wave overtopping, when $Rc > 0$, (Fig. 3.8a);

b) combined wave overtopping and overflow, when $h^* < Rc < 0$, (Fig. 3.8b);

c) overflow, after the full breach has been formed, i.e when $R_c = h^*$, (Fig. 3.8c).

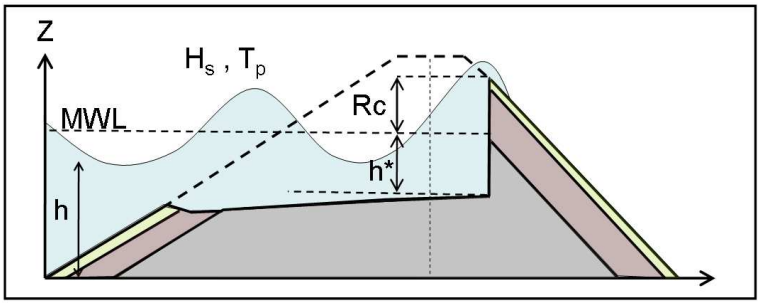

a) Wave overtopping ($Rc > 0$)

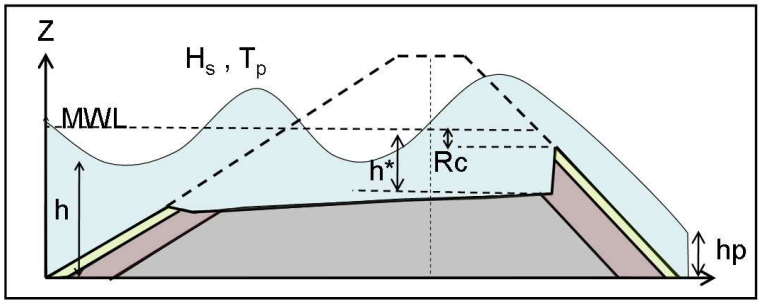

b) Combined wave overtopping and overflow ($h^* < Rc < 0$)

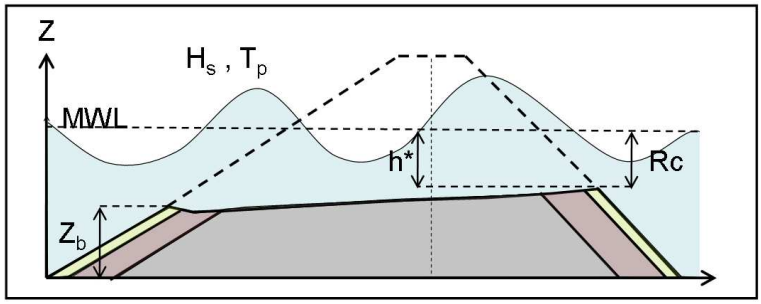

c) Overflow ($Rc = h^*$)

Figure 3.8: Flow through dike breach - loading cases

3.3.3 Wave overtopping

The model calculates the freeboard R_c as a difference between MWL and elevation of the highest point of the remaining part of the dike for every time step and applies the appropriate formula. The averaged volume of wave overtopping is calculated as proposed by Bleck et al. (2000):

$$q_{overtopping} = \frac{0.06}{\sqrt{\tan\alpha}} \cdot \xi \cdot exp^{(-4.7\frac{Rc}{H_s})} \cdot \sqrt{2gH_s^3} \tag{3.12}$$

3.3.4 Combined wave overtopping and overflow

Together with the progress of erosion in the x-direction the value of Rc decreases. After it reached zero, the overtopping becomes combined overtopping and overflow with the average volume of flow calculated as proposed by Bleck et al. (2000):

$$q_{overflow} = \frac{2}{3} \cdot 0.473 \cdot \xi \cdot \sqrt{2 \cdot g} \cdot \Big(Rc + \mu(t)\Big)^{1.5} \tag{3.13}$$

where:

- $\mu(t) = \frac{1}{2} \cdot H_s \cdot \sin \cdot \frac{2\pi}{T_p} \cdot t$

3.3.5 Overflow

The specific discharge ($m^3/s \cdot m$) through the breach without the effect of the backwater is calculated with the weir formula of Poleni (D'Eliso, 2007):

$$q = \frac{2}{3} \cdot \mu_{over} \cdot \sqrt{2 \cdot g} \cdot h_{of}^{1.5} \tag{3.14}$$

and with $Q = q \cdot B_b$

$$Q = \frac{2}{3} \cdot \mu_{over} \cdot \sqrt{2 \cdot g} \cdot h_{of}^{1.5} \cdot B_B \tag{3.15}$$

where:

- μ_{over} is the discharge coefficient for a broad-crest weir taking the value $\mu_{over} = 1.3/\sqrt{3} \approx 0.75$ (Visser, 1998)
- B_B is the width of the breach at the location of overflow head (Fig. 3.7)
- h_{of} - overflow head (Fig. 3.7)

The discharge through the breach by considering the effect of the backwater is calculated as (D'Eliso, 2007):

$$Q_{corr} = Q \cdot S_Q \tag{3.16}$$

where S_Q is the backwater level coefficient :

$$\begin{aligned} S_Q &= \left(1 - \left(\frac{h_p - Z_b}{h - Z_b}\right)^{1.5}\right)^{0.385} && h_p > Z_b \\ S_Q &= 1 && h_p < Z_b \end{aligned} \tag{3.17}$$

where:

- h_p - backwater level calculated as the function of discharge through the breach and the polder area (Fig. 3.8b)
- Z_b - elevation of the breach bottom at the breach entrance (Fig. 3.8c)

The flow velocity and depth are calculated with an explicit forward calculation (D'Eliso, 2007):

$$\frac{H_{i+1} - H_i}{dx_{i,i+1}} = -J_{i,i+1} \Rightarrow z_{i+1} + h_{i+1} + \frac{v_{i+1}^2}{2g} = z_i + h_i + (1 - \alpha_{ce}) \cdot \frac{v_i^2}{2g} - J_{i,i+1} dx_{i,i+1} \tag{3.18}$$

where:

- J - energy slope:

  $$J_{i,i+1} = \frac{J_i + J_{i+1}}{2} \tag{3.19}$$

  and using the Manning's formula:

  $$J = \frac{n^2 \cdot v^2}{R^{4/3}}; \quad n - \text{Manning coefficient} \tag{3.20}$$

  where R denotes the hydraulic radius

- α_{ce} - contraction-expansion coefficient for the breach

$$\alpha_{ce} = \left(1 - \frac{\Omega_{i+1}}{\Omega_i}\right) \cdot \frac{v_{i+1}^2}{2 \cdot g} \quad \text{for} \quad \Omega_{i+1} \leq \Omega_i \tag{3.21}$$

$$\alpha_{ce} = \left(1 - \frac{\Omega_i}{\Omega_{i+1}}\right) \cdot \frac{v_{i+1}^2}{2 \cdot g} \quad \text{for} \quad \Omega_{i+1} > \Omega_i \tag{3.22}$$

where Ω denotes the wetted cross-section

3.3.6 Additional simplifications and assumptions

Wave breaking is a very complex natural process, especially in the case of irregular waves. Some assumptions and simplifications are therefore necessary to simulate this process. The most important assumptions implied in the hydrodynamic module are as follows:

- a two-dimensional description (plane x-z) is adopted
- each wave is treated as a single event that is independent from the preceding wave,
- no influence of obliquely incident waves is taken into account - only normal wave incidence is considered,
- no calculation of the velocity fields of wave run-up and run-down is performed, since the morphodynamic module calculates the progress of erosion directly as a function of wave parameters, not as a function of flow depth and velocity.

3.4 Morphodynamic module

The main purpose of the morphodynamic module is the calculation of the breach profile evolution in time. The information on the loads provided by the hydrodynamic module (Section 3.3) is used as input data for the calculation of breach initiation, formation and development. The entire breaching process is divided into the following phases (Fig. 3.9) :

Phase 1: - erosion of grass cover, surface erosion of the cover directly subject to the repeated action of the breaking waves;

Phase 2: - discrete local erosion of the clay cover up to the exposure of the sand core to the breaking wave impacts;

Phase 3: - discrete erosion of the sand core, cliff formation and development of the horizontal bottom of the breach;

Phase 4 - continuous breach deepening and widening due to erosion during the overflow

The following general assumptions for the preliminary morphodynamic module are made:

- only the erosion of the seaward slope is calculated during Phases 1 and 2, the possible erosion of the inner slope resulting from the wave overtopping is neglected,

- during Phases 1 and 2 the shape of the scour hole is calculated as a function of the pressure distribution on the slope (Fig. 3.5). In Phase 3 the horizontal breach bottom and vertical cliff are assumed. In Phase 4 the breach profile is calculated according to the sediment transport model applied for the rectangular channel cross-section (Fig. 3.7)
- no change in the material properties due to mixing of clay and sand occurs, the properties of sand are considered to be constant during the entire breaching process,
- during Phases 1, 2 and 3 the simulation is performed in two-dimensional plane x-z. In Phase 4 the simulation becomes 2D+2D (x-z and x-y planes). The initial conditions for the simulation in x-y plane are assumed based on the observations of historical dike failures (see Section 3.4.4.1 for more details),

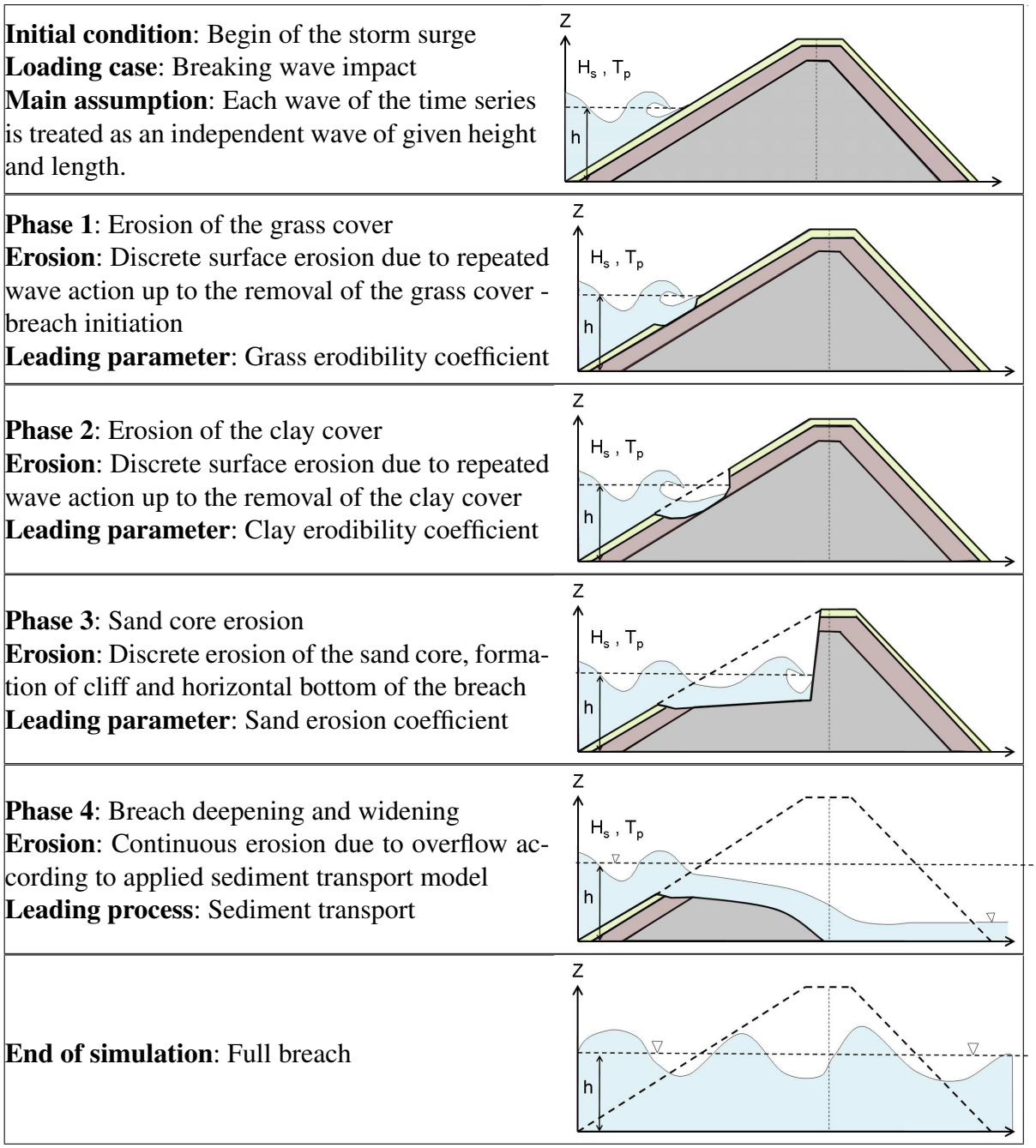

Figure 3.9: Phases of dike breach simulation

3.4.1 Erosion of the grass cover

The grass erosion module is based on the wave impact approach which assumes the total erosion depth to be the sum of the erosion caused by every single wave impact (Larson et al, 2004). The depth of the soil eroded after a single breaking wave impact is calculated based on an empirical relationship (Eq. 3.23) of the depth of erosion after a given time period and the significant height of the waves attacking a dike during this period. The erodibility coefficients that are needed for the grass erosion simulation are calibrated using the information on the tests with the grass cover performed by Smith et al. (1994) in the Delta Flume (Fig. 3.10).

Figure 3.10: Laboratory tests on the erosion resistance of the grass cover (Smith et al, 1994)

The maximal depth of erosion $d_{g,max}$ after a single breaking wave impact is then calculated as a function of a wave height H_s, period T_p and erodibility coefficient for the grass cover $E_{g,max}$:

$$d_{g,max} = T_p \cdot H_s^2 \cdot E_{g,max,\alpha} \tag{3.23}$$

with:

- $d_{g,max}$ - maximal depth of erosion for a single impact of breaking wave [m]
- $E_{g,max,\alpha} = E_{g,max} \cdot \tan\alpha$ - grass erosion coefficient [$\mathrm{m}^{-1}s^{-1}$]

As Eq. 3.23 provides information only on the maximal erosion depth , the shape of the scour hole is calculated based on the proportionality relationship:

$$\frac{d_{g,max}}{p_{max}} = \frac{d_{g,i}}{p_i} \tag{3.24}$$

with

- $d_{g,i}$ - depth of erosion at the i-th point,
- p_i - pressure at the i-th point (Eq. 3.5 and Fig. 3.5)

The total erosion depth is than calculated as a sum of erosion due to each single impact:

$$d_{g,tot,n} = \sum_{1}^{i=n} d_{g,max,i} \tag{3.25}$$

The grass is assumed to fail as soon as the total erosion depth $d_{g,tot,n}$ has reached the critical erosion depth $d_{g,crit}$ expressed in terms of grass root percentage (see Section 4.3.3 for more details on the critical erosion depth)

3.4.2 Erosion of the clay cover

Immediately after the grass revetment is removed, the **clay cover erosion** begins. The following formula for the maximal depth of the clay cover erosion subject to a single breaking wave impact is used:

$$d_{c,max} = T_p \cdot H_s^2 \cdot E_{c,max,\alpha} \tag{3.26}$$

with

- $d_{c,max}$ - maximal depth of clay erosion for a single impact of breaking wave [m]
- $E_{c,max,\alpha} = E_{c,max} \cdot \tan\alpha$ - clay erodibility coefficient [m^{-1}]

Eq. 3.26 forms the basis of the clay erosion module. It is derived combining the assumptions implied in the PC-Ring model (INFRAM, 1999) with the wave-impact approach (Larson et al, 2004). The clay erosion coefficient $E_{c,max}$ is calibrated using the available information from other erosion models (INFRAM, 1999) and may vary from $E_{c,max} = 1.4 \cdot 10^{-4}[m^{-1} \cdot s^{-1}]$ for the clay of weak quality to $E_{c,max} = 1.2 \cdot 10^{-5}[m^{-1} \cdot s^{-1}]$ for the clay of good quality. However, these values are subject to large variations as the clay cover is a very inhomogeneous material. Identically as in the case of the grass erosion module (Sec. 3.4.1), the linear dependency of the erosion depth in i-th point on the impact pressure in the i-th point is assumed (Eq. 3.24). For every time step, the condition for the phase end (and therefore also the clay cover removal) is controlled. It is assumed that the clay cover is removed when the erosion depth has reached a critical depth of erosion $d_{c,crit}$ which is equal to the thickness of the clay cover.
The most important simplifications and assumptions that are made in the clay erosion module can be summarised as follows:

- although the variability of the erodibility coefficient for the clay cover used in the model is the result of the laboratory experiments, no cracks along the dike profile are considered. In fact, clay cover contains a large number of cracks that may lead to additional damage when subject to impact pressure. However, due to lack of experimental verification of the available conceptual models that describe the process of shear failure in crack, this simulation of this phenomenon will be first included in the detailed model, after a series of clarifying laboratory experiments will be performed;
- no interaction between the materials is considered, i.e. the clay is assumed to be homogenous during the entire clay erosion phase;
- the erosion is simulated with no separation between the erosion due to the impact pressures and the erosion due to flow associated with wave run-up and run down since this is the main assumption of the clay erosion model selected for the application;
- after the local removal of the clay cover the entire revetment is assumed to be removed and the dike core becomes unprotected.

3.4.3 Front-face erosion of the sand core

After the removal of the entire revetment, i.e. grass and clay layers, the sand core of the dike becomes unprotected and the last phase of the simulation - sand core erosion - begins. Due to variable flow conditions, the entire erosion of sand core consists of two phases: (i) erosion of the front face due to repeated action of breaking waves (this Section) and (ii) breach deepening and widening after the erosion has reached the inner slope and overflow occurred (Section 3.4.4). The simulation of erosion during the front-face erosion of sand core is performed based on the wave impact theory and the information on the erosion of sand dunes (Larson et al, 2004). The applied approach estimates the sediment transport from the sand core (Q_{single}) and associated progress of erosion in the direction of waves (x_{single}) for each single wave that hits the sand core (see Fig. 3.11) as a function of impact force F_{impact}. The total erosion rate is then calculated as a sum of the erosion rate resulting from each single wave impact.

The governing equation for this phase reads (Larson et al., 2004):

$$Q_{single} = C_E \cdot F_{impact} \tag{3.27}$$

with:

- Q_{single} - erosion rate of the sand core induced by a single wave impact [m^3];
- F_{impact} - impact force calculated as a function of impact pressure and impact area [kN] (Section 3.3.1)
- C_e - sand erodibility coefficient [m^3/kN]

$$C_E = \frac{2 \cdot C_S \cdot C_U \cdot \rho_s^2 \cdot (1-p)^2}{\rho_w}$$

with:

$$C_S = A_s \cdot e^{-b\frac{H}{D_{50}}}$$

where:

- p - soil porosity [-]
- A_s - non-dimensional empirical coefficient equal $A_s = 1.34 \cdot 10^{-3}$
- b - non-dimensional empirical coefficient equal $b = 3.19 \cdot 10^{-4}$
- C_U - non-dimensional empirical coefficient equal $C_U = 1.83$

The progress of erosion in the direction of waves in the i-th time step is calculated as a function of the eroded volume and height of the cliff as:

$$x_{single,i} = \frac{Q_{single,i}}{z_{single,i}} \tag{3.28}$$

with:

- $z_{single,i} = z_{max,i} - z_i$ - height of the vertical cliff

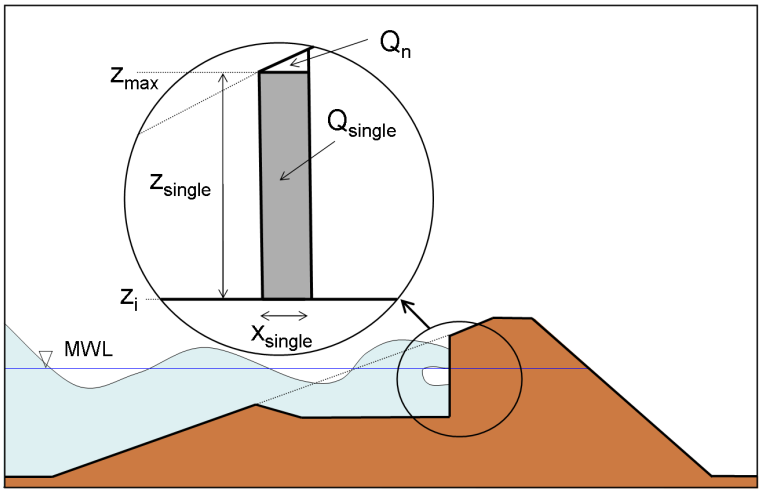

Figure 3.11: Wave impact approach for the sand core

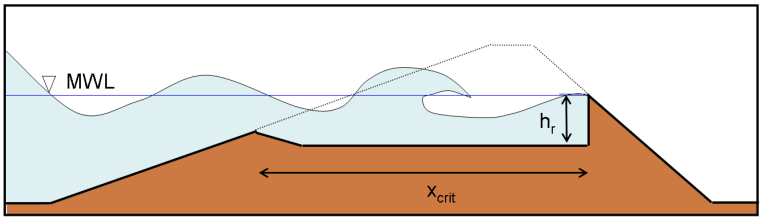

Figure 3.12: Definition of the end of Phase 3 (front-face erosion of the sand core)

The total progress of the erosion of the sand core in the x-direction is the sum of the erosion induced by every impact:

$$x_{total,n} = \sum_{1}^{n} x_{single,i} \tag{3.29}$$

The phase ends when the progress of erosion x_{total} reaches the critical value x_{crit} (Fig. 3.12) The shape of the breach is not calculated as during the grass and clay erosion phases, but assumed based on the available literature (Laustrup et al, 1990). The bottom of the breach is horizontal, while the front wall is assumed to be vertical. No scheme for distributing the eroded sediment on the foreshore is applied. It is only assumed that the eroded soil is transported offshore by the wave action immediately after the erosion and the deposited sediment has no influence on the wave breaking.

The following simplifications were already included in the adopted models or were assumed during the development of the preliminary dike breaching model:

- the mass failure is not simulated directly, but implicitly included in the empirical coefficients of Eq. 3.27
- the shape of the breach is not calculated but assumed based on the model of Lautstrup et al (1990) - see Fig. 3.8;
- the material of the sand core is assumed to be homogenous, no mixing of materials and no interaction with clay is accounted for.

3.4.4 Breach deepening and widening

After the erosion has reached the inner slope and overflow occurred, the last phase of the simulation, i.e. breach channel widening and deepening, starts. For the calculation of the changes in the breach channel shape two approach were selected: (i) the one-dimensional Exner equation (D'Eliso, 2007) and, alternatively (ii) the volume-averaged approach (Tuan, 2007).

3.4.4.1 Introduction of the third dimension

The erosion of the grass and clay cover as well as the front face erosion of the sand core are simulated as 2D processes in the $x - z$ plane. However, in order to calculate the breach widening and deepening it is necessary to introduce the third dimension (y-dimension).

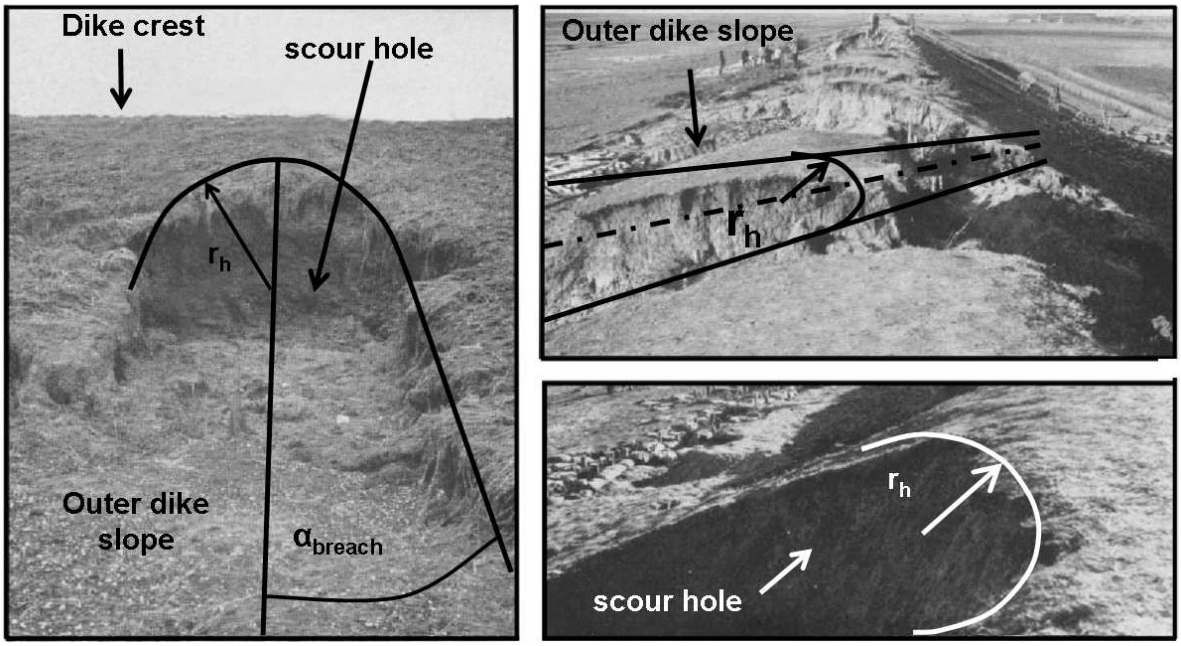

Figure 3.13: Shape of the partial breach at the outer slope of sea dikes

Based on the reported damages of the sea-dikes (Landesamt für Wasserwirtschaft - Schleswig-Holstein,1962; Zitscher,1962; Wohlenberg,1963; Stephan,1981) and available pictures (examples in Fig. 3.13) taken after the flood events, the shape of the scour hole in the $x - y$ plane (Fig 3.14) is assumed.

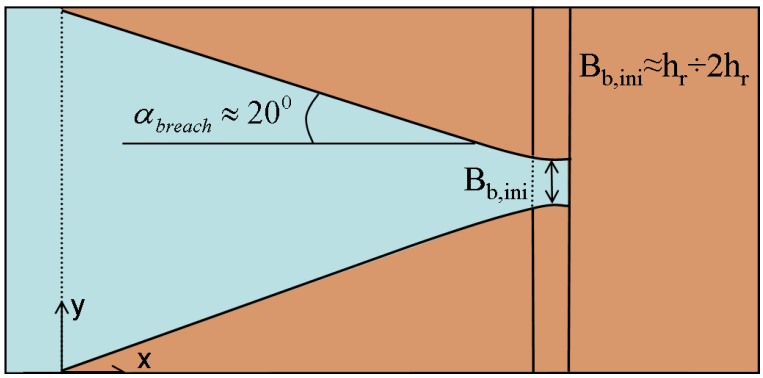

Figure 3.14: Initial conditions for the 3D modeling - $y - z$ plane

According to those reports the width of the initial breach $B_{B,ini}$ (Fig. 3.14) is usually in the range $B_{B,ini} = h_r$ to $B_{B,ini} = 2h_r$ where h_r denotes the height of the initial breach (see Fig. 3.12). During the progress of the erosion, the side walls of the breach are not formed parallel but the breach remains wider at the seaside. The angle between side walls and x-axis α_{breach} can be roughly estimated to be equal $\alpha_{breach} = 20^0$.

3.4.4.2 Energetic approach

Two sediment transport models based on the energetic approach were selected: (i) Bagnold-Visser sediment transport formula (Visser, 1998) and (ii) Bagnold-Bailard formula (Bailard, 1981). Both formulae were already used for the simulation of dike breaching under overflow conditions (D'Eliso, 2007). One of the following sediment transport models can be freely selected by the user. Generally, the two models are similar, but the Bagnold-Visser model is suggested for use, as it was reported that the Bagnold-Bailard model can provide too high erosion rate (D'Eliso, 2007).

1. Bagnold-Visser sediment transport formula:

   The volumetric bed load transport q_{sb} $[m^3/s \cdot m]$ is calculated as:

   $$q_{sb} = \frac{\tau_0 \cdot v}{\rho_w \cdot g \cdot \Delta} \cdot \frac{e_b}{\tan\phi - \tan\beta \cdot \cos\beta} \tag{3.30}$$

   $$q_{sb} \leq \zeta_2 \cdot (1-p) \cdot D_{50} \cdot v; \qquad \zeta_2 \approx 2 \tag{3.31}$$

   with:

   - Δ - relative density of soil particles $\Delta = (\rho_s/\rho_w) - 1$
   - e_b - bed-load efficiency coefficient, $e_b = 0.13$
   - ϕ - internal friction angle $[deg]$
   - τ_0 - bed shear stress (see Eq. 3.36)
   - β - angle of dike inner slope [^{0}]
   - p - soil porosity
   - D_{50} - mean sand size $[mm]$
   - ρ_w - water density $[kg/m^3]$

   The volumetric suspended sediment transport q_{ss} $[m^3/m \cdot s]$:

   $$q_{ss} = \frac{\tau_0 \cdot v}{\rho_w \cdot g \cdot \Delta} \cdot \frac{e_s}{w_s/v(\cos\beta)^2} \tag{3.32}$$

   with:

   - e_s - suspended load efficiency coefficient, $e_s = 0.01$
   - w_s - settling velocity $[m/s]$

The total volumetric sediment transport Q_{st} $[m^3/s]$:

$$Q_{st} = P \cdot (q_{sb} + q_{ss}) \tag{3.33}$$

with:

- P - wet perimeter of the breach channel $[m]$

2. Bagnold-Bailard formula:

   the volumetric bed-load sediment transport q_{sb} $[m^3/m \cdot s]$ is calculated as:

$$q_{sb} = \frac{\tau_0 \cdot v}{\rho_w \cdot g \cdot \Delta} \cdot \frac{e_b}{\tan\phi - \tan\beta} \tag{3.34}$$

   while the volumetric suspended sediment transport $q_s s$ $[m^3/m \cdot s]$ is calculated as:

$$q_{ss} = \frac{\tau_0 \cdot v}{\rho_w \cdot g \cdot \Delta} \cdot \frac{e_s}{w_s/v\cos\beta} \tag{3.35}$$

The bottom shear stress τ_0 is a function of the flow characteristics and surface roughness calculated as:

$$\tau_0 = g \cdot \rho_w \cdot h \cdot J \tag{3.36}$$

The energy slope J can be calculated by selecting one of the two following formulae which are implemented in the model:

1. Manning formula:

$$J = \frac{n^2 \cdot v^2}{R^{4/3}} \tag{3.37}$$

2. Chezy formula

$$J = \frac{v^2 \cdot C_f}{g \cdot R} \tag{3.38}$$

   with:

   - C_f - Chezy's friction coefficient calculated as :

$$C_f = \frac{0.4}{[\ln(12R/z_0)]^2}$$

   - z_0 - roughness height calculated as:

$$z_0 = 3 \cdot \theta \cdot D_{90} \tag{3.39}$$

The Shields parameter θ is calculated as:

$$\begin{aligned} \theta &= \frac{C_f \cdot v^2}{\Delta \cdot g \cdot D_{50}} \quad \text{for} \quad \theta \geq 1 \\ \theta &= 1 \quad \text{for} \quad \theta < 1 \end{aligned} \tag{3.40}$$

The roughness height describes the influence of the high concentration of the sediments near the breach bottom as the viscosity of the water-sediment mixture is significantly larger that

the viscosity of water (D'Eliso, 2007). When θ is greater than one, the friction coefficient C_f is calculated iteratively.

The sediment fall velocity w_s can be calculated by using one of the following approaches, which can be freely chosen by the user. The formula of van Rijn (1993) was already implemented in available models of dike breaching due to overflow. The formula of Ahrens (2000) is suggested for use, as it is much simpler and derived explicitly for coastal areas.

1. Van Rijn formula (Van Rijn, 1993):

$$\begin{aligned} w_s &= \frac{\Delta \cdot g \cdot (D_{50})^2}{18 \cdot v} && \text{for} \quad 0.001 \leq D_{50} \leq 0.1 \\ w_s &= \frac{10 \cdot \nu}{D_{50}} \Big((1 + 0.01 \cdot \Delta \cdot g (D_{50})^3 \cdot \nu^{-2})^{0.5} - 1 \Big) && \text{for} \quad 0.1 \leq D_{50} \leq 1 \\ w_s &= 1.1 (\Delta \cdot g \cdot D_{50})^{0.5} && \text{for} \quad D_{50} > 1 \end{aligned} \tag{3.41}$$

   Where the kinematic viscosity of water ν $[m^2/s]$ depends on the water temperature $T_w[^0C]$ and is calculated as (NBS,1975):

$$\nu = \frac{\rho_w + 1505}{2500 \cdot \rho_w} \cdot 10^{(\frac{13}{10 - 0.081(20 - T_w)} - 4.3)} \quad \text{for} \quad 0 < T < 20 \tag{3.42}$$

$$\nu = \frac{\rho_w + 1505}{2500 \cdot \rho_w} \cdot 10^{(\frac{1.33 \cdot (20 - T_w)}{T + 104} - 3)} \quad \text{for} \quad 20 < T < 40$$

2. Ahrens formula (Ahrens, 2000)

$$w_s = C_1 \cdot \frac{\Delta \cdot g \cdot D_{50}^2}{\nu} + C_2 \sqrt{\Delta \cdot g \cdot D_{50}} \tag{3.43}$$

   with:

   - $C_1 = 0.055 \cdot \tanh(12 \cdot A_h^{-0.59} \exp(-0.0004 \cdot A_h))$
   - $C_2 = 1.06 \cdot \tanh(0.016 A_h \cdot A_h^{-0.50} \exp(-120/A_h))$
   - $A_h = \frac{\Delta \cdot g \cdot D_{50}^3}{\nu^2}$

   The kinematic viscosity of water $\nu[m^2/s]$ is calculated as a function of water temperature $T_w[^0C]$

$$\nu = 10^{-4}(0.0000069 \cdot T_w^2 - 0.000529 \cdot T_w + 0.0182) \tag{3.44}$$

The breach growth can be then calculated by the following, one-dimensional Exner equation (D'Eliso, 2007):

$$\frac{dQ_{st}}{dx} + (1 - p)\frac{dA}{dt} = 0 \tag{3.45}$$

where

- A - breach cross-section
- p - porosity of the soil

Eq. (3.45) is solved using the following finite difference scheme (D'Eliso, 2007) :

$$\frac{1}{2}\cdot\left(\frac{Q_{st,i+1}-Q_{st,i}}{\Delta x_{i+1,i}}+\frac{Q_{st,i}-Q_{st,i-1}}{\Delta x_{i,i-1}}\right)+(1-p)\cdot\frac{A_{t-1}-A_t}{\Delta t}=0 \tag{3.46}$$

$$A_{t-1}=A_t-\frac{\Delta t}{2\cdot(1-p)}\cdot\left(\frac{Q_{st,i+1}-Q_{st,i}}{\Delta x_{i+1,i}}+\frac{Q_{st,i}-Q_{st,i-1}}{\Delta x_{i,i-1}}\right) \tag{3.47}$$

where:

- $Q_{st,i}$ - total sediment transport rate for the i-th Section
- A_i - breach cross-section for the i-th Section
- Δx_i - grid space for the i-th Section
- Δt - time step

At the first and the last section of the dike the following equations are applied (D'Eliso, 2007)

$$A_{1,t+1} = A_{1,t}-\frac{\Delta t}{1-p}\cdot\left(\frac{Q_{st,2}-Q_{st,1}}{\Delta x_{2,1}}\right) \tag{3.48}$$

$$A_{N,t+1} = A_{N,t}-\frac{\Delta t}{1-p}\cdot\left(\frac{Q_{st,N}-Q_{st,N-1}}{\Delta x_{N,N-1}}\right) \tag{3.49}$$

Sections 1, i and N are defined as in Fig. 3.15.

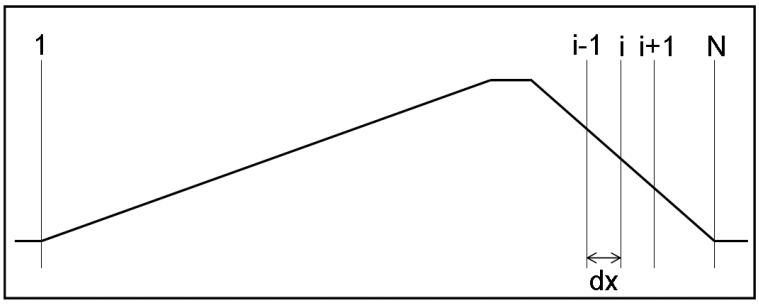

Figure 3.15: Finite difference scheme

The calculation of the change in the breach profile is then performed assuming that the breach channel is rectangular and the ratio between lateral (d_b) and vertical (d_z) erosion (Fig.3.16) $c_{db/dz,b}$ is given. The following equation for the calculation of the vertical erosion is introduced (D'Eliso, 2007):

$$dz=\frac{-B_b+\sqrt{B_b^2+8c_{db/dz,b}dA}}{4c_{db/dz,b}} \tag{3.50}$$

the lateral erosion is then calculated as:

$$db=dz\cdot c_{db/dz,b} \tag{3.51}$$

More details and derivations can be found in the original publication (D'Eliso, 2007)

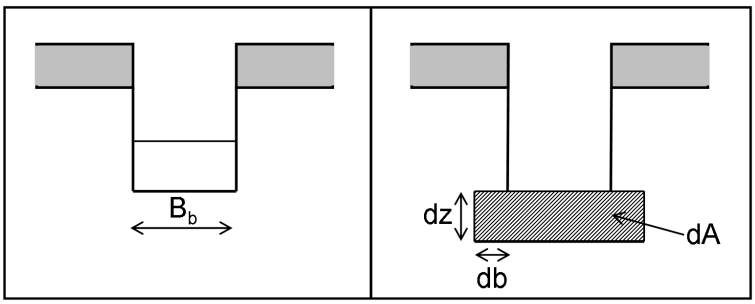

Figure 3.16: Breach channel evolution (modified from D'Eliso, 2007)

3.4.4.3 Volume averaged approach

Alternatively to the Bagnold-Visser/Bagnold-Bailard formulae combined with the 1D-Exner equation, a recent, volume-averaged approach (Tuan, 2007) may used. This approach was originally developed for the breaching of coastal barriers and is based on the power-law sediment transport model (Nielsen, 1992) and on the application of the empirical breach growth coefficient Kvl which describes the relationship between lateral and vertical breach growth.

In this approach the total transport rate q_s $[m^3/s \cdot m]$ is calculated as (Tuan, 2007):

$$q_s = M(\tau_b - \tau_{b,cr})^{n_t} \tag{3.52}$$

with:

- n_t - dimensionless transport exponent, of the order of 1.5
- M - transport coefficient $[m^4/N]$, of the order of $1 \cdot 10^{-7}$
- τ_b - bed shear stress, here calculated as:

$$\tau_b = \rho \cdot g \cdot h \cdot I \approx \rho \cdot g \cdot h \cdot \tan\beta \tag{3.53}$$

- $\tau_{b,cr}$ - critical bed shear stress, given as:

$$\tau_{b,cr} = \theta_{cr} \cdot \rho \cdot g \cdot \Delta \cdot d_{50} \tag{3.54}$$

- θ_{cr} - critical Shields parameter $[-]$

The rate of lateral channel growth is then calculated as a function of the **volume averaged channel width $\mathbf{B_v}$** (Tuan, 2007):

$$B_v = \frac{\int_{Lb} B_{hc} \cdot h_c dx}{\int_{Lb} h_c dx} = \frac{V_c}{\int_{Lb} h_c dx} \tag{3.55}$$

where:

- V_c - channel volume $[m^3]$ (see Fig. 3.17 for the notation)
- B_{hc} - depth-averaged width over the channel depth $[m]$

$$B_{hc} = b + \frac{h_c}{tan\gamma} \tag{3.56}$$

where b denotes the width at the channel bottom, h_c channel depth and γ the side slope, which is usually equal the internal friction angle of the sand

- B_h - depth-averaged width over the water depth $[m]$:

$$B_h = b + \frac{h}{tan\gamma} \tag{3.57}$$

- L_B - breach channel length $[m]$

The increase of the volume-averaged channel width B_v is given as (Tuan, 2007):

$$(h_L + K_{vl}B_v) \cdot \frac{\partial B_v}{\partial t} = \left(\frac{\partial A}{\partial t}\right)_{L_B} \tag{3.58}$$

where:

- h_L - averaged channel depth $[m]$ given as:

$$h_L = \frac{1}{L_B}\int_L h_c dx \tag{3.59}$$

- K_{vl} - non-dimensional channel growth index which defines the relationship between lateral and vertical channel growth. The values obtained from the laboratory experiments are in the range $K_{vl} = 0.02$ to $K_{vl} = 0.2$ for overwash. For overflow rather the smaller values should be used

- A - breach cross-section $[m^2]$

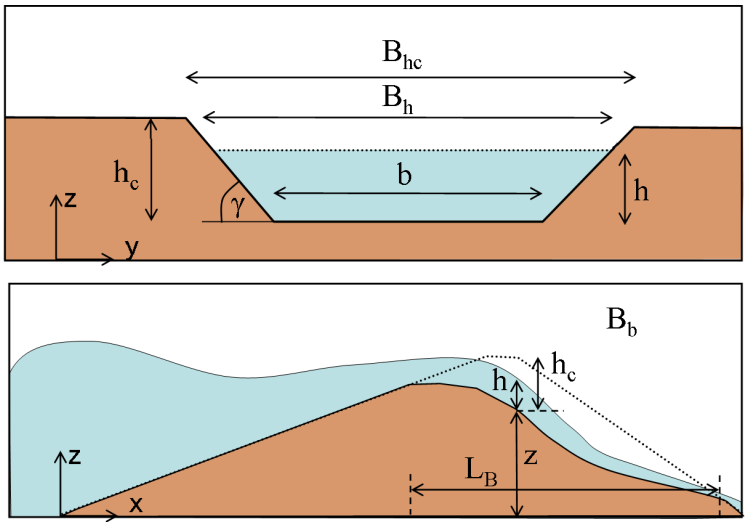

Figure 3.17: Definition sketch for the volume-averaged approach (modified from Tuan, 2007)

Consequently, the updated channel width B_v is calculated as (Tuan, 2007):

$$B_v(t+1) = B_v(t) + \frac{\Delta t}{(1-p)} \cdot \frac{B_v(t)}{h_L(t) + K_{vl}(t)B_v(t)} \cdot \frac{q_s^*(t)}{L_B(t)} \tag{3.60}$$

where $q_s^* = (q_{s,LB} - q_{s,0})$ denotes the net transport rate over the channel. The updated channel widths can be now calculated as:

$$B_{hc} = B_v - \frac{1}{tan\gamma} \cdot h_L - h_c \tag{3.61}$$

$$B_h = B_v - \frac{1}{tan\gamma} \cdot h_L - h \tag{3.62}$$

The bed level is then calculated according to the following relationship:

$$-\frac{\partial}{\partial t}(B_{hc} \cdot h_c) + \frac{1}{(1-p)} \cdot \frac{\partial(q_s \cdot B_{hc})}{\partial x} = 0 \tag{3.63}$$

It has to be however emphasised, that although this approach provides fast and relatively good results, the values of the channel growth index K_{vl} which is the most crucial parameter of the calculation were obtained from only one series of laboratory experiments. Therefore, this approach should be used with caution and further laboratory tests on this topic are recommended

3.4.4.4 Further simplifications and assumptions

For the dike core wash-out simulation the following assumptions are imposed:

- the initial breach shape for the sand wash-out in the $x - y$ plane is assumed based on the available information on the historical dike breaches
- in the energetic approach, the shape of the cross-section breach channel is assumed to be rectangular (See Fig. 3.7b)
- the erosion is assumed to be continuous, no mass failure is simulated
- the breach growth index Kvl is constant during the entire simulation

3.4.5 Limitations of the mathematical formulation

The preliminary model is subject to a number of limitations. The most important can be summarised as follows:

- no water infiltration into the dike is simulated, therefore the possible changes in the erosion resistance of soil that occur due to variations in water content are not accounted for;
- the erosion processes and breach initiation are oversimplified, no shear failure in cracks is simulated, which can result in the overestimation of the dike strength and consequently of the clay cover failure time;
- the simulated erosion of grass cover is not progressive but linear. In fact the erosion resistance of the grass decreases together with the increase of depth which results in the different course of the erosion progress. However, since erosion resistance applied in the model represents the mean erosion resistance, this simplification has no significant influence on the overall results ;
- no separation between erosion due to impact pressures and due to flow is made, since the selected erosion models are based on the dependency of erosion progress on the wave parameters, not on the flow properties. This simplifications might lead to unreliable calculation of the shape of the scour hole and consequently to unreliable prediction of the boundary conditions for the successive phases;

- the shape of the breach is calculated only during grass and clay erosion as well as during overflow. During front face erosion of the sand core the shape of the scour hole is assumed, not calculated, which can lead to unrealistic assumptions of the boundary conditions for the simulation of overflow;
- the applied sediment transport models are not strictly valid under breaching conditions, which can result in unreliable prediction of the breach widening and deepening;
- during overflow no slope stability is calculated, it is assumed that soil from the eventually collapsed walls is instantaneously transported from the site. Therefore, the possible decrease of the erosion rate which results from the decrease of the flow velocity caused by the collapsed soil blocks, is neglected.
- non-erodible dike base is assumed (stable foundation)

3.5 Model implementation

The preliminary model is entirely coded in MatLab v7.0, the flow chart of the model is given in Figure 3.18, while the sets of equations that are implemented are given in Tab. 3.2. During each phase, the hydrodynamic and morphodynamic modules are applied iteratively until the conditions for the end of the phase are fulfilled.

	Phase	Model (Equation)	Reference
Loading cases	Wave impact on the slope	Eqs. 3.1 - 3.9	Führböter (1966) Schüttrumpf (2001) Stive (1984)
	Overflow	Eqs. 3.14 - 3.44	D'Eliso (2007)
Breaching phases	Grass erosion	Eqs. 3.23 - 3.24	Smith et al (1994)
	Clay erosion	Eqs. 3.26 and 3.24	INFRAM (1999)
	Core erosion (front face)	Eqs. 3.27 - 3.29	Larson et al (2004)
	Core erosion (overflow)	Eqs. 3.45 - 3.51 Eqs.3.52 - 3.63	D'Eliso (2007) Tuan(2007)

Table 3.2: Summary of the models implemented in the preliminary model - c.f Fig.2.9

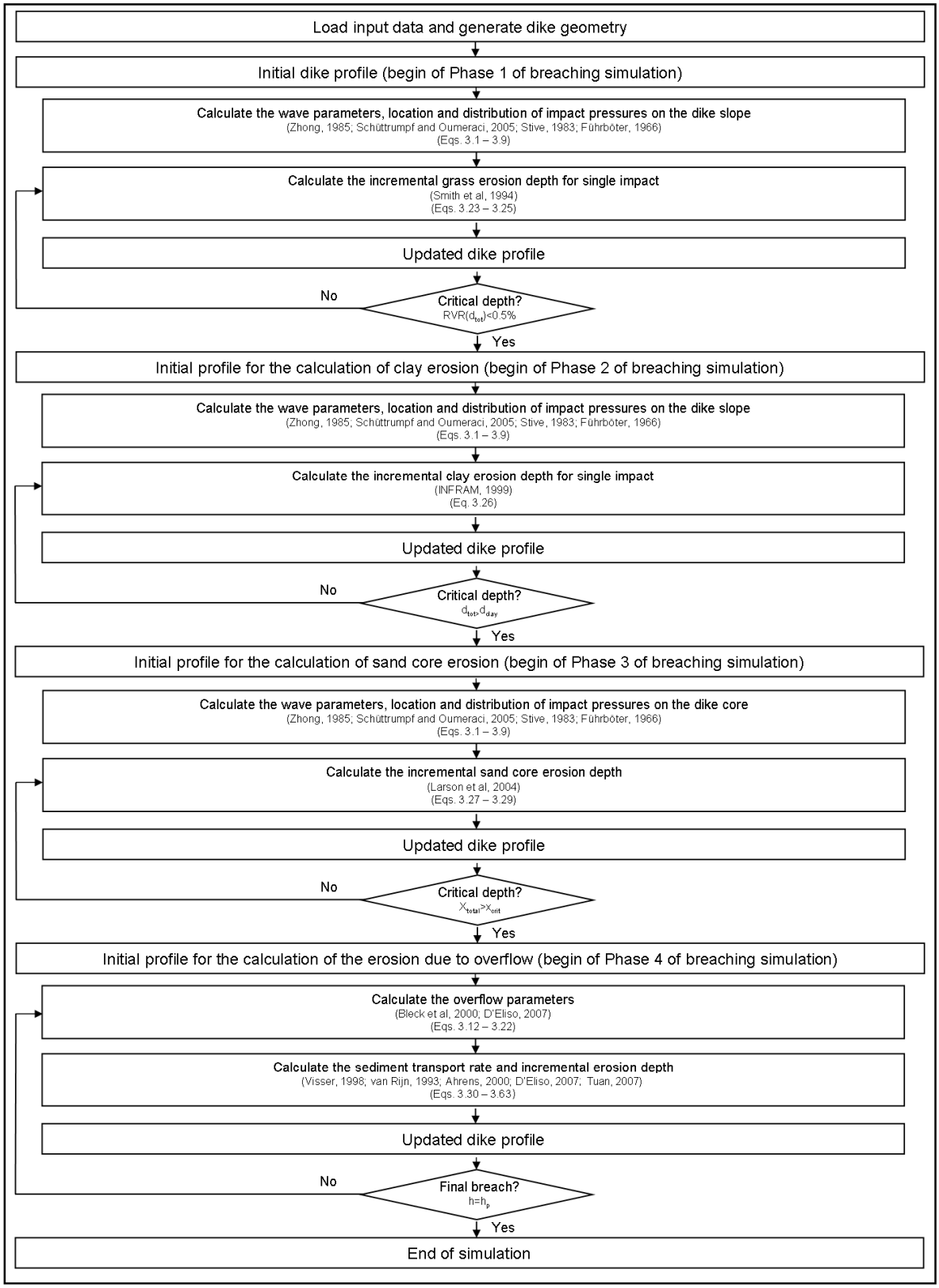

Figure 3.18: Flow chart of the preliminary model

3.5.1 Computational aspects, results and discussion

After the input data are loaded, the dike geometry is generated. Three regions: **seaside**, **crest** and **landside** are defined, and the computational nodes are located along the dike profile ac-

cording to the given grid size. The grid size (Δx) is given as input and although there are no limitations due to numerical stability, it is recommended to restrict the maximal Δx to 0.2m as the breaking wave impacts act locally and on very limited area. The time step Δt during grass, clay and front-face core erosion is equal to the period of individual wave. Therefore, the time step is constant if regular waves are assumed, while it varies for irregular waves. During the overflow simulation the time step Δt should be specified by the user.

3.5.1.1 Example application

The model is applied for the simulation of breaching of a prototype sea dike (Fig. 3.19). The main parameters used for the simulation are provided in Tab. 3.3.

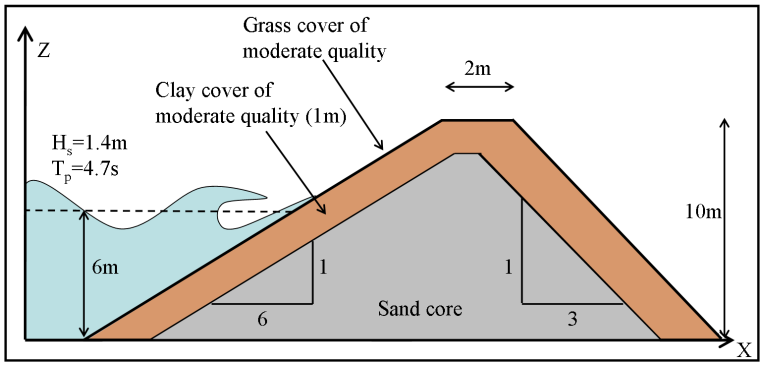

Figure 3.19: Geometry of the prototype dike

INPUT PARAMETER	SYMBOL	VALUE	UNIT
Type of waves	Waves	Irregular	$[-]$
Significant wave height (at the dike toe)	H_s	1.4	$[m]$
Peak period (at the dike toe)	T_p	4.7	$[s]$
Mean water level (at the dike toe)	mwl	6	$[m]$
Dike height	H_D	10	$[m]$
Dike crest	B_D	2	$[m]$
Outer slope	m	6	$[-]$
Inner slope	n	3	$[-]$
Thickness of the clay layer	d_c	1	$[m]$
Polder area	A_p	1000000	$[m^2]$
Grass erosion coefficient	$E_{g,max}$	$2 \cdot 10^{-6}$	$[m^{-1}s^{-1}]$
Clay erosion coefficient	$E_{c,max}$	$8 \cdot 10^{-5}$	$[m^{-1}s^{-1}]$
Sediment size	D_{50}	0.2	$[mm]$
Internal friction angle	ϕ	32	$[deg]$
Porosity of the sand	p	0.4	$[-]$

Table 3.3: Input parameters for the simulation of breaching

The main outcomes from the model are given in Table 3.4. The velocity of the erosion

OUTCOME	SYMBOL	PHASE	VALUE	UNIT
Time of grass erosion	t_{gf}	1	16.03	$[h]$
Time of clay erosion	t_{cf}	2	14.15	$[h]$
Time of core erosion	t_{sf}	3 and 4	5.57	$[h]$
Total time of dike breaching	t_t	1,2,3,4	35.75	$[h]$
Erosion rate in Phase 1	dx/dt	1	0.001	$[mm/s]$
Erosion rate in Phase 2	dx/dt	2	0.038	$[mm/s]$
Erosion rate in Phase 3	dx/dt	3	2.211	$[mm/s]$
Breach widening rate	dB_B/dt	4	0.007	$[m/s]$
Peak outflow discharge	Q_p	4	1367	$[m^3/s]$
Final breach width - maximum	$B_{B,max}$	4	93.26	$[m]$
Final breach width - minimum	$B_{B,min}$	4	44.24	$[m]$

Table 3.4: Main outcomes from the model

progress (Fig. 3.20) can be clearly divided into three phases: (i) grass erosion, (ii) clay erosion and (iii) front-face core erosion. The failure of the sand core develops significantly faster than the erosion of the revetment - $t_{sf} = 0.18 \cdot (t_{gf} + t_{cf})$, while the progress of the cover erosion is dominated by the grass erosion $t_{gf} = 0.52 \cdot (t_{gf} + t_{cf})$;

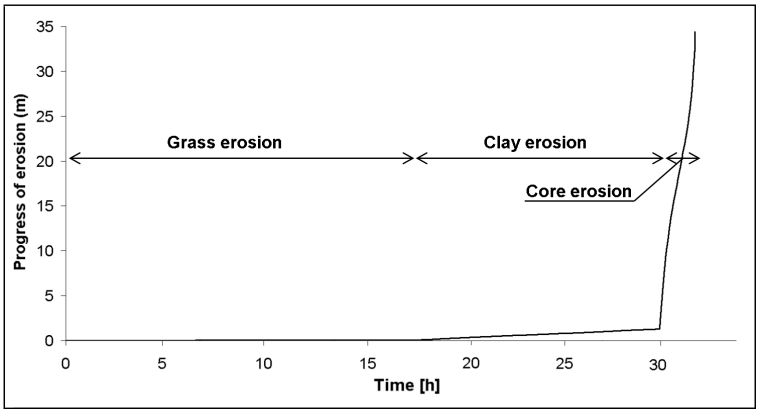

Figure 3.20: Progress of erosion in x-direction

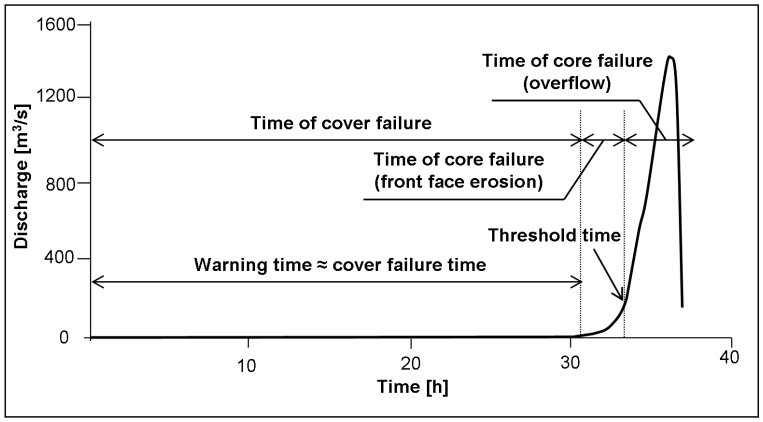

Figure 3.21: Outflow hydrograph

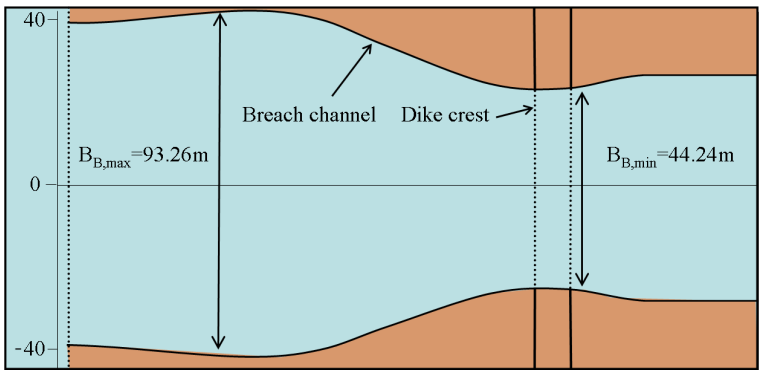

Figure 3.22: Shape of the full breach channel - $x - y$ plane

Analyzing the outflow from the breach (Fig. 3.21) it can be clearly seen that after reaching a certain **threshold time** the discharge increases rapidly and the process of breaching becomes nonreversible - when the core erosion reached the point where overflow occurred, the dike is seriously vulnerable.

The **warning time** could be therefore defined as the sum of cover failure time and front face erosion time, but as the overtopping, which could cause an additional damage of the dike is not accounted for, it is recommended to define the warning time only as the cover failure time.

3.5.2 Tentative validation of the preliminary model

At the moment, no laboratory experiments or field measurements that would be suitable for the model validation are available. Very limited and usually only qualitative information on the experienced dike failures initiated from the seaside by breaking wave impact can be found in the reports made after the disastrous flood events in 1953 in The Netherlands (Rijkswaterstaat, 1961) and 1962 in Germany (Wohlenberg, 1963, for instance). Two cases were selected among them and are used for the tentative validation of the model prediction capabilities: (i) partial breach that occurred in Neuwerk (Germany) in 1962 and (ii) full dike breach that was observed in the Ülversbüller Koog (Germany) in 1962:

- a damage of the dike (Figure 3.23) reported by Führböter et al (1976) which occurred after the dike was subject to a storm surge in 1962 with $H_s = 0.75m$. In this case, the entire grass and clay covers were removed and the dike core was partially damaged (which corresponds to Phase 3 of the simulation). The progress of the erosion was interrupted by the end of the storm surge.

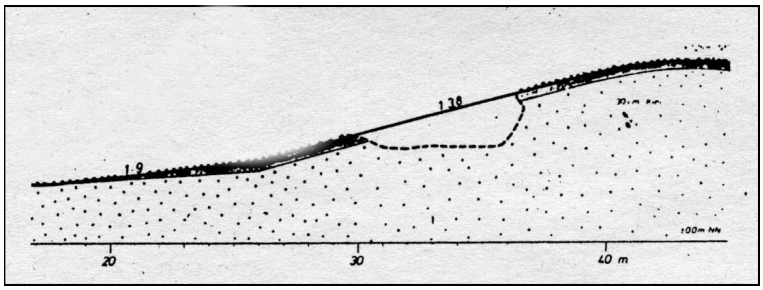

Figure 3.23: Damage of the sea dike in Neuwerk observed in 1962 (Führböter et al, 1976)

The obtained results of the simulation are compared with the observed ones (Figure 3.24 and Table 3.5) providing very good agreement (difference in the range 0-3%) for the prediction of the breach dimensions and relatively good (difference 35%) for the prediction of the breaching time.

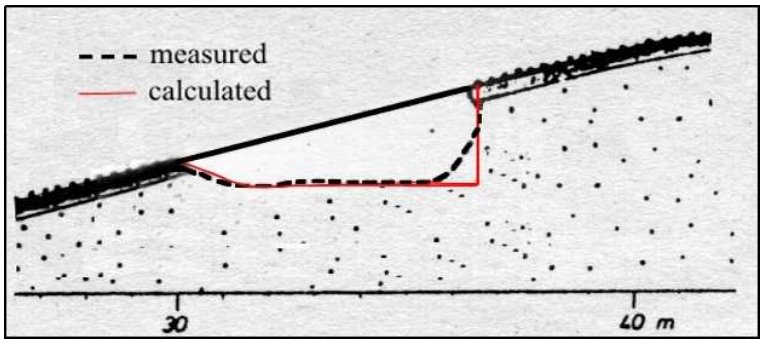

Figure 3.24: Comparison of calculated and measured damage of the dike

Outcome	Observed	Calculated	Difference [%]
Depth of the eroded hole [m]	≈ 2.0*	2.11	$\approx 3\%$
Diameter of the eroded hole [m]	≈ 6.0*	6.0	$\approx 0\%$
Time needed for the damage to occur [h]	unknown	13.52	-
* Führböter et al (1976)			

Table 3.5: Comparison of the measured and calculated dike damage

- information on the full dike breach in Ülversbüller Koog (Germany) in 1962 (Wohlenberg, 1963) was compared with the results provided by the model. Although no information on the breach initiation time is provided, based on the records of mean water level provided by Landesamt für Wasserwirtschaft - Schleswig-Holstein (1962) it can be assumed that the erosion has reached the crest of the dike about 23 hours after the begin of the storm surge. In comparison, the time of this erosion progress calculated by the model is equal to $27h10min$ which gives pretty fair agreement. The slight difference is caused by the lack of information on the grass cover quality - for the purposes of the simulation therefore, the parameters for the grass of moderate quality were used. After the erosion has reached the inner slope and overflow occurred it took about two hours to inundate a $105ha$ ($1.05 \cdot 10^6 m^2$) large polder compared to $3h20min$ calculated using the model. Once again the difference is to be explained by the lack of information on the dike parameters - the mean grain size D_{50} was therefore assumed to take the value $D_{50} = 0.2mm$ for the purposes of the simulation. The calculated dimensions of the full breach channel fit almost perfectly the measured ones - on the seaside calculated width $B_{B,calc} = 88.2m$ is comparable with the measured width $B_{B,obs} \approx 80m$, while on the landside $B_{B,calc} = 37.6m$ compared to $B_{B,obs} \approx 35m$ - see also Figure 3.25 and Table 3.6

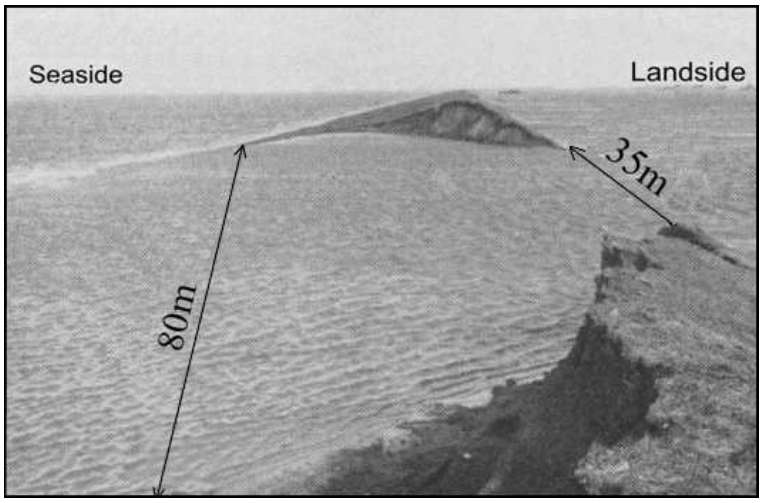

Figure 3.25: Dike breach in the Ülversbüller Koog

Outcome	Observed	Calculated	Difference [%]
Time of breach initiation [h]	$\approx$ 23.0*	27.07	30.4%
Overflow time [h]	$\approx$ 2.0**	3.33	33.6%
Final breach width (min) [m]	$\approx$ 35**	37.6	-7.4%
Final breach width (max) [m]	$\approx$ 80**	88.2	-10.3%
* Landesamt für Wasserwirtschaft - SH (1962); ** Wohlenberg (1963)			

Table 3.6: Comparison of the observed and calculated dike breach parameters

3.6 Capabilities and limitations of the preliminary model

The preliminary model represents the first part of the tiered approach for the simulation of the dike breaching initiated by the breaking wave impact on the outer slope of. The first application of the model for the simulation of historical dike breaches revealed the following issues:

- the model predicts the final breach dimensions very good, within 10% of relative error for both partial and full breaches (c.f. Tables 3.5 and 3.6). Since the final breach dimensions depend mostly on the applied sediment transport model, it can be stated, that the selected models for the sediment transport provide reliable results so that they can be further used in the detailed model. Nevertheless, the application of an alternative model (Tuan, 2007, for instance) should be at least considered;

- the breaching times provided by the model are generally overestimated, which suggest that the either soil resistance is overestimated or, that the loading on the dike is underestimated. The former may arise from the lack of the water infiltration calculation and consequently from the disregard of the resulting decrease of the soil erosion resistance. The latter occurs from the fact that the empirical models for the calculation of loading are case-specific and therefore not full reliable

The following implications for the development of the detailed models can be therefore drawn after the analysis of the results provided by the preliminary model:

- the changes in the water content resulting from the water infiltration into the dike and

the consequent decrease of the soil resistance has to be necessarily accounted for thus improving the prediction of the breaching time;

- the empirical hydrodynamic models selected for the application in the preliminary model should be replaced by the numerical models, which are not case-specific and provide more reliable results
- the sand-core wash out module of the preliminary model can be directly used in the detailed model, since the obtained final breach dimensions are satisfactory.

Furthermore, the following issues should be verified based on the results of laboratory experiments:

- the assumed progress of grass erosion is linear, which probably does not fit the reality - laboratory experiments tests on this subject are however lacking;
- local damage in cracks and fissures in clay layer is neglected, but according to Führböter (1966) is of crucial importance - clarifying laboratory tests are therefore needed;

The focus of the detailed model should be therefore on the improvement of the above listed issues. However, before embarking into the development of the detailed model a number of the clarifying experimental tests on (i) grass reinforcement properties, (ii) gras erosion resistance, (iii) clay erosion resistance and (iv) shear failure in cracks in clay layer will be performed. Furthermore, the small-scale experiments will be performed in order to gain at least qualitative information on the entire breaching process, from the breach initiation till the final breach.

4 Laboratory experiments on the erosion and breaching processes

The conceptual models for the surface erosion of the soil due to impact pressures and for the shear failure in cracks listed in Section 2.2.3 were either verified against limited amount of data (model of Woolhiser et al, 1990), or even not verified experimentally at all (the model of Führböter, 1966). In order to validate, calibrate and if necessary also to improve the selected conceptual models and to gain more knowledge on the processes of grass and clay erosion, a number of laboratory experiments are performed in the framework of this study. The focus of the experimental investigations is on the following issues:

1. Prediction of the erosion resistance of clay against impact pressures of breaking waves.
2. Assessment of the effect of the grass cover on the erosion resistance of the clay cover against breaking wave impact;
3. Estimation of the effect of grass roots on the shear strength of the soil.
4. Verification and if necessary improvement of the conceptual model of Führböter (1966) on the shear failure in water-filled cracks in a clay layer (see Section 2.2.3.2).
5. Analysis of the entire breaching process, using a small-scale dike model.

Issues 1,2 and 4 will be investigated by means of wave impact simulator, Issue 3 will be investigated in the soil mechanics laboratory while Issue 5 will be investigated in a wave flume.

4.1 Experiments on the surface erosion of clay cover

The experiments were performed using the so-called wave impact simulator which was developed and described by Pachnio (2005) - see Fig. 4.1. The experimental set-up consists of a vertical pipe that is used to contain the mass of water to be suddenly dropped from a given height h_f. The pipe can be placed in a range of $h_f = 50cm$ up to $h_f = 165cm$ above the soil sample. A computer-controlled system fills the pipe with given amount of water ($m = 2kg$) and releases the mass using a pneumatic-steered valve. Falling mass of water hits the soil sample generating an impact pressure. The dependency upon the fall height of pressures at the surface of the soil sample was measured and described by Pachnio (2005), the values of the impact pressures and energy are not directly measured but calculated as a function of fall height h_f.

For the purposes of the tests, **three samples of clay** taken from the following locations in Lower Saxony are used:

- sea dike in Cäciliengroden
- sea dike in Elisabethgroden, km 9.0
- sea dike in Elisabethgroden, km 3.5

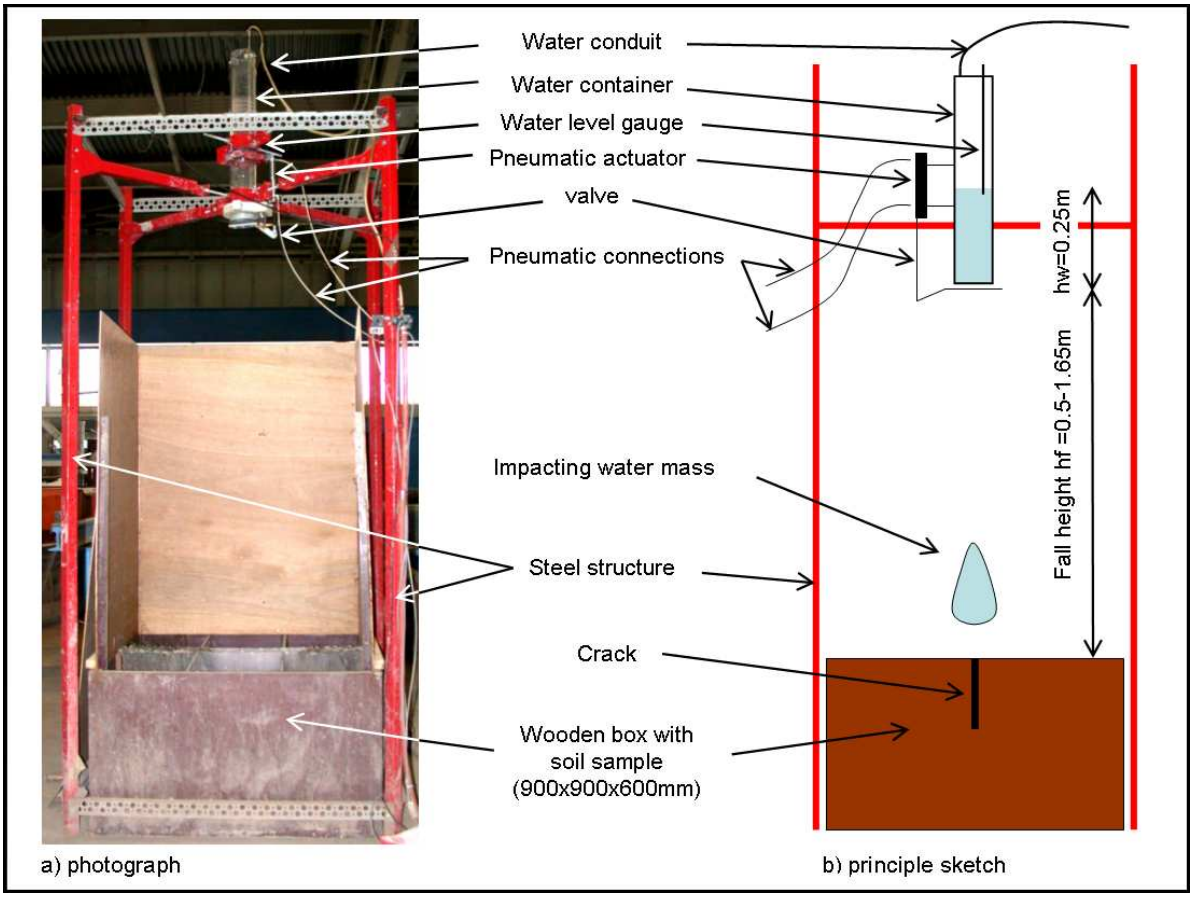

Figure 4.1: Wave impact simulator

Characteristic value	Cäciliengr.	Elisabethgr., km 9.0	Elisabethgr., km 3.5
Clay percentage [%]	35	20	10
Silt percentage [%]	53	45	30
Sand percentage S_p [%]	12	35	60
Proctor density [g/cm^3]	1.458	1.643	1.835
Infiltration rate k_s [m/s]	$1.37{\cdot}10^{-9}$	$1.22{\cdot}10^{-8}$	$3.23{\cdot}10^{-6}$
Plasticity index I_p [-]	0.45	0.2706	0.0649
Undrained cohesion[kPa]	22.6-70.7	18.6-40.0	8.6-24.1
Flow limit w_l[-]	0.77	0.41	0.25

Table 4.1: Properties of the three clay types used in the laboratory tests (IGBFT,2001)

The samples of soil used in the tests are evaluated using the Dutch approach for the classification of the erosion resistance of clay for dikes (Tab. 4.2).

Category	w_l[-]	I_p[-]	Sand content S_p [%]
Category 1: Erosion resistant	>0.45	>0.73·(w_l-20)	<40
Category 2: Moderately erosion resistant	<0.45	>0.18	<40
Category 3: Little erosion resistance	-	<0.18	>40

Table 4.2: Classification of clay for dikes according to the Dutch requirements (TAW,1996)

The three soil samples used in the tests are therefore classified as:

- Cäciliengroden - $w_l = 0.77$, $I_p = 0.45$, $S_p = 12\% \Rightarrow$ Category 1
- Elisabethgroden, km.9.0 - $w_l = 0.41$, $I_p = 0.208$, $S_p = 35\% \Rightarrow$ Category 2
- Elisabethgroden, km. 3.5 - $w_l = 0.25$, $I_p = 0.06$, $S_p = 60\% \Rightarrow$ Category 3

For every type of clay the experiments are performed applying wide range of impact energies and using water layer of variable thickness. Tests without water layer are performed as well. The complete list of all the measured volumes of eroded soil $k_d[cm^3]$ can be found in the original publication (Stanczak et al, 2007a). The results obtained from the tests without water layer are used to calibrate the detachability parameter k_d in Eq. 2.1, which is defined as the mean volume of eroded soil by a unit of energy of a single impact. However, as no linear dependency of detachability parameter k_d on the kinetic energy E_k can be observed after the tests, an additional parameter $k_{d,p}[cm^3/kPa]$ is introduced. This parameter is calculated as the mean value of soil volume eroded by a unit impact pressure (1kPa) when no water layer is present. Consequently, taking the damping effectiveness of a water layer into consideration, the volume of soil eroded by each impact $R_{d,p}[cm^3]$ is calculated as:

$$R_{d,p} = p_{max} \cdot k_{d,p} \cdot e^{-w \cdot h} \tag{4.1}$$

Based on the experimental results, the detachability coefficients used in Eqs. (2.1) and (4.1) are obtained in Table 4.3.

Type of the soil	$k_d\ [cm^3/J]$	$k_{d,p}\ [cm^3/kPa]$	$w\ [-]$
Weak clay	1.17	1.09	0.25
Moderate clay	1.01	0.99	1.0
Strong clay	0.88	0.85	0.1

Table 4.3: Detachability coefficients for the tested types of clay

A clear dependency of the detachability coefficient k_d on the type of the soil can be observed as the value of k_d decreases with the increasing quality of the clay. The parameter w that describes the damping effectiveness of the water layer doesn't seem to depend on the type of soil for the tested samples. In the case when the volume of eroded soil is calculated based on the detachability parameter k_d for unit energy, the correlation coefficient R calculated for all the measurements takes the value $R_{kd} = 0.570$ for weak clay, $R_{kd} = 0.812$ for moderate clay and $R_{kd} = 0.31$ for strong clay. For the calculations based on the dependency of the volume of eroded soil on the impact pressure $k_{d,p}$ the correlation coefficient is of the value $R_{kd,p} = 0.742$ for weak clay, $R_{kd,p} = 0.842$ for moderate clay and $R_{kd,p} = 0.336$ for strong clay. This would suggest that rather the calculations based on the $k_{d,p}$ should be used in further investigations. The comparison of eroded volume R_d for a unit impact pressure with the mean value of all measurements performed with given water layer thickness is presented in Fig. 4.2a for weak clay, Fig. 4.2b for moderate clay and Fig. 4.2c for strong clay.

A relatively good agreement can be observed. For the tests with weak and moderate clay, quite significant influence of the water layer thickness on the progress of erosion can be reported, while for the good clay the damping effect of the water layer is not so significant. In Fig. 4.3 the comparison between the volume of eroded soil measured for all performed

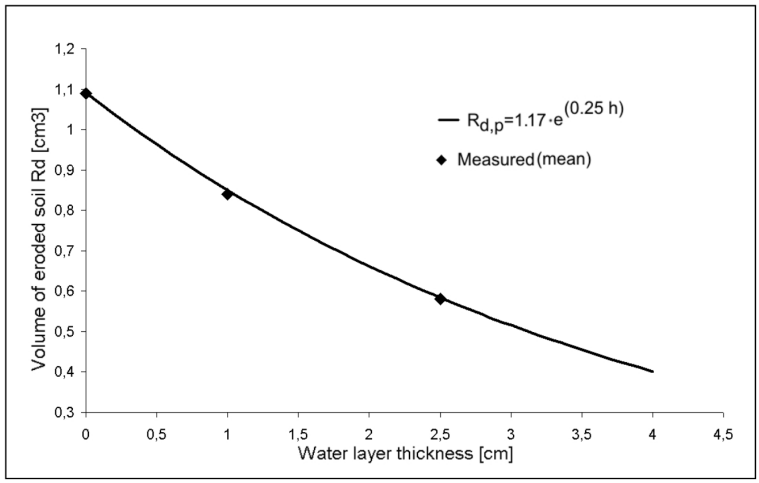

a) Weak clay

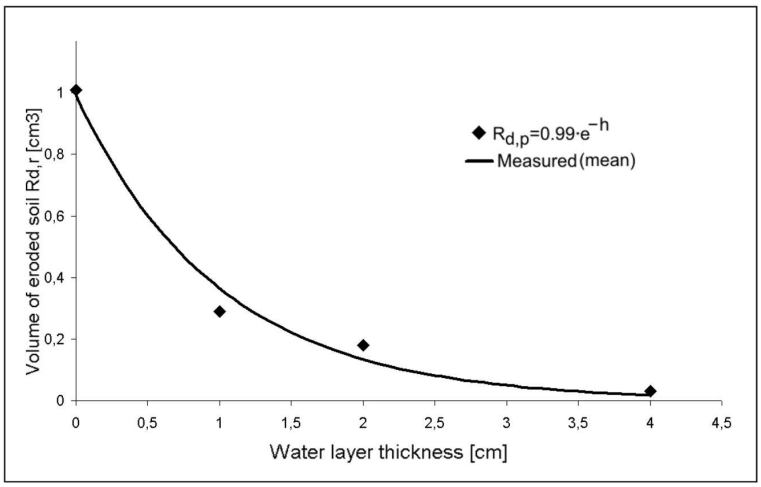

b) moderate clay

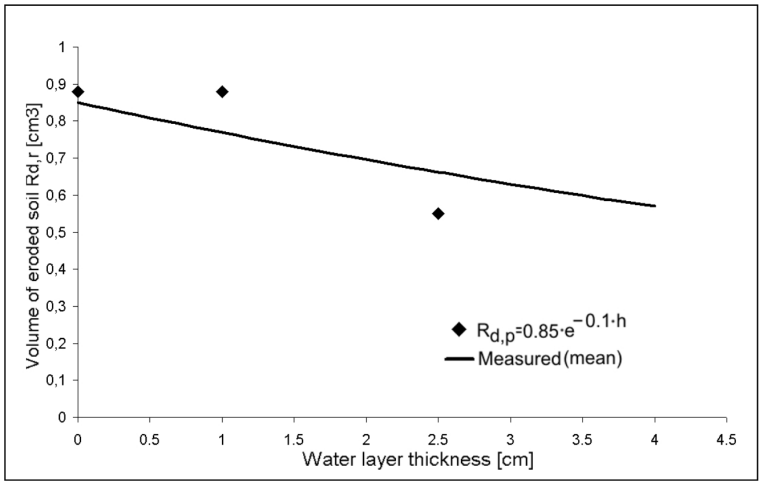

c) strong clay

Figure 4.2: Volume of eroded clay vs. water layer thickness

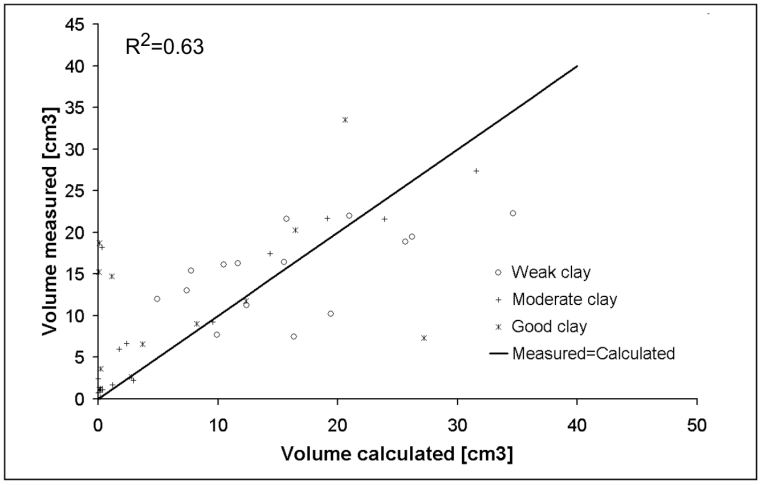

Figure 4.3: Measured volume of eroded soil vs volume calculated using Eq. 2.1

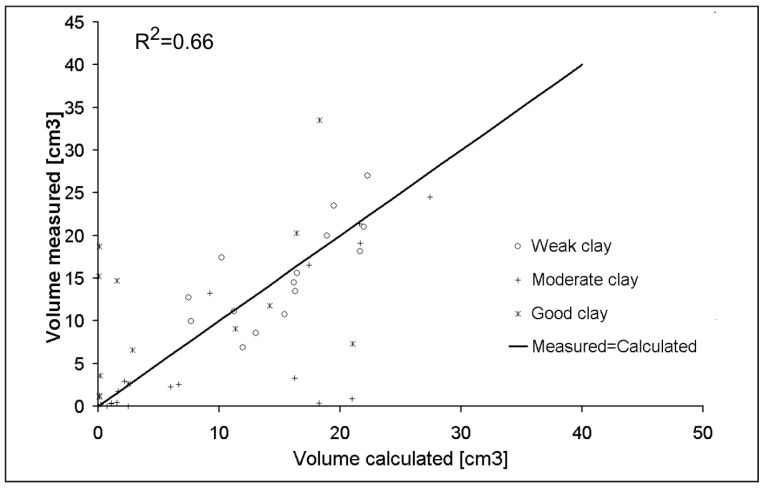

Figure 4.4: Measured volume of eroded soil vs volume calculated using Eq. 4.1

experiments and the values calculated using Eq. 2.1 is presented. In Fig. 4.4 the results of comparison between measured values and the ones calculated according to Eq. 4.1 are shown. Based on the above results one may state that (i) rather the formulae based on the maximal impact pressure should be used than the formula based on the energy of impact, since using the former provides slightly better results than applying the formula based on the kinetic energy of the impact. The correlation coefficient R^2 for the latter takes the value $R^2_{Rd} = 0.63$ while for the former $R^2_{Rd,p} = 0.66$. Furthermore, the results of the performed laboratory experiments show very strong damping effect of the water layer that remains on the dike slope and this effect has necessarily to be included in the detailed dike breaching model

4.2 Experiments on the shear failure in cracks

4.2.1 Experimental verification of the model by Führböter (1966)

According to the conceptual model proposed by Führböter (1966), if a water-filled crack of depth a and length L_c is subject to an impact pressure p_{max} then the pressure is instantly transferred in the full magnitude to the two side walls of the crack. The force acting on the wall of

the crack can then be calculated as follows - see also Fig. 4.5:

$$F_{crack} = a \cdot L_c \cdot p_{max} \tag{4.2}$$

with:

- F_{crack} - force acting on the wall of crack $[N]$
- a - depth of crack $[m]$
- L_c - length of the crack $[m]$

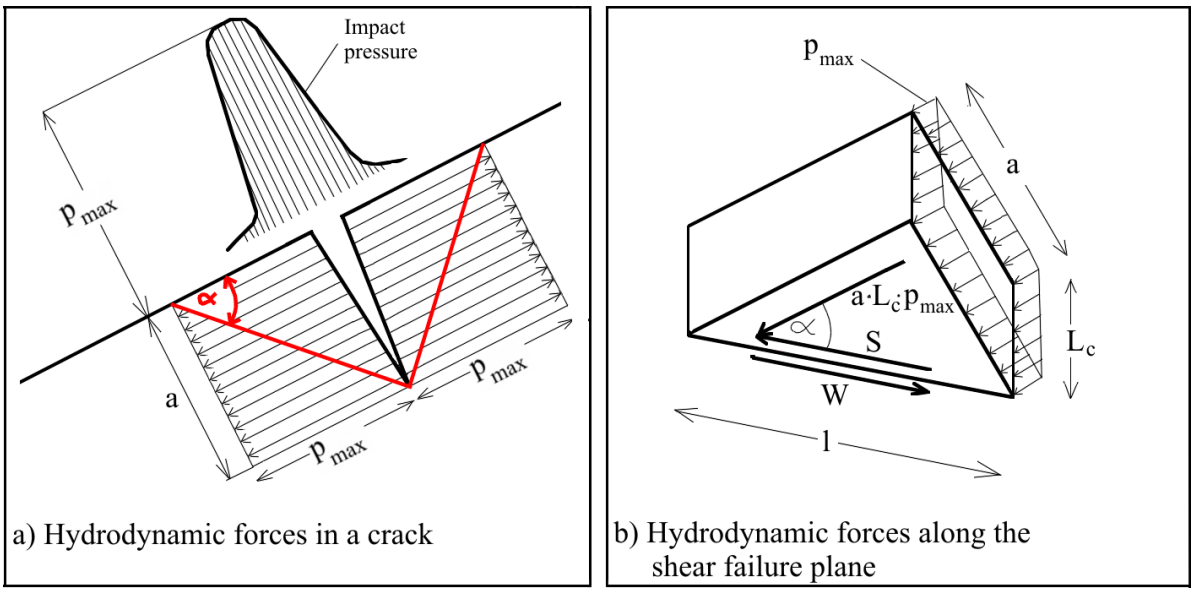

Figure 4.5: Forces inside a crack subject to an impact pressure (after Führböter,1966)

These forces are absorbed by the compression and the shear strength of the soil behind the walls of the crack. The shear stress acts on a plane leaning to the surface with an angle α and provides the following shear force:

$$S = a \cdot L_c \cdot p_{max} \cdot cos\alpha \tag{4.3}$$

the resistance force is provided by the shear strength described by cohesion c only, as the weight of the soil body is considered by Führböter (1966) to be negligibly small :

$$W = \frac{a \cdot L_c \cdot c}{sin\alpha} \tag{4.4}$$

Solving the limit state equation $S = W$ for $sin\alpha$ provides the angle of shear failure α :

$$sin\alpha = \sqrt{\frac{1}{2} \pm \sqrt{\frac{1}{4} - \left(\frac{c}{p_{max}}\right)^2}} \tag{4.5}$$

which leads to $p_{max} = 2c$ as the critical impact pressure, i.e. the shear failure occurs for impact pressures p_{max} greater or equal to the double of cohesion. This conceptual model was never verified experimentally, and before implementing it into a dike breaching model, at least its tentative validation is needed. In order to achieve this goal, the laboratory experiments are performed using the same experimental set-up as described in Section 4.1. All tests are performed using the following procedure:

1. the clay is put into a wooden box with glass windows and compacted;
2. a crack is made in the middle of the sample, at the location where the falling water mass hits the soil. The crack is 150mm deep, 10mm wide and 100mm long. Figures 4.6 and 4.7 show the side and top views of the crack, respectively;
3. the crack is filled up with water;

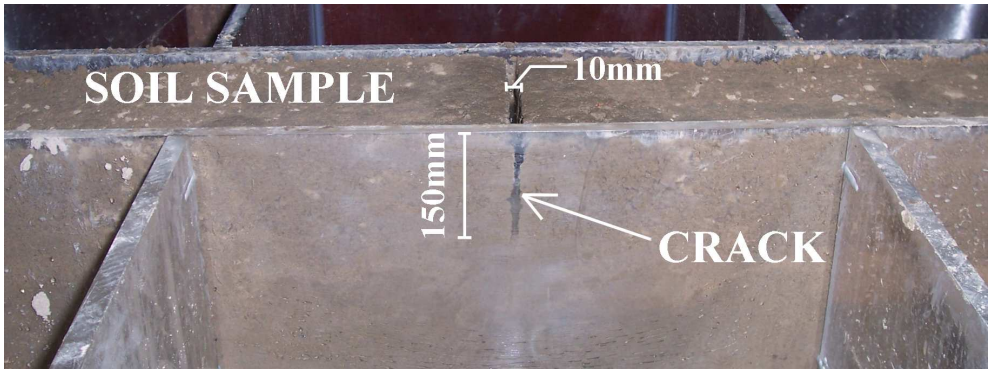

Figure 4.6: Artificial crack in the soil sample - side view

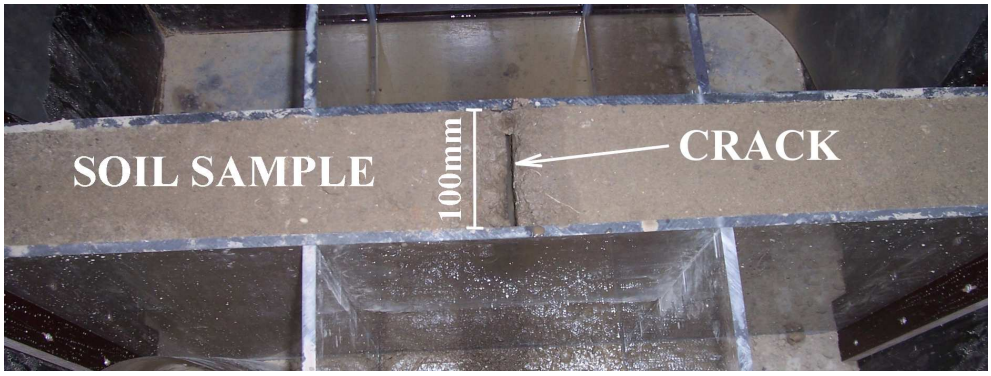

Figure 4.7: Artificial crack in the soil sample - top view

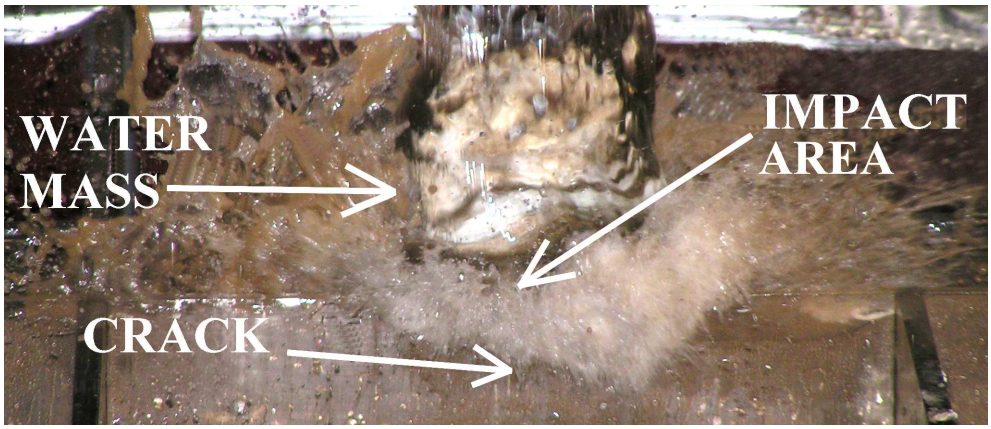

Figure 4.8: Mass of water impacting the sample

4. the automatically released mass of water (see Section 4.1) is used to generate an impact pressure in the crack at the surface of the sample (see Fig. 4.8);
5. After an impact event for which shear failure occurred, a picture of the crack development is taken, then the angle of shear failure α (Fig. 4.9) between the failure plane and the surface of the soil sample is measured

6. For every single test a soil sample is taken in order to measure the water content w_c. This represents an indirect measurement of the shear strength, as an empirical equations for the calculation of shear strength depending on the water content for every type of tested soil are provided (Kortenhaus, 2003):

$$\begin{aligned} c &= 2550 \cdot e^{-33 \cdot w_c}[kN] && \text{for the weak clay} \\ c &= 2800 \cdot e^{-20 \cdot w_c}[kN] && \text{for the moderate clay} \\ c &= 7230 \cdot e^{-12 \cdot w_c}[kN] && \text{for the strong clay} \end{aligned} \tag{4.6}$$

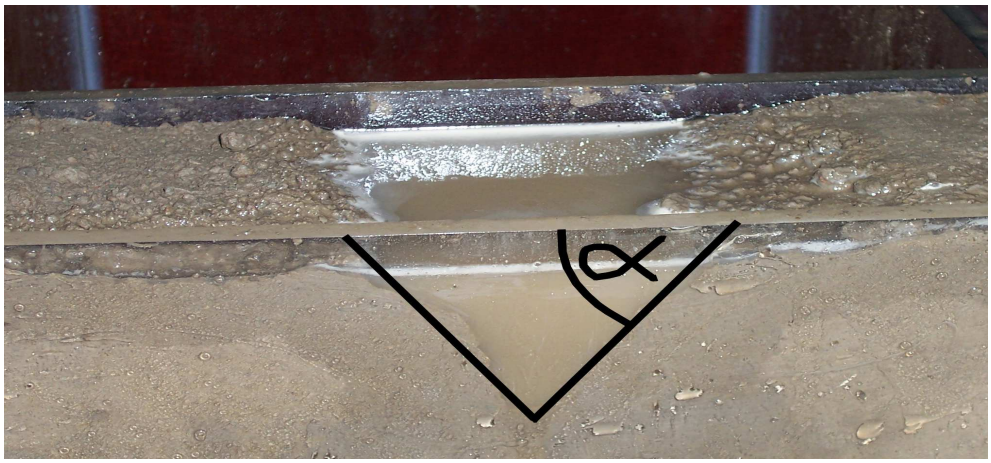

Figure 4.9: Crack development recorded after an impact - angle of shear failure α

The test procedure was performed for each type of clay applying wide range of impact pressures and soil conditions (see Stanczak et al, 2007a for full test programme). The results of the laboratory experiments confirmed the conceptual model of Führböter (1966) only partially. During the experiments the shear failure itself occurs, but the observed process of failure differs from the predicted one (see Fig. 4.10).

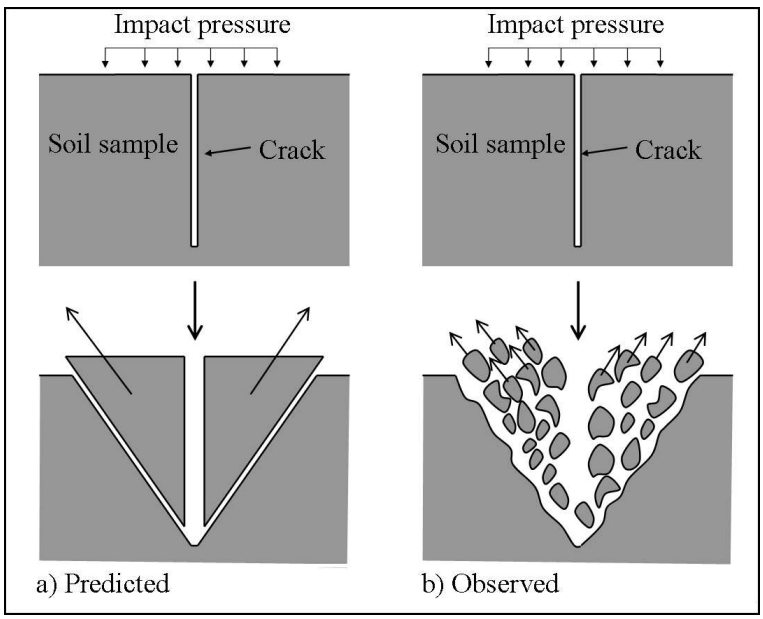

Figure 4.10: Predicted and observed shear failure - principle sketch

The soil from the scour hole is quarried out in the form of particles and small aggregates instead of being removed as a single soil block . The measured angle of shear failure α_{meas} for every single test run is compared with the value calculated using the model of Führböter (1966) - Eq. 4.5. The values of maximal impact pressures are here calculated with the formula of Pachnio (2005) while the cohesion of the soil is calculated as a function of the measured water content. For all soil samples the measured angle of shear failure α_{meas} is smaller than the calculated one (Fig.4.11). That suggests that either the soil cohesion in all the cases is underestimated or, which is more reasonable, also the neglected forces affect the process of shear failure. Therefore the model of Führböter (1966) is improved by taking also additional resisting forces into consideration.

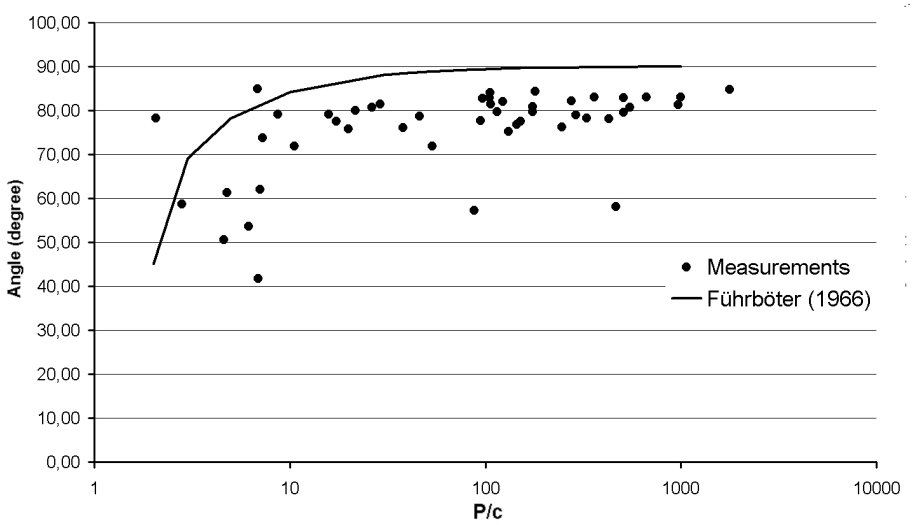

Figure 4.11: Calculated and measured shear failure angle α

4.2.2 Improvement of the Führböter (1966) model

In order to improve the model by Führböter (1966), it is necessary to include also the forces that were originally neglected i.e. weight of the soil and shear strength at the both sides of the block (Fig. 4.12).

The weight of the soil block is calculated as:

$$G = (0.5 \cdot a^2 \cdot L_c \cdot \gamma)/\text{tan}\alpha \tag{4.7}$$

The shear resistance W_A on both sides of the block is given as:

$$W_A = A \cdot c = \frac{a^2 \cdot c}{\text{ctan}\alpha} \tag{4.8}$$

The limit state equation can be now rewritten as:

$$\frac{a \cdot L_c \cdot c}{sin\alpha} + 0.5 \cdot a^2 \cdot L_c \cdot \text{ctan}\alpha \cdot \gamma \cdot sin\alpha + \frac{a^2 \cdot c}{\text{ctan}\alpha} = a \cdot L_c \cdot p_{max} \cdot cos\alpha \tag{4.9}$$

A comparison between measured angle of shear failure α_{meas} with values calculated using Eqs. 4.5 and 4.9 is given in Tab. 4.4 and Fig. 4.13. Taking additional resisting forces into account, the results are improved from $\alpha_{meas}/\alpha_{calc}$ =1.165 in the case of unmodified approach of Führböter (1966) to $\alpha_{meas}/\alpha_{calc}$=0.971 for approach that includes also the weight of the block and shear resistance on both sides of the block. The coefficient of variation σ' is also getting smaller.

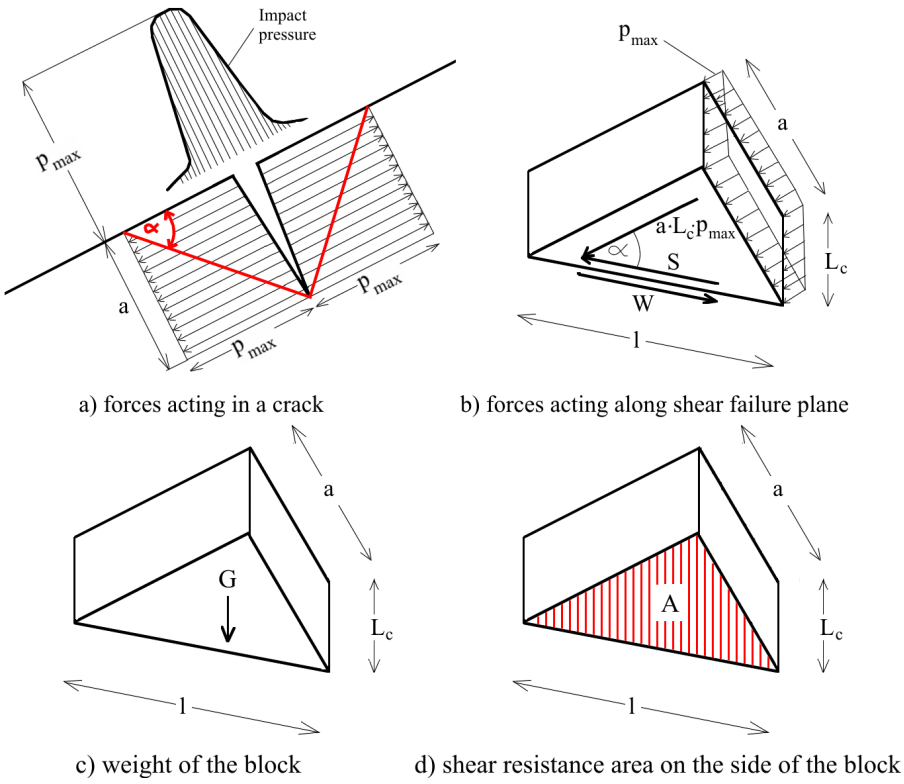

Figure 4.12: Forces acting on the block of soil

Approach	Mean $\alpha_{meas}/\alpha_{calc}$	Std.deviation $\alpha_{meas}/\alpha_{calc}$	σ'
Model of Führböter (1966) - Eq. (4.5)	1.165	0.187	0.161
Modified model of Führböter (1966) - Eq. (4.9)	0.971	0.135	0.139

Table 4.4: Comparison of the mean and standard deviation of $\alpha_{meas}/\alpha_{calc}$ for the original and modified approach

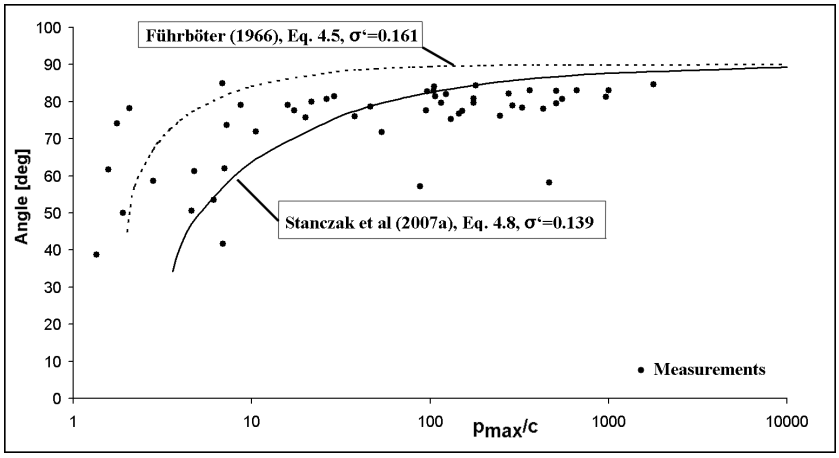

Figure 4.13: Comparison of the original and modified approach of Führböter (1966)

The performed laboratory experiments represent the first ever physical verification of the existing conceptual model of Führböter (1966). Since it was found, that the forces originally neglected by Führböter (1966) also play an important role, the model was improved. In com-

parison to the original model, the improved one predicts better the possibility of shear failure in the cracks, and if a failure occurs, also the angle of shear failure. Therefore, the improved model should be applied in the detailed clay erosion model thus improving the prediction of the clay failure time, since the shear failure in the cracks subject to impact pressure of breaking waves was recognised as one of the leading failure modes for the clay cover of a sea dike (Stephan, 1981, for instance).

4.3 Reinforcement properties of the grass roots

Two mechanisms of the grass root reinforcement are subject to investigations:

- increase in the shear strength of the soil (*apparent root cohesion*), which results in the improved resistance against the shear failure in cracks and against the revetment sliding;
- chemical and mechanical bonding of the soil particles by the dense network of fine roots that improves the surface erosion resistance

4.3.1 Laboratory experiments on the root volume ratio

According to Wu et al (1979) the increase in the shear strength of the soil (*apparent root cohesion*) due to bonding action of roots can be calculated as:

$$c_r = T_R \frac{V_R}{V}(cos\theta_r \cdot tan\phi + sin\theta_r) \tag{4.10}$$

with:

- c_r - apparent root cohesion [N/m^2]
- T_R - root tensile strength [N/m^2]
- V_R - volume of roots in soil [m^3]
- V - total volume of soil including the roots [m^3]
- θ_r - root angle of shear rotation [deg]

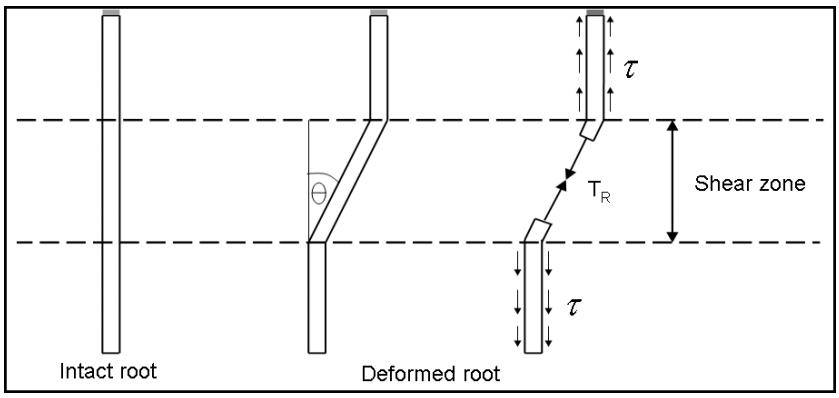

Figure 4.14: Flexible elastic perpendicular root reinforcement (Wu et al, 1979)

In order to investigate the influence of the root network on the strength of reinforced soil, the knowledge of root percentage in the soil sample is needed. The laboratory experiments to obtain the root volume ratio RVR were performed at the Leichtweiß-Institute using the following procedure:

1. a sample of the grass cover is extracted from a sea dike ("Alter Störtebeker Deich" in Leybucht, Lower Saxony, Germany) using a steel pipe of inner diameter of 48mm inserted perpendicularly to the surface of the dike up to the depth of 20cm;

2. the extracted, cylindrical sample is cut into slices of 2cm thickness. Each slice represents a given depth under the surface and is used to provide an information on the RVR for this particular depth;

3. for every single slice the roots are separated from the soil , carefully cleaned with water and dried in 105° C for 24 hours

4. the dry mass of roots m_R separated from each single slice is obtained. The density of dry grass roots γ_R is known ($\gamma_R = 300kg/m^3$ (Young, 2005)). The volume of roots V_R in a single slice is calculated as:
$$V_R = \frac{m_R}{\gamma_R} \tag{4.11}$$

5. the root volume ratio RVR is calculated as:
$$RVR = \frac{V_R}{V_{ss}} \cdot 100 \qquad [\%] \tag{4.12}$$
where V_{ss} is the total volume of a single slice, including the roots ($V_{ss} = 36.2cm^3$)

6. the same procedure is repeated 10 times, using samples extracted at different locations on the dike slope.

The results of all the ten measurements as well as the mean value of root volume ratio for each depth are presented in Tab. 4.5.

Depth [cm]	RVR										Mean
2	2.43	0.99	0.96	1.45	0.50	0.77	3.28	1.93	2.15	1.35	1.58
4	1.82	0.50	0.48	0.73	0.26	0.56	0.36	0.71	1.07	0.67	0.72
6	0.91	0.73	0.31	0.31	0.76	0.28	0.17	0.36	0.64	0.99	0.55
8	0.52	0.36	0.15	0.15	0.38	0.36	0.13	0.17	0.31	0.50	0.30
10	0.26	0.86	0.09	0.21	0.07	0.17	0.07	0.09	0.10	0.16	0.21
12	0.03	0.43	0.05	0.10	0.03	0.10	0.01	0.06	0.05	0.08	0.10
14	0.01	0.07	0.01	0.00	0.00	0.05	0.00	0.03	0.13	0.03	0.03
16	0.01	0.03	0.00	0.00	0.00	0.00	0.00	0.00	0.00	0.01	0.01

Table 4.5: Measured root volume ratio for the ten samples taken from the dike.

Fig. 4.15 shows a comparison of root volume distribution measured during the laboratory experiments with the mean distribution measured for 24 Dutch dikes and reported by Sprangers (1999). Good agreement between these two distributions can be observed. The general form of the best fit function proposed by Sprangers (1999) that will be used for the purposes of further tests reads:
$$RVR = A \cdot D^{(d-2)} \qquad [\%] \tag{4.13}$$

where A and D are empirical coefficients that depend on the quality of grass cover while d is the depth under the surface. The coefficients A and D are supposed to have a negative correlation with the clay quality, as stronger clay prevents the grow of a dense root network. For the tested samples of grass cover the coefficients are of the value $A = 1.58$ and $D = 0.75$

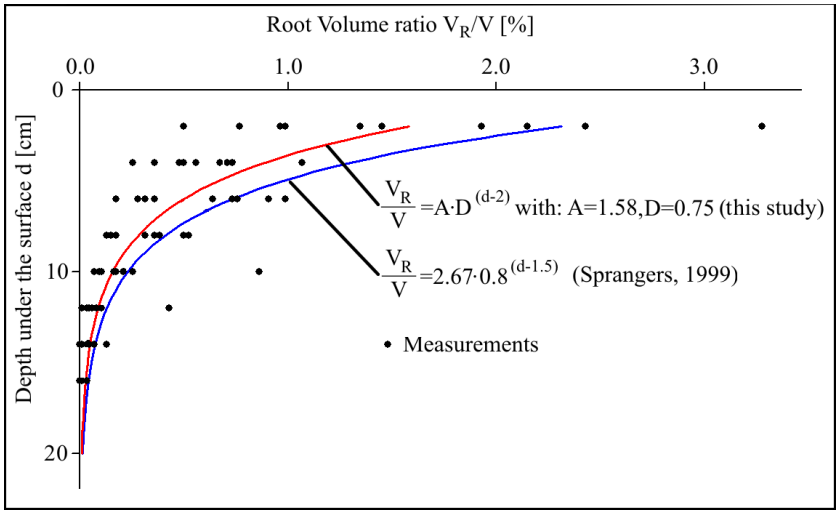

Figure 4.15: Measured root volume ratio for the samples taken from the dike

The second important parameter that describes the quality of the root network is the tensile strength of the roots. The tensile strength of ten single roots was measured, the obtained values are in a quite narrow range $300 - 800 N/cm^2$, with mean of $T_R = 500 N/cm^2$.

The information on the grass root distribution gained from the conducted laboratory investigations is of crucial importance for the estimation of the reinforcement effect of the grass roots on the clay cover. The root volume ratio RVR is the essential parameter in Eq. 4.10 which can be now directly applied in the detailed model for the calculation of the shear strength of grass-reinforced clay layer thus improving the overall estimation of the dike resistance.

4.3.2 Tests with grass cover - shear strength

In order to examine the influence of grass roots on the shear strength of the soil, the knowledge of the shear strength of the reinforced soil on different depths under the surface of the dike is needed. To achieve this goal, the direct shear measurements are performed with the shear plane set to 2,4,6,8 and 10 cm under the surface (Fig. 4.16)

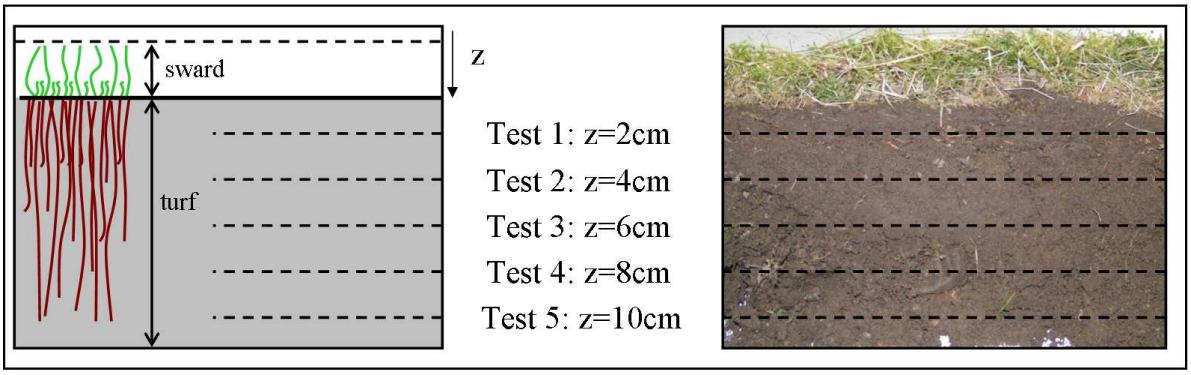

Figure 4.16: Planes of shear strength measurements

As a comparison, the tests on the sample of the same soil but without a vegetation are performed. Measured shear strength of the soil $\tau_S = 104kN/m^2$ with $\sigma_N = 200kN/m^2$. Measured internal friction angle of the soil $\phi = 25.4^0$ and measured cohesion of the soil $c_s = 7kN/m^2$. All of the tests on grass are performed with $\sigma_N = 200kN/m^2$. Summary of the results is given in Tab. 4.6.

Test no.	Depth d[cm]	Shear strength $[kN/m^2]$		
		Clay	Clay with roots	Apparent root cohesion
1	2	104	198	94
2	4	104	146	42
3	6	104	135	31
4	8	104	128	24
5	10	104	118	14

Table 4.6: Results of the direct shear tests.

In Fig. 4.17 the comparison of measured values with the increase of shear strength of the reinforced soil (apparent root cohesion) calculated using Eq. 4.10 by Wu et al (1979) is presented.

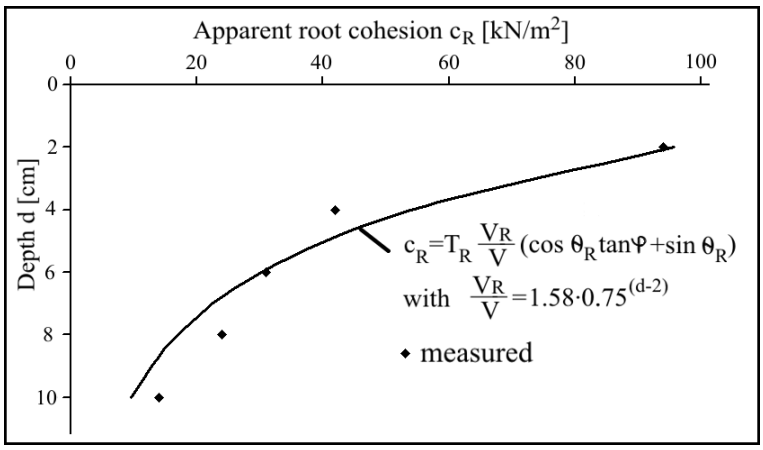

Figure 4.17: Measured and calculated increase of shear strength

According to the obtained results it can be stated that there is a good agreement with the root reinforcement model (Eq.4.10) proposed by Wu et al. (1979). Therefore, it can be applied in the detailed model for the calculation of shear strength of root reinforced soil with respect to depth under the slope surface.

4.3.3 Surface erosion of grass-reinforced clay cover

The surface erosion resistance is strongly increased by the bonding properties of the grass root network (TAW, 1997). As the density of roots depends on the depth under the surface (cf. Section 4.3.1), the focus of the experimental tests on the erosion resistance performed for the purposes of this work was on the dependency of erosion resistance on the depth under the surface. The complete test programme and all measured data of these experiments is summarised in Stanczak et al (2007a). As the soil that formes the substrate of the tested grass cover is classified as the weak clay, $k_{d,p} = 1.09$ and $w = 0.25$ (see Tab. 4.3) will be used in further considerations. The detachability parameter of the grass cover $k_{d,g,p}$ depends both on the properties of the soil itself and the percentage of the roots that reinforce the soil body

(RVR). The following empirical equation based on the results of the experimental tests gives the dependency of the detachability parameter $k_{d,g,p}$ on the root volume ratio:

$$k_{d,g,p} = \frac{k_{d,p}}{b \cdot RVR^2} \quad [cm^3] \tag{4.14}$$

where b is the parameter describing the influence of the roots on the erodibility of the grass cover. It takes the value $b = 5$ for the best fit function. In Fig. 4.18 the comparison of the measured values with the ones calculated using Eq. 4.14 is shown. Very good agreement is observed - the correlation coefficient takes the value of $R = 0.963$ and the coefficient of variation $CoV = 0.24$. At the depth where the $RVR = 0.44\%$ the detachability parameter of the grass cover $k_{d,g,p}$ reaches the value of the detachability parameter of the clay $k_{d,p}$ - the influence of the roots becomes negligible. This is the ***critical depth of erosion*** d_{crit}. The detachability parameter for the whole revetment $k_{d,t,p}$ is then calculated as:

$$\begin{aligned} k_{d,t,p} &= \frac{k_{d,p}}{b \cdot RVR^2} \qquad \text{for} \qquad d < d_{crit} \\ k_{d,t,p} &= k_{d,p} \qquad \text{for} \qquad d > d_{crit} \end{aligned} \tag{4.15}$$

The same damping effectiveness of the water layer as in the case of clay layer is observed, so that Eq. 4.1 can be applied also for the grass-reinforced clay layer.

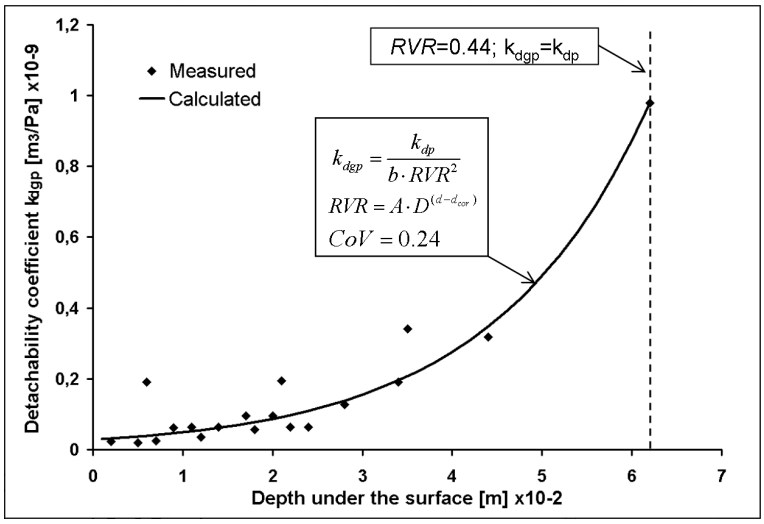

Figure 4.18: Measured and calculated values of the detachability parameter $k_{d,g,p}$ with respect to the depth under the surface

The results of the conducted laboratory experiments form the basis for the calculation of grass and clay erosion, taking into account the following processes:

- the erosion of the clay cover that results from the impact pressures of breaking waves;
- the reinforcement effect of the grass roots on the erosion resistance of clay cover;
- the possibility of shear failure in cracks subject to impact pressures;
- the increase of the shear strength of the soil that results from the apparent root cohesion of the grass cover.

The simulation of the listed processes should necessarily be included in the detailed dike breaching model thus significantly improving the prediction capabilities of the grass and clay erosion modules.

4.4 Dike breaching tests in a small wave flume

In order to analyse the full process of dike breaching, from the initiation till the full breach, a small scale (1:40) test was performed at the Leichtweiß-Institute using the following set-up:

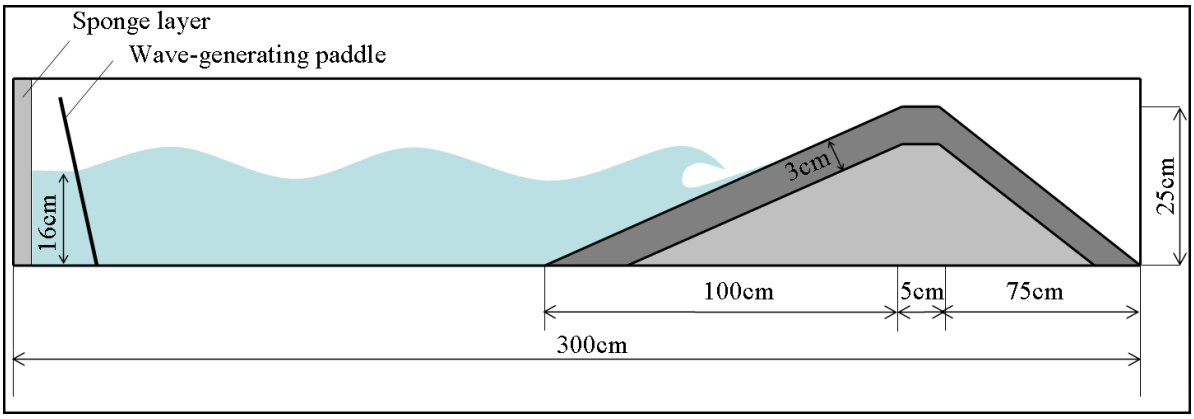

Figure 4.19: Experimental setup in the small LWI wave flume

The following parameters describe the set-up:

- Regular waves, H=0.06m, T=0.81s
- Water level h=16cm
- Outer slope 1:4, inner slope 1:3
- Dike height 25cm
- Clay layer thickness 3cm
- Grain diameter D_{50}=0.108mm

As clay is not scalable and the sand that was used is also not properly scaled, the experimental results cannot be evaluated quantitatively. Nevertheless, according to the observations made during the experiment, the process of breaching can be qualitatively described using the following steps (Fig. 4.20):

First step: Clay cover erodes in the area of largest impact pressures, almost no erosion due to flow of wave run-up is observed	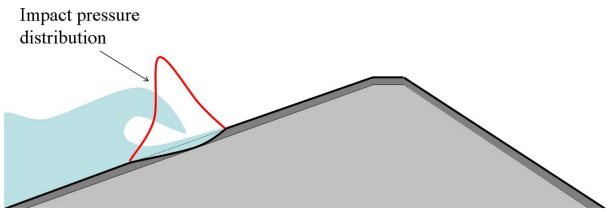
Second step: The erosion in the area of largest impact pressures decelerates due to damping effect of water pad that remains in the scour hole, the erosion due to flow of wave run-up becomes significant	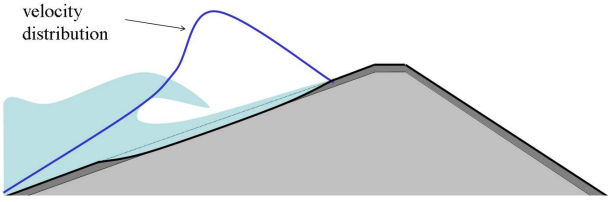

Third step: The eroded sediment is accumulated under the mean water level. After the sand core has been reached, it is washed out by the flow of run-up and run-down. The clay layer that remains above the washed out soil is still stable.	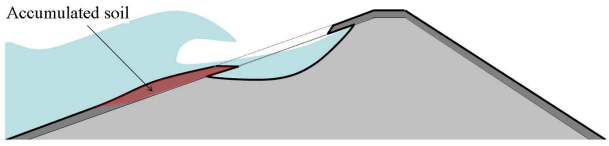
Fourth step: the undermined clay cover collapses	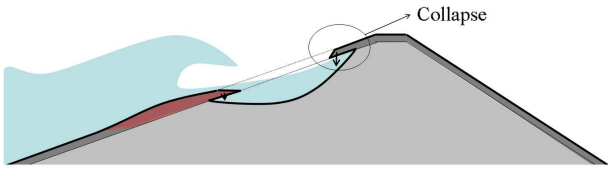
Fourth step - continued: the blocks of cohesive soil that collapsed act as breakwaters, protecting the remaining parts of the dike and decelerating the erosion impact pressures	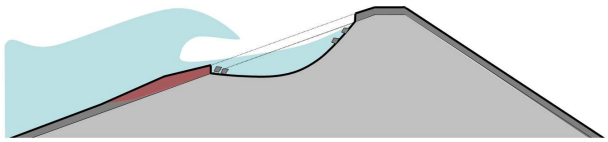
Fourth step - continued: the erosion continues, the clay cover is being continuously undermined and collapses	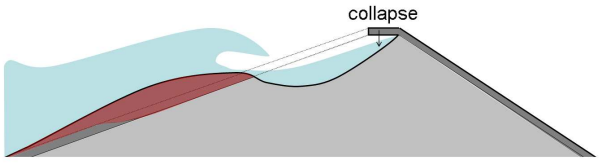
Fifth step: the clay cover on the inner slope is undermined	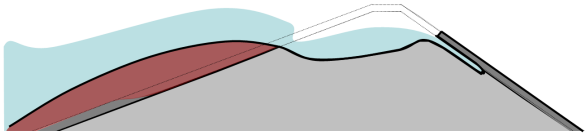
Fifth step - continued: a number of small holes in the cover on the landside is formed	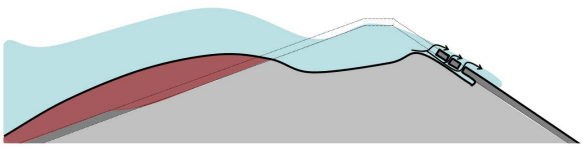
Fifth step - continued: the cover on the landside is completely removed	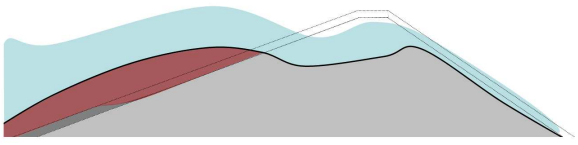

Sixth step: during the overflow the full breach is formed

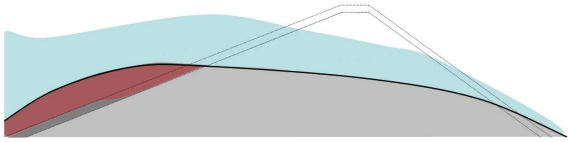

Figure 4.20: Progress of dike erosion and breaching observed in the small LWI flume

The following conclusions and observations made after the laboratory experiments in the small LWI flume:

- just after the local failure of the clay cover only a small part of the sand core becomes unprotected, the uncovered core erodes relatively slow.
- the eroded and afterwards deposited clay is mixed with the sand which decelerates the erosion of the core just after it begins;
- during the sand core erosion, the sand is eroded which undermines the clay cover, but the cover itself is still stable, it collapses just after a critical depth of undermining is reached;
- the collapsed parts of the clay cover significantly decelerate the progress of core erosion;
- the eroded sediment that is deposited on the foreland and on the lower part of the slope influences the process of wave breaking, i.e. the breaking point moves offshore. The process of beach profile formation is clearly observed;
- no mass failure was observed during the erosion of sand core, the sand is removed continuously.

Based on the above listed observations, the following implications for the detailed models arise:

- the observed transition phase between clay and sand core erosion is relatively long, and consists of surface erosion of the clay cover, erosion of the sand core, undermining and collapse of the clay cover. All those processes have necessarily to be included in the detailed model, since the assumption made in the preliminary model, which stated that the clay cover do not fail instantaneously, does not fit the reality;
- the shape of the scour hole during sand core erosion represents clearly a beach profile, so that an appropriate beach profile model should be used in the detailed model, instead of assuming the breach shape as it was done in the preliminary model;
- the eroded sediment that is deposited on the foreland influences the wave breaking processes, this phenomenon has to be accounted for in the detailed model.

5 Development of the detailed model

The detailed model represents the main part of this study. The experience gained from the preliminary model provides the indications for the improvements and extensions which are required for the development of the detailed model. Since it is found (Section 3.5.1) that the time of cover failure constitutes the key parameter needed for the estimation of the warning time, the focus should be put on the improvement of the grass and clay erosion prediction and the application of the knowledge on grass and clay erosion which has been gained from the laboratory experiments described in Chapter 4. Moreover, the detailed model should include new processes, especially water infiltration and failure in cracks, that were neglected in the preliminary model. Further improvements are made in the simulation of the processes that were already included in the preliminary model. This especially concerns the erosion of sand core, which has been shown to be of crucial importance by the new wave flume tests described in Section 4.4. The most important improvements made in the detailed model in comparison to the preliminary model can be summarized as follows:

1. The calculation of the hydraulic loading represents the main task of the improvements made in the **detailed hydrodynamic module**:

    - The impact forces on the slope, the flow field associated with wave run-up and run down, including the water layer thickness on the outer slope are calculated by a numerical model that solves the Reynolds Averaged Navier-Stokes equations using the Volume-of-Fluid method (RANS-VOF COBRAS model);
    - The effect of the water infiltration due to the mean water level and wave run-up is simulated;
    - During the erosion of the front-face of the sand core the complete wave height distribution and energy dissipation rate are calculated using a numerical model initially developed for sand dune and beach erosion (SBEACH model);
    - During two last breaching phases, i.e. front-face core erosion and core wash-out wave overtopping as well as combined overtopping and overflow are also accounted for.

2. Although a number of improvements concerning the core erosion are also made, the focus of the improvements of the **detailed morphodynamic module** is rather put on the grass and clay erosion processes:

    - Grass and clay erosion is simulated as a sum of the erosion increments induced by repeated impact pressures and flow associated with wave run-up and run-down;
    - The empirical models for grass and clay surface erosion that were developed through the laboratory experiments described in Chapter 4 are implemented;
    - The grass root reinforcement model (Section 4.3.2) is used for the calculation of the shear strength of the grass cover;
    - The shear failure in water-filled cracks in the grass and clay layers is simulated;
    - The influence of the water content in the soil on the erosion properties is accounted for;
    - A numerical equilibrium profile model (SBEACH model) is applied for the calculation of the sand core erosion;

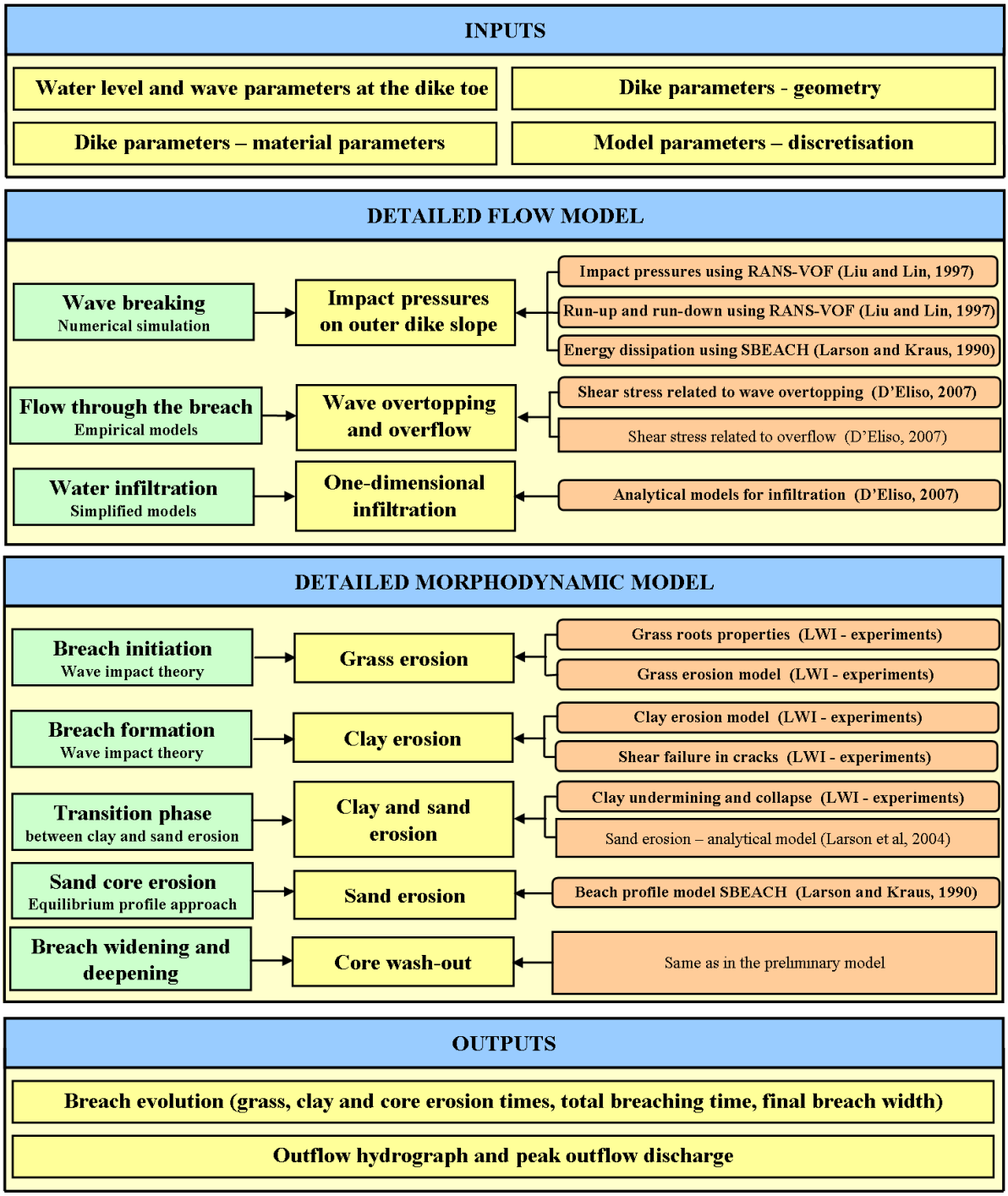

Figure 5.1: Strategy for the detailed computational model

A more detailed description of the improvements made in the hydrodynamic and morphodynamic module is given in Section 5.1 and Section 5.2, respectively. Figure 5.1 shows briefly the flow chart of the detailed model, also indicating the new processes and improvements (bold and in slightly rounded boxes) as compared to the preliminary model (Fig.3.1)

5.1 Improvements of the hydrodynamic module

The most important improvements made in the detailed hydrodynamic module compared to the preliminary model concern the completely new approach for the free surface flow which

is now calculated by a numerical RANS-VOF model instead of the empirical approach used in the preliminary model (Section 5.1.1). Furthermore, the simulation of the water infiltration into the dike is introduced (Section 5.1.2).

5.1.1 Free surface flow - simulation of breaking wave impact and flow field on the outer slope

Although the empirical models used in the preliminary model are considered to be of sufficient engineering accuracy for a simple dike geometry, this will certainly not be the case for more complicated boundary conditions. Therefore, a numerical model COBRAS which is much more versatile, has been introduced. The COBRAS (COrnell Breaking Wave And Structures) model is based on the Reynolds Averaged Navier Stokes 2DV equations, with a nonlinear, three-dimensional $k - \varepsilon$ turbulence model . The model was originally developed by NASA (Kothe et al, 1991), and after modifications made at the Cornell University (Liu and Lin, 1997) is able to deal with breaking wave impacts. The main features of the model are summarised as follows:

- A Volume-of-Fluid method is used to track the free surface;
- The equation of motion are solved using two finite difference methods, which significantly improves the accuracy of the results;
- Information on pressure, kinetic energy, horizontal and vertical velocities, free surface configuration, mass conservation is given at the model output providing a complete and very accurate information on the temporal and spatial distribution of all the essential parameters that are necessary for the simulation of sea dikes breaching.

5.1.1.1 Numerical formulation of the COBRAS model

The motion of an incompressible fluid is described using the Reynolds Averaged Navier-Stokes equations:

Continuity:

$$\frac{\partial < u_i >}{\partial x_i} = 0 \tag{5.1}$$

Momentum:

$$\frac{\partial < u_i >}{\partial t} + < u_j > \frac{\partial < u_i >}{\partial x_j} = -\frac{1}{\rho}\frac{\partial < p >}{\partial x_i} + g_i + \frac{1}{\rho}\frac{\partial < \tau_{ij} >}{\partial x_j} \tag{5.2}$$

with:

- i, j - 1,2,3 - for each of the fluid three dimensions
- u_i - $i-$th component of velocity vector
- g_i - $i-$th component of the gravity acceleration
- τ_{ij} - viscous stress
- $<>$ - symbol representing time-averaging

Kinematic boundary condition:

$$\frac{\partial < \rho >}{\partial t} + < u_i > \frac{\partial < \rho >}{\partial x_i} = 0 \tag{5.3}$$

k-ε turbulence transport model

$$\frac{\partial k}{\partial t} + < u_j > \frac{\partial k}{\partial x_j} = \frac{\partial}{\partial x_j}\left[\left(\frac{v_t}{\sigma_k} + v\right)\frac{\partial k}{\partial x_j}\right] - < u_i' u_j' > \frac{\partial < u_i' >}{\partial x_j} - \varepsilon \tag{5.4}$$

$$\frac{\partial \varepsilon}{\partial t} + < u_j > \frac{\partial \varepsilon}{\partial x_j} = \frac{\partial}{\partial x_j}\left[\left(\frac{v_t}{\sigma_\varepsilon} + v\right)\frac{\partial \varepsilon}{\partial x_j}\right] + 2C_{1\varepsilon}\frac{\varepsilon}{k} v_t S_{ij} \frac{\partial < u_i >}{\partial x_j} - C_{2\varepsilon}\frac{\varepsilon^2}{k} \tag{5.5}$$

with:

- $k = \frac{1}{2} < u_i' u_i' >$ - turbulent kinetic energy
- $\varepsilon = v\left\langle \left(\frac{\partial u_i'}{\partial x_k}\right)^2 \right\rangle$ - turbulent dissipation rate
- $v_t = C_d \frac{k^2}{\varepsilon}$ - eddy viscosity

where:

- $\sigma_k = 1.0$
- $\sigma_\varepsilon = 1.3$
- $C_{1\varepsilon} = 1.44$
- $C_{2\varepsilon} = 1.92$
- $C_d = \frac{2}{3}\left(\frac{1}{7.4 + S_{max}}\right)$
- $S_{max} = \frac{k}{\varepsilon} max\left(\left|\frac{\partial < u_i >}{\partial x_i}\right|\right)$

Linear closure model for Reynolds stresses - isotropic eddy viscosity

$$< u_i' u_j' > = -2 v_t S_{ij} + \frac{2}{3} k \delta_{ij} \tag{5.6}$$

VOF function

$$\frac{\partial F}{\partial t} + \frac{\partial}{\partial x}(uF) + \frac{\partial}{\partial y}(vF) = 0 \tag{5.7}$$

where:

- $\rho(x, y, t) = F(x, y, t)\rho_f$
- $F(x, y, t)\rho_f$ is the cell density

Partial cells treatment - obstacle boundaries

$$\frac{\partial(\theta u_i)}{\partial x_i} = 0$$

$$\frac{\partial(\theta u_i)}{\partial t} + \theta u_j \frac{\partial(\theta u_i)}{\partial x_j} = \frac{\theta}{\rho}\frac{\partial p}{\partial x_i} + \theta g_i + \theta \frac{\partial}{\partial x_j}\tau_{ij}$$

where:

- θ - relation between the cell surface open to flow and the total cell surface.

The complete description of the COBRAS model can be found in Liu and Lin (1997).

5.1.1.2 Application of the COBRAS model for the calculation of wave loads on a dike

The COBRAS model provides the complete information on the temporal and spatial distribution of all the essential parameters that are necessary for the simulation of sea dikes breaching, including breaking wave impact pressure as well as the velocity and layer thickness of the flow associated with wave run-up and run-down. However, the **latest stable version** of the model (built 250605) has still a number of limitations:

- significant computational effort - the simulation of 1 second of flow requires about 1 hour of CPU time, when a PC computer with two processors running at 2GHz is used
- the model is capable to **properly** simulate only the regular waves;
- only constant still water level can be assumed
- as one of the model constrains is that the assumed water level has to be equal thorough the entire computational domain, i.e. on the seaside and on the landside (see also Figure 5.2), the proper simulation of the flow is possible only up to the dike crest. The overtopping and overflow parameters on the inner slope during the breach widening and deepening phase have to be calculated by using other available models.

The model was used to simulate wave breaking on the slope. The main input parameters for the calculation of loading on a prototype dike are listed in Tab. 5.1. The **simplest possible dike profile** , i.e. with the horizontal foreland and without berms, was used.

Dike geometry			
Dike height H_d [m]		Outer slope n [-]	
10		6	
Incident wave parameters			
Wave height H [m]	Wave period T [s]	Water depth h [m]	Surf similarity par. ξ [-]
2.75	7	6	0.88
Numerical parameters			
Δx [m]	Δz [m]	Δt [s]	t_{max} [s]
0.2	0.1	0.1	200

Table 5.1: Main inputs for the calculation of the wave loading on the prototype dike

Figure 5.2 shows a series of free surface elevations during the wave breaking on the dike slope calculated by the model using input data summarized in Tab. 5.1. The pressure distribution, flow velocity and layer thickness for a single wave impact are shown in Figures 5.3a - 5.3c. Figures 5.3a and 5.3b provide the comparison between the impact pressures calculated by the preliminary and detailed model. Both models provide almost the same maximal impact pressure (44.0kN and 43.8kN for the preliminary and detailed model, respectively). Differences in the location and shape of the impact area can be however observed - the RANS-VOF model predicts significantly (63%) smaller impact area that is located about 0.1H lower than the preliminary model. Since the preliminary model does not calculate the flow velocity and layer thickness, the comparison of the results provided by the RANS-VOF model cannot be performed.

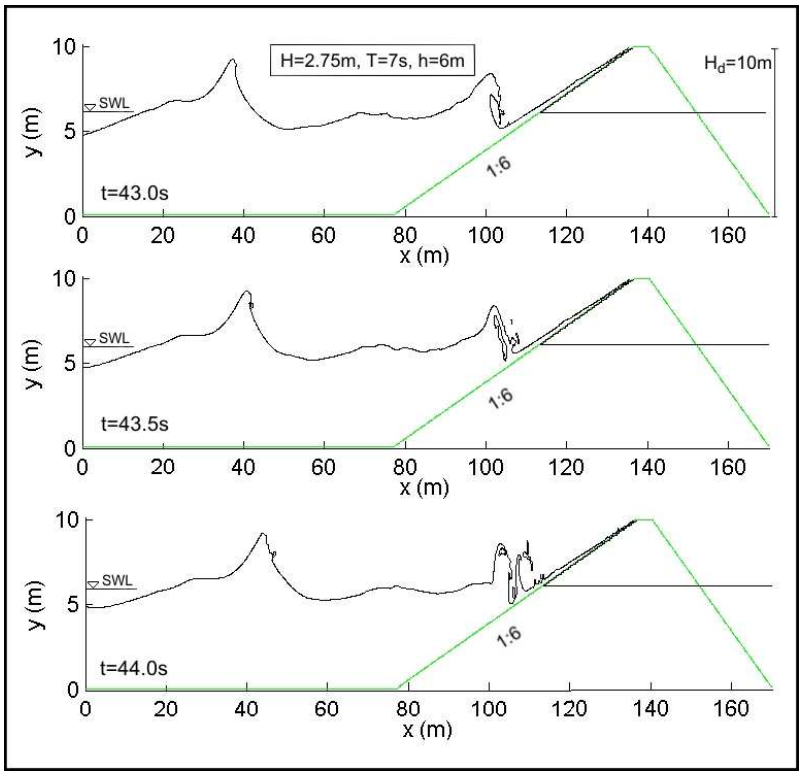

Figure 5.2: Wave breaking simulated by COBRAS - free surface elevation

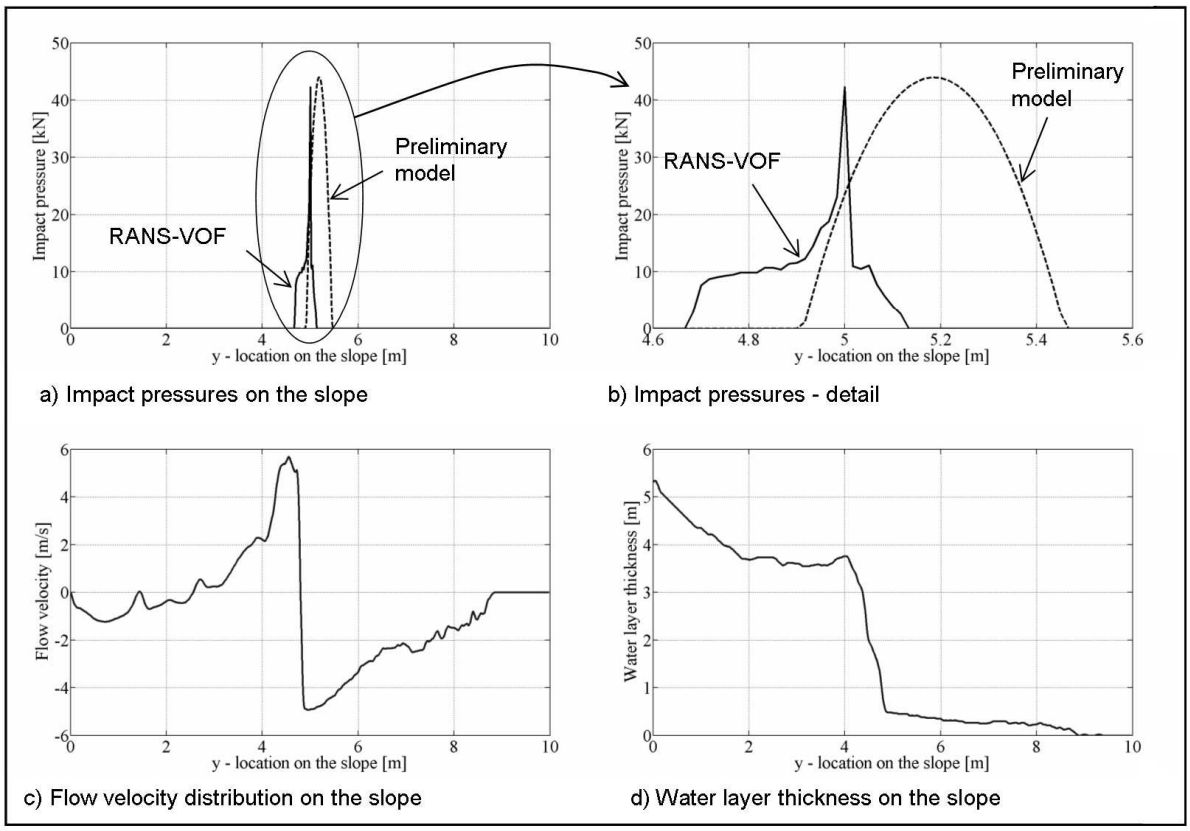

Figure 5.3: Distribution of impact pressures, velocity and layer thickness on the dike slope

5.1.2 Simulation of the erosion of the front face of the sand core

The results of the small-scale laboratory tests on the dike breaching (Husrin, 2007, Stanczak et al, 2007a) show that during the front-face erosion of the sand core rather a beach profile is formed than a vertical cliff with a horizontal bottom as assumed in the preliminary model. Based on the analysis of the available beach profile models was made (Stanczak et al, 2007b), the SBEACH model (Storm-induced BEAch CHanges) developed by Larson and Kraus (1990)) is selected for the application in the detailed model. The main advantages of the SBEACH model can be briefly summarised as follows:

- the dynamics of macroscale profile change including growth and movement of berms and breakpoints is reliably simulated;
- breaking waves represent the sole driving force causing sediment transport;
- the possibility of avalanching is accounted for;
- the model is easy to implement and economical to run.

The SBEACH model calculates the wave characteristics across-shore from a specified water depth offshore (dike outer toe) to the break point using a linear wave theory. Shoreward of the break point, a generalized form of the wave decay by Dally, Dean and Dalrymple (1984, 1985) is used for the calculation of the wave height distribution across-shore. Assuming the wave conditions to be uniform alongshore and the bottom contours to be straight and parallel, the equation for conservation of energy flux incorporating energy dissipation associated with wave breaking may be written as:

$$\frac{d}{dx}(F \cdot \cos\theta_w) = \frac{\kappa}{h}(F - F_s) \tag{5.8}$$

where:

- F - incident wave energy flux $[N \cdot m/m \cdot s]$
- F_s - wave energy flux corresponding to an equilibrium beach profile $[N \cdot m/m \cdot s]$
- θ_w - wave angle with respect to the bottom contours
- κ - empirical wave decay coefficient, recommended value $\kappa = 0.15$
- h - water depth $[m]$

Energy dissipation that is used for the sediment transport calculation is assumed proportional to the excess energy flux beyond a stable energy flux below which a wave will not decay. The incident wave energy flux is given by:

$$F = E \cdot C_g \tag{5.9}$$

where:

- E - wave energy density, $[Nm/m^2]$
- C_g - wave group velocity $[m/s]$

The wave energy density is written using linear wave theory as:

$$E = \frac{1}{8} \cdot \rho \cdot g \cdot H^2 \tag{5.10}$$

Wave group speed is a function of wave phase speed C and a factor n

$$C_g = n \cdot C \tag{5.11}$$

where:

- n - factor dependant on the water depth and on the local wave length at water depth h:

$$n = \frac{1}{2} \cdot \left[1 + \frac{\frac{2\pi h}{L}}{\sinh\left(\frac{2\pi h}{L}\right)}\right] \tag{5.12}$$

The wave celerity is determined through the dispersion relationship from linear wave theory:

$$C = C_0 \cdot \tanh\left(\frac{2\pi h}{L}\right) \tag{5.13}$$

where:

- C_0 - wave celerity in deep water $[m/s]$:

$$C_0 = \frac{gT}{2\pi} \tag{5.14}$$

- T - wave period $[s]$

The energy flux F_s determines the amount of energy dissipation necessary for an equilibrium beach profile to occur once breaking is initiated:

$$F_s = E_s \cdot C_g \tag{5.15}$$

where:

- E_s - wave energy density corresponding to an equilibrium beach profile $[N \cdot m/m^2]$:

The wave energy flux F_s corresponds to a wave height H_s that is a function of water depth h :

$$H_s = \Gamma \cdot h \tag{5.16}$$

where:

- Γ - wave height coefficient $[-]$, recommended value $\Gamma = 0.4$

Wave setup or setdown is determined from the momentum equation (radiation stress):

$$\frac{dS_{xx}}{dx} = -\rho g h \frac{d\mu}{dx} \tag{5.17}$$

where:

- S_{xx} - radiation stress component directed onshore $[m/s]$:

$$S_{xx} = \frac{1}{8}\rho g H^2 \left[n - \frac{1}{2} \right] \tag{5.18}$$

The setdown at the most seaward point is determined analytically as:

$$\eta = -\frac{\pi H^2}{4L \sinh\left(\frac{4\pi h}{L}\right)} \tag{5.19}$$

The point of incipient wave breaking is determined from an empirical criterion expressed in terms of surf similarity parameter ξ:

$$\frac{H_b}{h_b} = 1.14 \cdot \xi^{0.21} \tag{5.20}$$

Shoreward of the break point κ is set to zero, and no energy dissipation takes place since bottom friction is neglected. Once the breaking is initiated, the wave energy dissipation per unit water volume is calculated as:

$$D = \frac{\kappa}{h^2}(F - F_s) \tag{5.21}$$

The obtained wave energy dissipation forms the input data for the sediment transport calculation and consequently for the profile change calculation.

5.1.3 Wave overtopping, overflow and combined overtopping and overflow

Together with the onshore directed progress of erosion, the dike crest becomes lower and overtopping occurs, resulting in the erosion of the landside slope of the dike. As the available version of the RANS-VOF model applied for the calculation of the flow parameters on the outer slope cannot provide the required information for the inner slope, a selection of the model for the simulation of the flow on the inner slope was made. This recently developed model for dike breaching initiated by wave overtopping (D'Eliso, 2007) contains the formulae that enable one to calculate the relevant parameters of wave overtopping, overflow as well as combined wave overtopping and wave overflow.

5.1.3.1 Wave overtopping

In order to calculate the flow parameters that are necessary for the assessment of shear stress on the landside slope i.e. flow velocity and layer thickness, the approach proposed by Schüttrumpf and Oumeraci (2005) is applied. The principle sketch and definitions for the calculations is shown in Figure 5.4.
The following steps are needed for the calculation of the maximal velocity and layer thickness of wave run-up for ***regular waves***:

1. the calculation of wave run-up:

$$z_r = 2.25 \cdot \tanh(0.5 \cdot \xi_d); \quad \xi_d = \frac{\tan\alpha}{\sqrt{H/L}}; \quad L = \frac{gT2}{^2\pi} \tag{5.22}$$

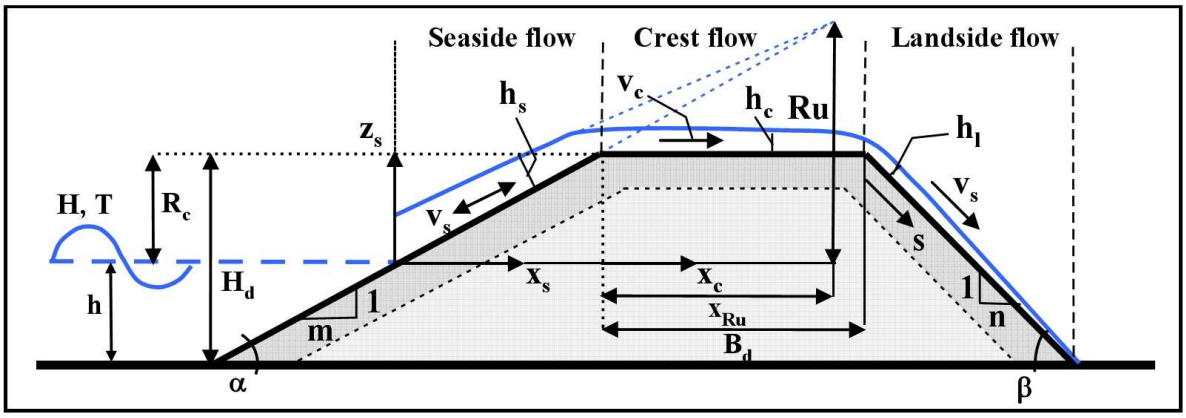

Figure 5.4: Definition sketch for the calculation of the overtopping parameters (D'Eliso, 2007)

2. the calculation of the layer thickness and velocity of the wave run-up on the outer slope, i.e $z_s \leq R_c$:

$$h_s(x_s) = 0.057 \cdot (x_{zr} - x_s) \tag{5.23}$$

$$v_s(x_s) = \frac{\pi \cdot H}{T} \cdot \frac{1.03}{\tan\alpha} \cdot \xi_d \cdot \sqrt{\frac{z_r - z_s}{H}} \tag{5.24}$$

3. the calculation of the flow on the crest; $x_c < \left(\frac{R_c}{\tan\alpha} + B_d\right)$:

$$\frac{h_c(x_c)}{h_s(H_d)} = \exp\left(-0.58 \cdot \frac{c_x}{B_d}\right) \tag{5.25}$$

$$v_c(x_c) = v_s(H_d) \cdot \exp\left(-\frac{f \cdot x_c}{2 \cdot h_c(x_c)}\right); \quad f = 0.02; \tag{5.26}$$

4. the calculation of the landward flow; $s \leq H_d \cdot \sin\beta$:

$$v_l(s) = \frac{v_c(B_d) + \frac{k_l(s) \cdot h_l(s)}{f} \cdot \tanh\left(\frac{k_l(s) \cdot t}{2}\right)}{1 + \frac{f \cdot v_c(B_d)}{h_l(s) \cdot k_l(s)} \cdot \tanh\left(\frac{k_l(s) \cdot t}{2}\right)} \tag{5.27}$$

$$h_l(s) = \frac{v_c(B_d) \cdot h_c(B_d)}{v_l(s)} \tag{5.28}$$

$$t \approx -\frac{v_c(B_d)}{g\sin\beta} + \sqrt{\frac{v_l(s)^2}{g^2\sin^2\beta} + \frac{2 \cdot s}{g\sin\beta}}; \quad k_l = \sqrt{\frac{2 \cdot f \cdot g \cdot \sin\beta}{h_l(s)}} \tag{5.29}$$

The flow discharge per unit width:

$$q = h_l \cdot v_l \tag{5.30}$$

The flow parameters obtained with Eqs. 5.22 - 5.30 represent the peak flow within a wave period. In order to take also the flow variation into consideration, each overtopping event is divided into five time steps, with the following assumptions imposed (D'Eliso, 2007):

- the flow discharge variation in time are assumed to have a triangular shape (Fig. 5.5a)
- the Froude number defined at each point along the dike profile $Fr = v_l/\sqrt{g \cdot h_l}$ is constant with time (Fig. 5.5b)
- the flow velocity and depth are calculated as (Figs. 5.5c and 5.5d):

$$q = h_s \cdot v_l; \quad Fr = \frac{v_l}{\sqrt{g \cdot h}} \Rightarrow h = \left(\frac{q}{Fr \cdot \sqrt{g}}\right)^{2/3}; \quad v_l = \frac{q}{h_l} \tag{5.31}$$

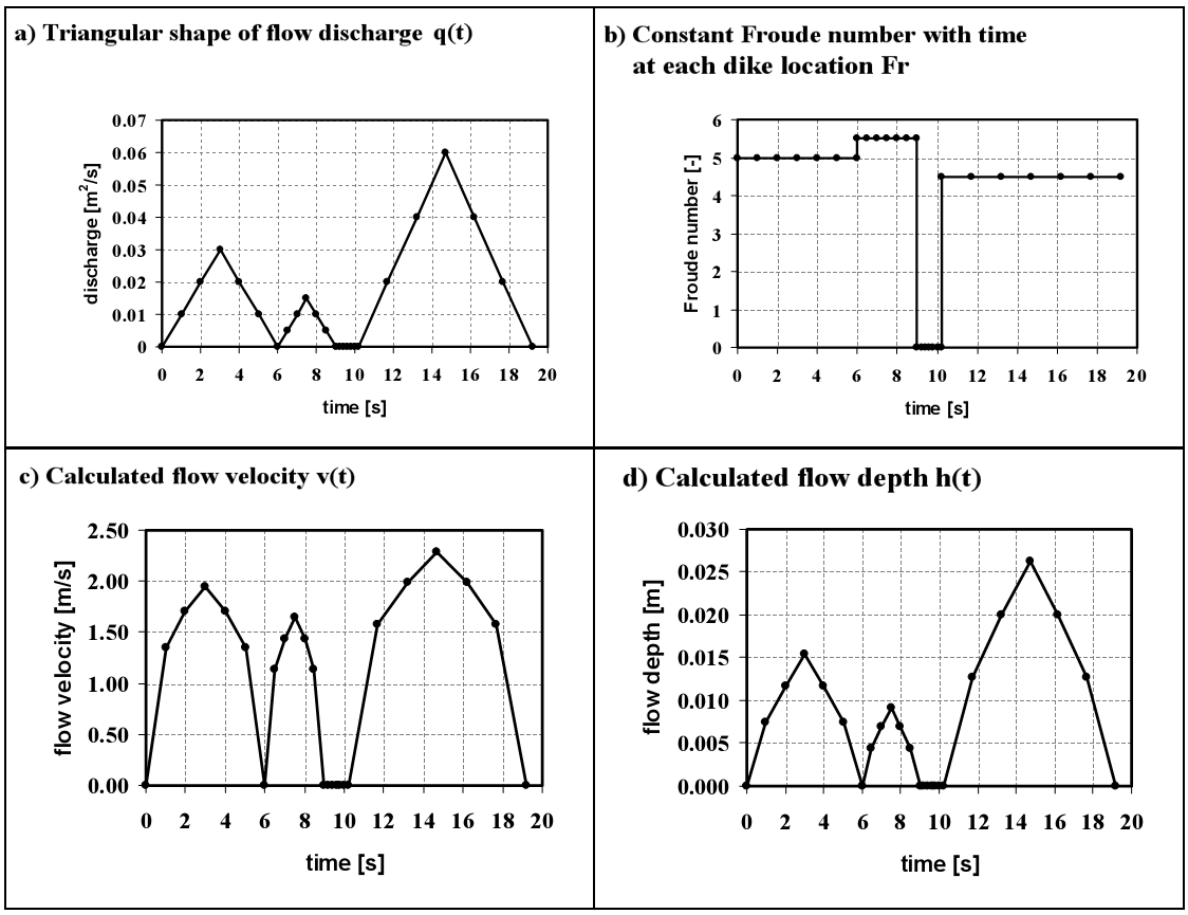

Figure 5.5: Flow properties at the dike within a wave period (D'Eliso, 2007)

5.1.3.2 Combined wave overtopping and overflow

Combined wave overtopping and overflow is defined as the sum of the wave overtopping and overflow due to high water level. The combined flow region consisting of two flow transitions and two subregions is shown in Figure 5.6. In the model an approach developed by D'Eliso (2007) for the dike breaching initiated by wave overtopping is selected for the implementation.

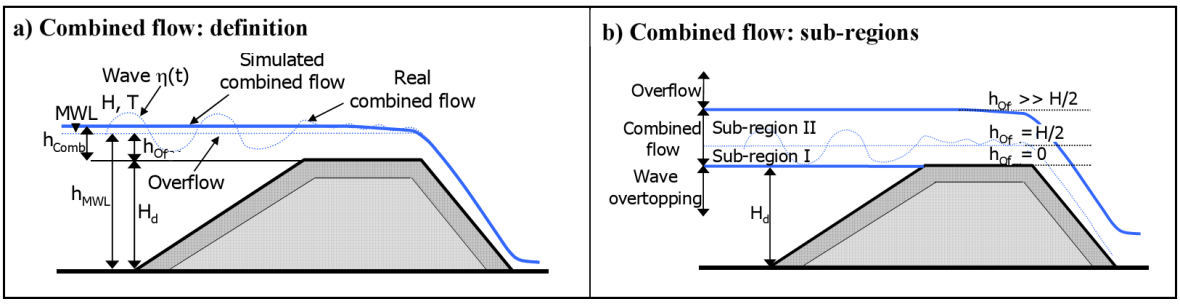

Figure 5.6: Combined flow - definition sketch (D'Eliso, 2007)

The flow discharge in the first region, i.e. between wave overtopping and combined flow ($h_{of} < H/2$) is calculated as:

$$q_{\overline{comb}} = \left| q_{comb} - \left(\frac{H/2 - h_{of}}{H/2} \right) \cdot (q_{comb} - q)_{h_{of}=0} \right| \tag{5.32}$$

where:

$$h_{over} = MWL - H_d \tag{5.33}$$

$$q_{comb} = \frac{1}{T} \int_0^T \left(\frac{2}{3} \cdot \mu_{comb} \cdot \sqrt{2 \cdot g} \cdot (h_{of} + \eta(t))^{1.5} \right) \mathrm{dt}; \qquad \mu_{comb} = 0.4728 \cdot \xi_d \tag{5.34}$$

In the second region, i.e $h_{of} > H/2$ the flow discharge is calculated as:

$$q_{comb} = \frac{2}{3} \cdot \sqrt{2 \cdot g} \left(\mu_{comb} \cdot h_{comb}^{1.5} + \left(\frac{h_{of} - H/2}{h_{comb} - H/2} \right) \cdot (\mu_{over} \cdot h_{of}^{1.5} - \mu_{comb} \cdot h_{comb}^{1.5}) \right) \tag{5.35}$$

After the combined wave overtopping and overflow becomes overflow, the flow through the breach channel is calculated

5.1.4 Water infiltration

Recently performed experimental tests on the clay erosion resistance (Husrin, 2007) confirmed significant influence of the water content on the erosion properties of the cohesive soils used for the construction of the dike revetment. Furthermore, the increase of water content resulting from infiltration determines the cohesion decrease and consequently the increased possibility of shear failure occurrence in water-filled cracks. Therefore a reliable model for the calculation of water infiltration into the soil is needed. Since the problem of infiltration

was deeply treated in the companion PhD of D'Eliso (2007) and successfully implemented into a dike breachin model, in the present study generally the same approach will be used.

This section addresses the Richard's equation (Richards, 1931) which is a non-linear partial differential equation that represents the movement of water in unsaturated soils. The Richards equation is difficult to solve since it does not have a closed-form analytical solution, so usually simplified solvers are used.

5.1.4.1 Richard's equation

The 2D Richard's equation is the continuity equation of the flow in the unsaturated soil and reads (Richards, 1931):

$$\frac{\partial}{\partial x}\left(k_x \frac{\partial \Psi}{\partial x}\right) + \frac{\partial}{\partial y}\left(k_y \frac{\partial \Psi}{\partial y}\right) + Q = \frac{\partial \theta_c}{\partial t} \tag{5.36}$$

where:

- k - hydraulic conductivity; $\mathbf{k}(\psi) = (k_x(\psi), k_y(\psi))$
- ψ - flow head; $\psi = z + \frac{u}{\rho_w g}$
- θ_C - volumetric water content; $\theta = \frac{V_w}{V_s}$
- Q - boundary flux.

In order to solve the Richard's equation, the following soil properties have to be known:

- **saturated hydraulic conductivity** (soil permeability) - empirical parameter, decreasing from sand to clay soils. A number of references with typical values for different types of soil is available (Table 5.2). At the location of cracks in clay cover the permeability increases and this effect has necessarily to be accounted for during the simulation of water infiltration.

Material	k_s	Reference
Grass	$1.30 \cdot 10^{-7} \div 10^{-5}$	Holtan, 1961; Pilarczyk,2003
Clay	$5.56 \cdot 10^{-8} \div 1.67 \cdot 10^{-7}$	Weissmann, 2003; Rawsl et al, 1992
Sand	$8.25 \cdot 10^{-5} \div 5.83 \cdot 10^{-5}$	Weissmann, 2003;Rawsl et al, 1992
Cracks in clay	$1 \cdot 10^{-4} \div 1 \cdot 10^{-5}$	TAW, 1996

Table 5.2: Typical values of the hydraulic conductivity k_s (D'Eliso et al, 2007)

- **soil-water characteristic curve** that describes the relationship between suction pressure and volumetric water content. Two methods to obtain the soil-water characteristic curve are given:
  - van Genuchten's curve (1980);
  - Brooks and Corey's curve (1964).

  both of them are the function of the pore size distribution index N (see Table 5.3) and air entry value h_b (see Table 5.4).

As already discussed by D'Eliso et al (2007) the application of the numerical solver of the Richard's equation is unfeasible for the purposes of a dike breaching module and the implementation of one of the available simplified solutions is suggested. Therefore only the application of two simplified models (Wang, 2000 and Wang et al, 2003) will be here addressed.

Type of soil	N	Reference
Sand	$0.4 - 1.68$	Brankensiek et al., 1981; Carsel and Parrish, 1988
Sandy loam	$0.40 - 0.89$	Brankensiek et al., 1981; Carsel and Parrish, 1988
Clay loam	$0.28 - 0.40$	Brankensiek et al., 1981; Carsel and Parrish, 1988
Clay	$0.09 - 0.41$	Brankensiek et al., 1981; Carsel and Parrish, 1988

Table 5.3: Typical values of the pore size distribution index N (D'Eliso et al, 2007)

Type of soil	h_b	Reference
Sand	$3.58 - 35.30$	Brankensiek et al., 1981; Carsel and Parrish, 1988
Sandy loam	$9.09 - 29.21$	Brankensiek et al., 1981; Carsel and Parrish, 1988
Clay loam	$31.25 - 69.55$	Brankensiek et al., 1981; Carsel and Parrish, 1988
Clay	$10.0 - 125.00$	Brankensiek et al., 1981; Carsel and Parrish, 1988

Table 5.4: Typical values of the air entry value h_b (D'Eliso et al, 2007)

5.1.4.2 Wang Z model

The Wang Z model (Wang, 2000) is a simplified infiltration model that calculates the saturated water front using the Darcy's equations as:

$$z_s(t) = \sqrt{2 \cdot \alpha \cdot k_s \int_0^t h(t)dt} \tag{5.37}$$

with:

- z_s- vertical coordinate of the saturated water front $[m]$
- α_c - coefficient, $\alpha_c = 4.5$ $[-]$

The infiltration water front is calculated as:

$$z_w(t) = \sqrt{2 \cdot \beta_c \cdot k_s \int_0^t h(t)dt} \tag{5.38}$$

where: β_c - coefficient, $\beta_c = 15 \cdot \alpha = 67.5[-]$
The volumetric water content θ can be calculated either using the model of Wang Q (Section 5.1.4.3) or assuming the linear distribution along the vertical infiltration path as:

$$\theta_c(z_s) = \theta_s \tag{5.39}$$
$$\theta_c(z_w) = \theta_i \tag{5.40}$$

and:

- θ_s - saturated volumetric water content $[m^3/m^3]$ - see Tab. 5.5
- θ_i - initial volumetric water content $[m^3/m^3]$ - see Tab. 5.6
- θ_r - residual volumetric water content $[m^3/m^3]$ - see Tab. 5.7

Type of soil	θ_s	Reference
Sand	$0.35 - 0.43$	Brankensiek et al., 1981; Weissmann, 2003
Sandy loam	$0.41 - 0.44$	Weissmann, 2003; Carsel and Parrish, 1988
Clay loam	$0.39 - 0.48$	Weissmann, 2003; Brankensiek et al., 1981
Clay	$0.36 - 0.48$	Weissmann, 2003; Brankensiek et al., 1981

Table 5.5: Typical values of the saturated volumetric water content θ_s (D'Eliso et al, 2007)

Soil condition	θ_i
Dry	$\theta_r \div \theta_r + 0.3(\theta_s\theta_r)$
Medium	$\theta_r + 0.3(\theta_s\theta_r \div \theta_r + 0.6(\theta_s\theta_r)$
Wet	$\theta_r + 0.6(\theta_s\theta_r) \div \theta_s$

Table 5.6: Typical values of the initial volumetric water content θ_i (D'Eliso et al., 2007)

Type of soil	θ_s	Reference
Sand	$0.020 - 0.054$	Brankensiek et al., 1981; Weissmann, 2003
Sandy loam	$0.045 - 0.118$	Weissmann, 2003; Carsel and Parrish, 1988
Clay loam	$0.095 - 0.185$	Weissmann, 2003; Brankensiek et al., 1981
Clay	$0.068 - 0.226$	Weissmann, 2003; Brankensiek et al., 1981

Table 5.7: Typical values of the residual volumetric water content θ_r (D'Eliso et al, 2007)

The following assumptions are imposed in the model:

- the hydraulic gradient is a function of the mean water depth on the surface of the dike
- the calculation domain is limited only to the saturated soil, the influence of the unsaturated soil on the process of infiltration is limited to the empirical coefficient α

5.1.4.3 Wang Q model

The Wang Q model (Wang et al, 2003) is based on the following assumptions:

- 1D vertical infiltration is simulated
- the water-soil characteristic curve by Brooks and Corey (1964) are used
- the Richard equation is solved analytically using a Taylor series method

The infiltration water front is calculated solving Eq. 5.41 while the volumetric water content is calculated using Eq. 5.42.

$$t = \frac{\theta_s - \theta_i}{(1 + \alpha_c)k_s}\left(z_w - \frac{ln(\beta z_w + 1)}{\beta}\right) \tag{5.41}$$

$$\theta_c(z) = \theta_r + \left(1 - \frac{z}{zw}\right)_c^{\alpha}(\theta_s - \theta_r) \tag{5.42}$$

where:

- $\alpha_c = N/M$; $M = 2 + 3N$

  with N - pore size distribution index $[-]$

- $\beta_c = M/h_b$

  with h_b - air entry value $[cm]$

5.1.4.4 Comparison of the infiltration models

In order to compare the results provided by the simplified infiltration model, an idealized simulation has been performed. The following data were used:

- dike height $H_d = 10m$
- mean water level at the toe of the dike $h = 6m$
- irregular waves, $H_s = 1.47m$ $T_p = 4.7s$
- thickness of the clay layer $d_c = 1.5m$
- time of simulation $t_{sim} = 120min$
- soil parameters for clay and sand as given in Tabs.5.2-5.4

In Fig. 5.7 the comparison of the results provided by the Wang Q and Wang Z models is shown. Although the same input data set were used, the results substantially differ. In the detailed model both methods for the calculation of the saturated front are implemented and the one to be used can be freely chosen by the user. The application of the Wang Q model in the dike breaching model provides more conservative results concerning breaching times, but the infiltration model itself is more demanding in terms of computational effort.

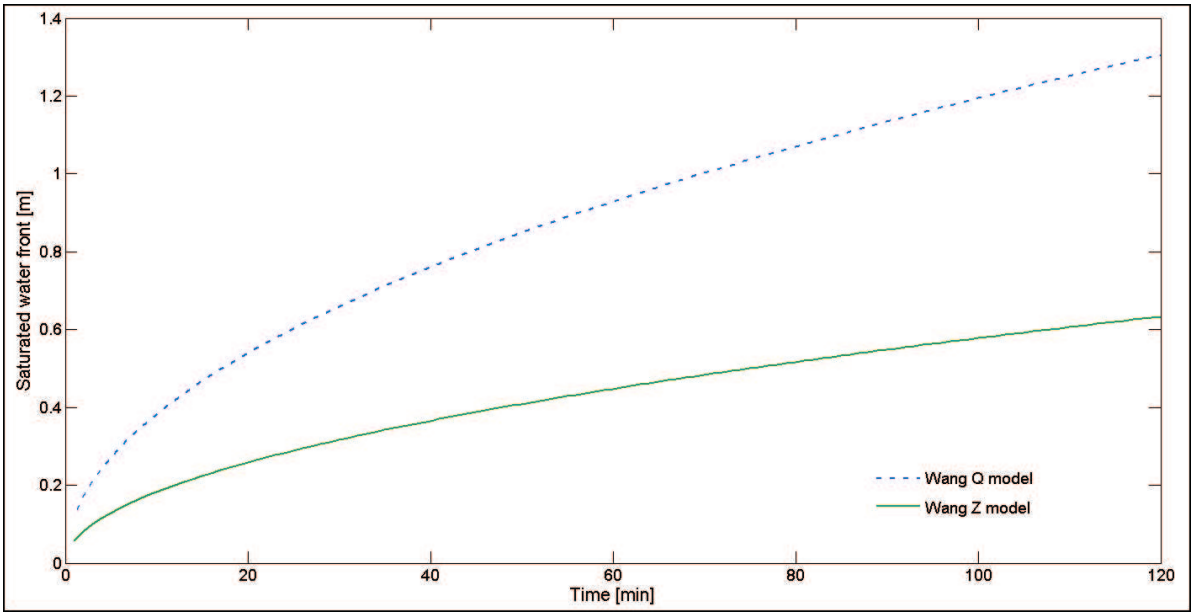

Figure 5.7: Comparison of the saturated fronts calculated using Wang Q and Wang Z models

5.2 Improvements of the morphodynamic module

The focus of the improvements made in the detailed morphodynamic module is on the phase of breach initiation, as it was found to be of crucial importance in the simulations using the preliminary model. The results of the laboratory experiments (Chapter 4) on the surface erosion of grass and clay and the local failure in cracks as well as the laboratory tests on the reinforcement properties of grass roots are implemented in the detailed model. Furthermore, the total progress of erosion during the first two phases is calculated as a sum of (i) erosion increments resulting from successive impact pressures, that act on a very limited area and (ii) erosion increments resulting from shear stress induced by the cyclic flow associated with wave run-up and run-down that acts on larger areas. For the simulation of the sand core erosion the results of the small scale tests on the entire process of dike breaching (Stanczak et al, 2007a, Husrin, 2007) are used. Furthermore, during the last two breaching phases also the erosion of the inner slope resulting from possible overtopping is accounted for.

5.2.1 Breach initiation - cover erosion

As already discussed in Section 3.5.1 the dike breach is considered to be initiated when the grass and clay cover failed. The laboratory experiments performed in the framework of this thesis show that it is not only possible, but also convenient, to treat the entire dike revetment as a clay layer that is partially reinforced by vegetation (Stanczak et al, 2007a). This approach allows one to simulate the grass and clay erosion processes continuously and to take the local variations in both materials into consideration. After the grass cover failed at one location, it still reinforces the remaining part of the slope. The assumption made in the preliminary model stating that grass cover fails simultaneously on the entire slope is therefore removed in the detailed model.

5.2.1.1 Combined action of impact pressures and flow associated with wave run-up and run-down

The data provided by the hydrodynamic module contains information on impact pressure, flow velocity and layer thickness for each time step and for each node of the numerical mesh, which enables one to calculate the erosion for each time step as a sum of the erosion increments due to impact pressure and erosion increments due to shear stress induced by the flow associated with wave run-up and run-down. The following models are selected for the simulation of grass and clay erosion:

- Excess shear approach (Temple et al, 1987) is used for the calculation of erosion due to the flow associated with run-up and run-down. The protective properties of the grass stems are accounted for in the grass cover factor (C_f) thus reducing the effective shear stress on the soil.
- The surface erosion model developed after the laboratory experiments described in Chapter 4 is applied for the calculation of the erosion due to impact pressures. The grass root reinforcement model is applied in order to include the effects of a grass cover;
- The presence of cracks and fissures is accounted for and the possible shear failure in cracks subject to impact pressure is simulated.

5.2.1.2 Erosion due to impact pressures

The following formula (see also Eq. 4.1) that was derived from the laboratory experiments forms the basis for the calculation of local surface erosion due to impact pressures:

$$d_i = k_{d,p,i} \cdot p_i \cdot e^{-wh_i} \tag{5.43}$$

where the following notation is used:

- d_i - depth of erosion at the *i*-th node resulting from a single impact pressure event $[m]$;
- $k_{d,p,i}$ - soil detachability coefficient for a unit area calculated at the *i*-th node $[m^3/N]$;
- p_i - impact pressure at the *i*-th node $[N/m^2]$;
- w - coefficient representing the damping effectiveness of a water layer $[-]$
- h_i - water layer thickness at the *i*-th node $[m]$

The empirical coefficient $k_{d,p,i}$ depends on the soil parameters - type of clay and on the water content. For the clay of the erosion resistance Category 1 according to the Dutch requirements (TAW, 1996) the erodibility coefficient $k_{d,p}$ can be calculated as the following function of the water content that was derived from laboratory experiments by Husrin (2007):

$$k_{d,i} = 0.35 \cdot \text{arctan}[110 - (wc - 0.43)] \cdot 10^{-12} \quad [m^3/Pa] \tag{5.44}$$

In Fig. 5.8 the comparison of the measured erodibility coefficients with Eq. 5.44 is provided. The increase of the erodibility coefficient even up to one order of magnitude that results from the variations in the water content may be observed. The measured values for other types of clay can be found in the progress report by Stanczak et al, (2007a).

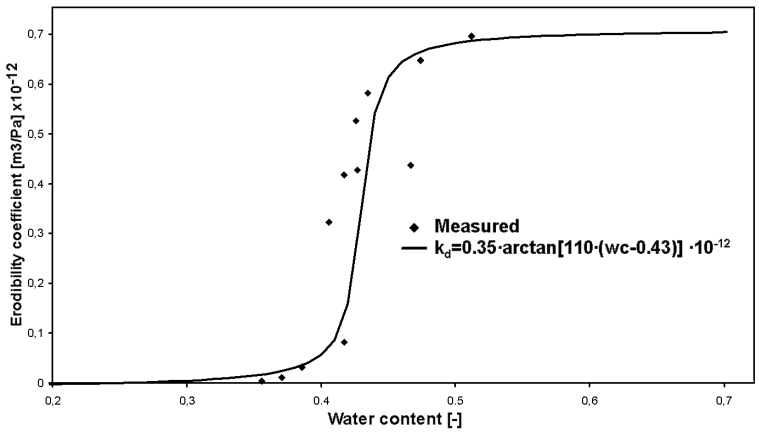

Figure 5.8: Erodibility of the clay as a function of water content

In the uppermost layer of the clay cover the soil is reinforced by the grass roots. The modified erodibility coefficient $k_{d,g,p}$ is a function of (i) the dimensionless parameter b that describes the influence of the roots on the erodibility and (ii) of the Root Volume Ratio RVR:

$$k_{d,g,p,i} = \frac{k_{d,p,i}}{b \cdot RVR_i^2} \quad [cm^3] \tag{5.45}$$

The Root Volume Ratio RVR can be calculated as a function of the depth under the grass surface. Two models that describe the distribution of the root volume ratio RVR underneath the soil surface are available (Sprangers, 1999 and Stanczak et al, 2007f):

$$RVR = A \cdot D^{(d-d_{cor})} \quad [\%] \tag{5.46}$$

where A, D and d_{cor} are the empirical coefficients that depend on the quality of grass cover while d is the depth under the surface given in centimeters. The coefficients A and D are supposed to have a negative correlation with the clay quality, since stronger clay prevents the grow of a dense root network. In Tab. 5.8 the coefficients suggested by different authors are given.

A	D	d_{cor}	b	Reference
2.67	0.8	1.5	-	Sprangers (1999)
1.58	0.75	2.0	5	Stanczak et al (2007a)

Table 5.8: Coefficients describing the grass roots distribution and their effect on soil erodibility

The erodibility parameter for the whole revetment $k_{d,t,p,i}$ can be then calculated taking the critical erosion depth into account as:

$$\begin{aligned} k_{d,t,p,i} &= \frac{k_{d,p,i}}{b \cdot RVR^2} \qquad \text{for} \qquad d < d_{crit} \\ k_{d,t,p,i} &= k_{d,p,i} \qquad \text{for} \qquad d > d_{crit} \end{aligned} \tag{5.47}$$

5.2.1.3 Erosion due to shear stress induced by the flow associated with wave run-up and run-down

The detachment of the soil particles during the surface erosion of the clay cover due to the flow associated with wave run-up and run-down occurs if the effective shear stress is greater than the critical shear stress for the soil. The erosion is then calculated according to the excess effective shear stress approach (Meyer, 1964) as:

$$\frac{dz}{dt} = k_d(\tau_0 - \tau_{0,cr})dt \tag{5.48}$$

with:

$$\tau_0 = \rho_w g h J \tag{5.49}$$

and:

- dz - incremental erosion depth $[m]$
- k_d - detachability coefficients that depend on the soil properties $[m \cdot N^{-1}s^{-1}]$
- $\tau_{0,cr}$ - critical shear stress for the given type of soil $[N/m^2]$
- h - water depth $[m]$
- J - energy slope $[-]$

The detachability coefficient is calculated as a function of the dry soil density $\rho_{c,d}$ and the weight percentage of the clay in the soil $c_{\%}$ as (Temple and Hanson, 1994):

$$k_d = 10^{-6}\frac{10\rho_w}{\rho_{c,d}}\exp\Big[-0.121c_{\%}^{0.406}\Big(\frac{\rho_{c,d}}{\rho_w}\Big)^{3.1}\Big] \tag{5.50}$$

where:

- ρ_w - water density $[kg/m^3]$
- $\rho_{c,d}$ - bulk soil density $[kg/m^3]$

The energy slope J is calculated using the Manning formula:

$$J = \frac{n^2 \cdot v^2}{h^{4/3}} \tag{5.51}$$

where the Manning roughness n is calculated as (Temple and Hanson, 1994):

$$n = \frac{D_{75}^{1/6}}{14.2301} \tag{5.52}$$

with:

- D_{75} - 75% sediment size $[mm]$

The critical shear stress $t_{0,ct}$ is calculated as (D'Eliso, 2007):

$$\tau_{0,cr} = 5.43 \cdot 10^{-6}\Big(\rho_{c,d} \cdot \frac{\rho_{cw} - \rho_w}{\rho_{c,d} - \rho_w}\Big)^{2.28} \tag{5.53}$$

where ρ_{cw} denotes the density of the clay-water mixture, which is typically equal to about 1100kg/m^3.

The protective properties of the grass cover are described by the grass cover factor C_f which represents the decrease of the effective shear stress due to the flow resistance of the stems. The calculation of the effective shear stress taking the influence of the vegetation into account is performed using the following approach (Temple et al, 1987);

$$\tau_{0,e} = \tau_0(1 - C_f)\Big(\frac{n_{soil}}{n_{tot}}\Big)^2 \tag{5.54}$$

with:

- $\tau_{0,e}$ - effective bottom shear stress $[N/m^2]$
- C_f - factor describing the influence of the grass cover on the effective shear stress $[-]$
- n_{soil} - Manning roughness of the soil $[s \cdot m^{-1/3}]$
- n_{tot} - total Manning roughness (taking the grass cover into account) $[s \cdot m^{-1/3}]$

The empirical factor C_f depends on the type of the grass cover and takes the values in the range 0-1. C_f-values for a number of grass species are given by Temple et al (1987).

The total Manning roughness is calculated using the following formula given by Temple et al (1987):

$$n_{tot} = 0.3048^{-\frac{1}{3}} \exp\{C_I[0.01331ln^2(10.7639q) - 0.0954ln(10.7639q) + 0.297] - 4.16\} \tag{5.55}$$

where C_I denotes the curve retardance factor calculated as $C_I = 2.5(L_s\sqrt{\rho_g})^{0.333}$, and:

- L_S - stem length $[m]$. The suggested values is in the range 0.08-0.2m
- ρ_g - number of stems per m^2 $[1/m^2]$. Typically takes value $\rho_g = 500 - 5500m^{-2}$, depending on the grass species.

In the case the grass species are unknown, the curve retardance factor C_I and grass cover factor C_f can be assumed as given in Tab. 5.9 (Temple and Hanson, 1994):

Grass cover quality	Grass cover factor C_f	Curve retardance factor C_I
Good	0.75	5.6
Moderate	0.5	5.0
Poor	0.25	4.4

Table 5.9: Grass cover factor and curve retardance factor for idealized scenarios

No formula for the critical shear stress for grass cover was found in the literature. The performed measurements however suggest values in the range of $\tau_{0,cr} = 34.8 - 184.2N/m^2$ depending on the grass quality (Fischerich, 2001).

5.2.1.4 Shear failure in fissures and cracks

Randomly located cracks are generated as a part of the definition of dike geometry. The maximal crack depth $d_{crack,max}$ expressed in centimeters is limited to $d_{crack,max} = 3 \cdot V_s$, where V_s is the soil shrinkage expressed in percent (Richwien, 2002). Since the soil shrinkage is in the range of $V_s = 5 \div 30\%$, depending on the soil parameters, the maximal crack depth is limited to $d_{crack,max} = 0.15 \div 0.9[m]$. At the cracks the limit state equation for the shear failure (Eq. 4.9) is solved, and if the failure occurs, the dimensions of the cracks are updated with the calculated angle of shear failure.

5.2.2 Undermining and mass instability of the clay cover

According to the simulations of dike breaching initiated from the seaside by breaking wave impact performed in the small LWI wave flume (Husrin, 2007, Stanczak et al, 2007a) the remaining part of the clay cover after breach initiation still plays an important protective role. The assumption made in the preliminary model, stating that the entire clay cover is removed from the dike after the breach initiation is therefore not fully consistent. Actually, a transition phase containing the erosion of both clay cover and sand core was observed between the clay erosion phase and the sand core erosion phase (Figure 5.9).

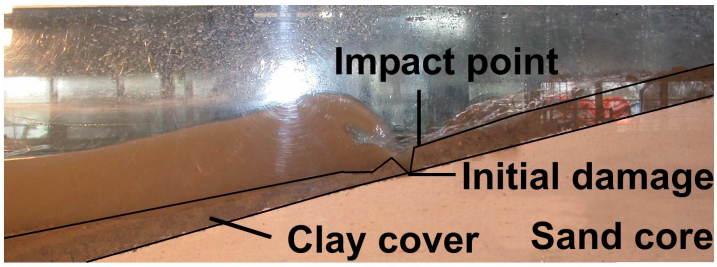

a) Begin of the transition phase

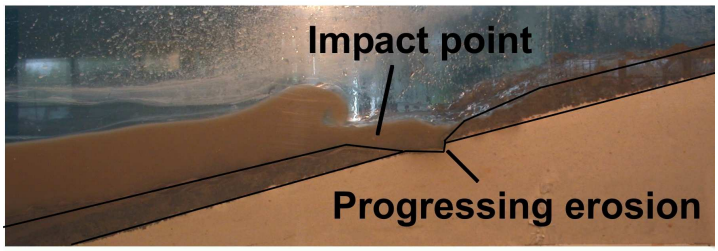

b) Transition phase

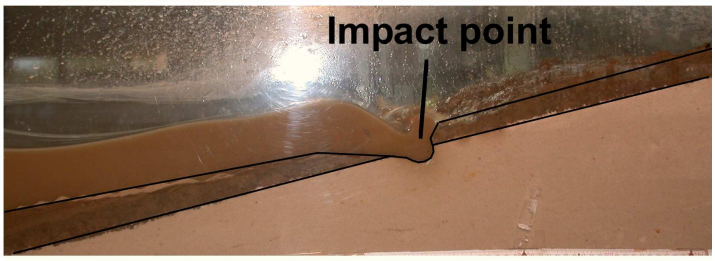

c) End of the transition phase

Figure 5.9: Transition phase between cover and core erosion

This transition phase begins immediately after the end of the clay erosion phase, i.e. when the eroded hole in the clay layer has reached at least one point of the sand core and ends when the dimensions of the scour hole have grown up to the point when the plunge point is located on the uncovered sand core. In the detailed model, during the transition phase the erosion of clay is calculated as in the preceding phase (Eqs. 5.43 - 5.52), while the progress of sand core erosion is calculated as in the preliminary model, i.e. by applying the wave impact approach of Larson et al (2004) for sand dune erosion (Eq. 3.27). Since the progress of sand core erosion is significantly faster than that of the clay layer undermining and consequently the collapse of the clay layer is observed (Fig. 5.10).

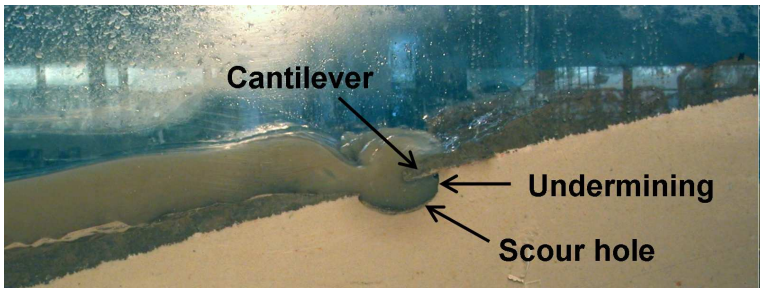

Figure 5.10: Undermining of the clay layer during the transition phase

Three failure modes for the clay cantilever can theoretically occur: bending, shearing and sliding. However, based on the observations during tests in the wave flume it can be stated, that bending is the dominant failure mode. The critical length of the undermined clay cantilever is

then calculated as (Fig. 5.11) :

$$l_{crit} = \sqrt{\frac{c \cdot d_c}{3 \cdot \rho_c \cdot g}} \tag{5.56}$$

with:

- l_{crit} - critical cantilever length $[m]$

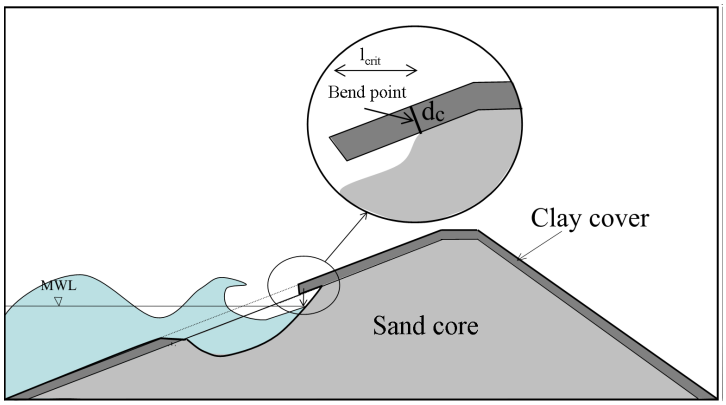

Figure 5.11: Bending of the undermined clay cantilever - definition sketch

5.2.3 Front face erosion of the sand core - beach profile formation

In the preliminary model the erosion of sand core was calculated as a linear dependency of the eroded soil volume on the impact force. The tests performed in small wave flumes (Husrin, 2007 and c.f. Chapter 4) clearly showed that in the reality this process is rather driven by the formation and evolution of a beach profile (see Figure 5.12a)

a) Beach profile development in the wave flume tests at LWI

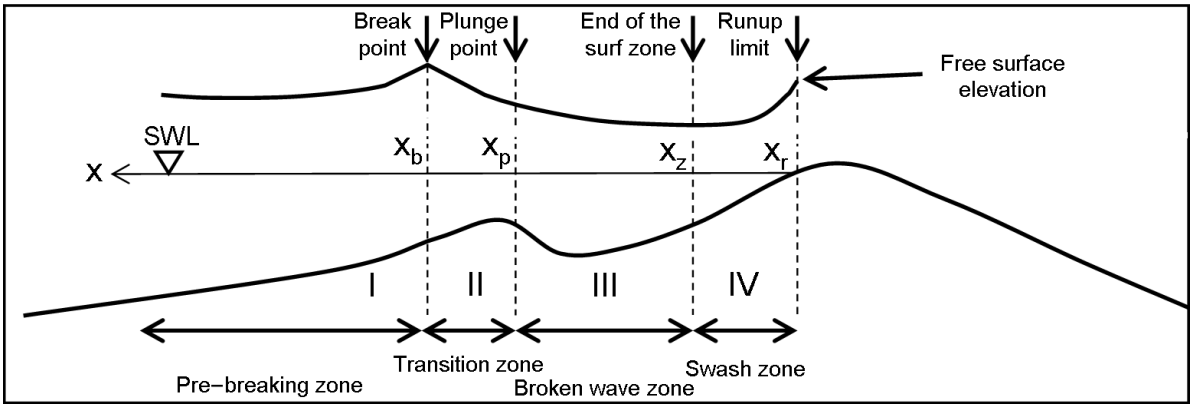

b) Principal zones of cross-shore transport

Figure 5.12: Formation of beach profile and cross-shore transport zones

The identification of regions with different wave characteristics requires an analysis of the net transport rates in the following zones (see also Figure 5.12b):

- **pre-breaking zone** (zone I) - from the seaward depth of effective sand transport to the breaking zone
- **breaker transition zone** (zone II) - from the break point to the plunge point
- **broken wave zone** (zone III) - from the plunge point to the swash zone
- **swash zone** (zone IV) - from the shoreward boundary of the surf zone to the shoreward limit of runup

The sediment transport rate relationships for each zone (see Fig.5.12b) are then given as (Larson and Kraus, 1989):

- Zone I ($x_b < x$):
$$q = q_b \cdot e^{-\lambda_1 (x - x_b)} \tag{5.57}$$
- Zone II ($x_p < x \leq x_b$)
$$q = q_p \cdot e^{-\lambda_2 (x - x_p)} \tag{5.58}$$
- Zone III ($x_z < x \leq x_p$)
$$q = \begin{cases} K\left(D - D_{eq} + \frac{\varepsilon}{K}\frac{\mathrm{dh}}{\mathrm{dx}}\right) & D > \left(D_{eq} - \frac{\varepsilon}{K}\frac{\mathrm{dh}}{\mathrm{dx}}\right) \\ 0 & D \leq \left(D_{eq} - \frac{\varepsilon}{K}\frac{\mathrm{dh}}{\mathrm{dx}}\right) \end{cases} \tag{5.59}$$
- Zone IV ($x_r < x \leq x_z$)
$$q = q_z\left(\frac{x - x_r}{x_z - x_r}\right) \tag{5.60}$$

where:

- q_s - net sediment cross-shore transport rate $[m^3/m \cdot s]$
- λ_1 and λ_2 - spatial decay coefficients for the transport rate $[1/m]$ - see Equations 5.62 and 5.63
- K - sediment transport rate coefficient $[m^4/N]$, assumed to be equal $K = 3 \cdot 10^{-6}$
- ε - slope-related transport rate coefficient $[m^2/s]$, equal $\varepsilon = 6 \cdot 10^{-4}$
- D_{eq} - energy dissipation associated with an equilibrium beach profile, calculated as:
$$D_{eq} = \frac{5}{24} \cdot \rho \cdot g^{1.5} \cdot \left(\frac{H_b}{h_b}\right)^2 \cdot A^{1.5} \quad [Nm/m^3/sec] \tag{5.61}$$
where A is the shape parameter calculated as: $A = 2.25 \cdot (w_s/\sqrt{g})^{2/3}$

The subscripts b,p,z and r stand for the quantities evaluated at the break point, plunge point. end of the surf zone and runup limit, respectively (Fig.5.12b). The spatial decay coefficients used in zones I and II describe the decrease in transport rate with distance and are calculated as:

$$\lambda_1 = 0.4\Big(\frac{D_{50}}{H_b}\Big)^{0.47} \tag{5.62}$$

and

$$\lambda_2 = 0.2 \cdot \lambda_1 \tag{5.63}$$

The locations of the break point, plunge point, end of the surf zone and runup height are calculated applying the following formulae (Larson and Kraus, 1989):

- The break point is calculated directly from the wave height calculations

$$H_B = 0.53 \cdot H_0\Big(\frac{H_0}{L_0}\Big)^{-0.24} \tag{5.64}$$

- The plunge point is located $3H_B$ shorewards from the impact point
- The end of the surf zone is defined arbitrarily as the point, where water depth $h < 0.4$m.
- The runup limit is calculated as a function of surf similarity parameter ξ_D (c.f. Eq. 5.22).

The transport rate is first calculated at the plunge point ($x = x_p$) and at the end of the surf zone ($x = x_z$), after that Equations 5.57, 5.58 and 5.60 are applied in order to completely define the transport rate distribution. In the model also the concept of avalanching is implemented, i.e. if the local slope exceeds the angle of initial yield ψ_i, soil is redistributed along the slope and a new stable slope with the angle ψ_r is formed. In the model, ψ_i is set to 28^0 while ψ_r takes the value of 18^0

5.2.4 Transition phase for the sand core erosion

The continuous erosion and formation of the sand beach profile results in the lowering of the dike crest which in turn can result in wave overtopping and consequently in the erosion of the inner slope. In order to account for this mechanism, from the begin of the sand core erosion till the begin of wave overtopping, also the possibility of the inner slope erosion is controlled. The dike cross-section is divided into two parts, with the outer edge of the dike crest being the border. The condition for wave overtopping is controlled by calculating the wave runup (Eq. 5.22). If overtopping occurs, the flow conditions are calculated by applying Eqs. 5.23 - 5.31 and the profile change is calculated using the excess shear approach as given by Eqs. 5.48. The progressive lowering of the dike crest may lead to the overflow and if the latter occurs the core wash-out begins. The simulation of the core wash-out is essentially performed by using the same two approaches as in the preliminary model.

5.3 Overall implementation of the model

In order to develop the detailed dike breaching model the information on the modeling of flow and erosion processes given in Chapters 5 are summarized and implemented into a computational dike breaching model. In this model, the flow model COBRAS is used to provide the

information on the loading on the dike slope during the grass and clay erosion phases, while the flow models for the front-face erosion of the sand core (Section 3.3.1) and for the core wash-out (Section 3.3.2) are coded in MATLAB v7.0. The complete morphodynamic module is also coded in MATLAB. The flow chart of the detailed model is shown in Figure 5.13. In Section 5.3.1 the modeling of the grass and clay cover erosion is summarized, while the modeling of sand core erosion including the transition phase between erosion of clay and sand is reported in Section 5.3.2.

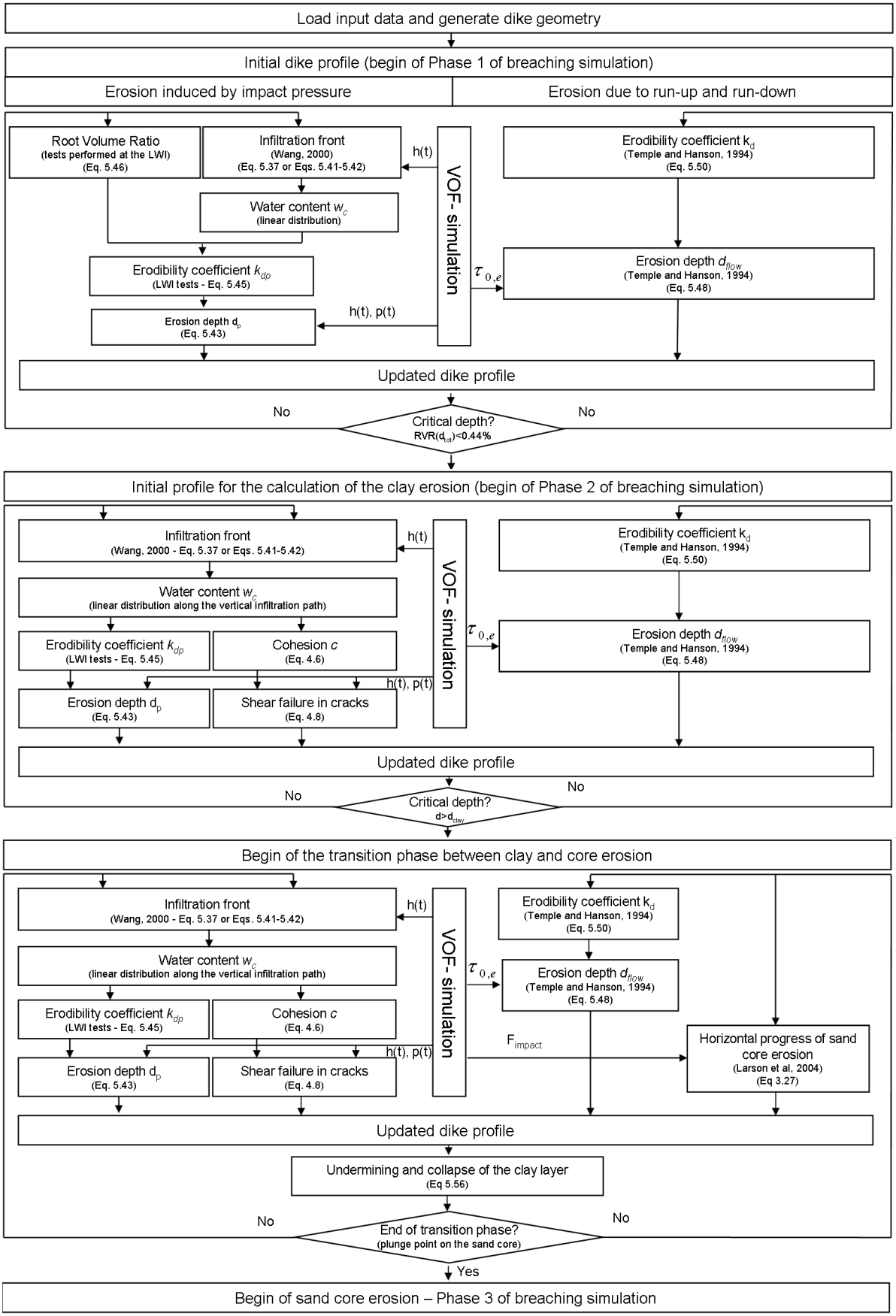

Figure 5.13: Detailed model - complete flow chart

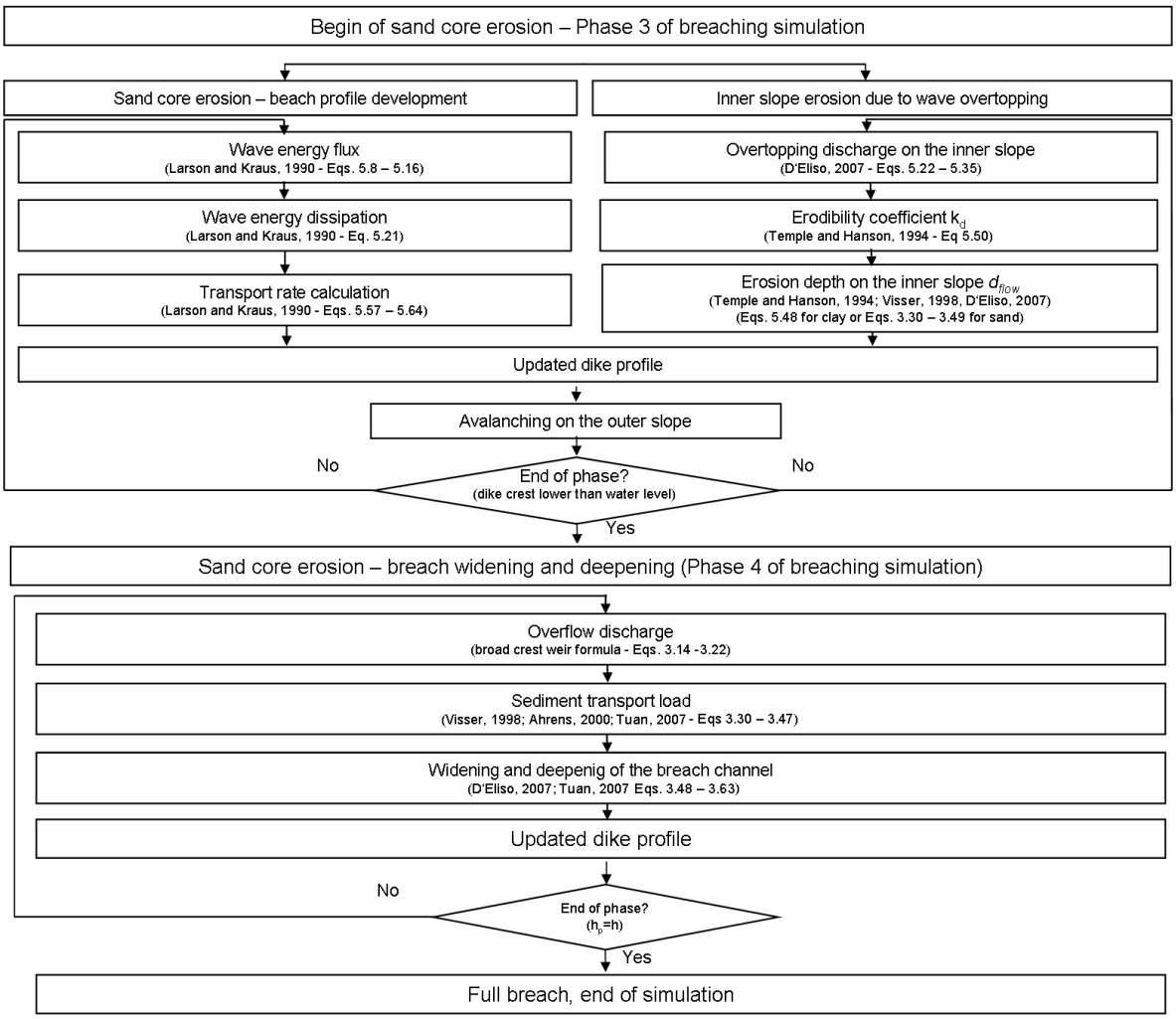

Figure 5.14: Detailed model - complete flow chart (continued)

5.3.1 Simulation of the dike cover erosion

The grass erosion phase and the clay erosion phase form the entire cover erosion phase which starts with the incipient wave action and ends when the erosion reaches the sand core of the dike. The hydrodynamic module is essentially the same during the erosion of grass and clay and contains the numerical simulation of free surface flow and the calculation of infiltration using simplified solvers of Richard's equation. The outputs of the hydrodynamic module are used as inputs for the morphodynamic module. During the simulation of the grass erosion the focus is on the reproduction of the roots reinforcement properties, while during the clay erosion, the shear failure in cracks is the leading process.

5.3.1.1 Free surface flow on the outer slope and infiltration

During the erosion of the grass and clay cover only the flow conditions on the outer slope are calculated. The RANS-VOF model COBRAS is used to simulate the free surface flow. A MATLAB subroutine for the postprocessing of the defaults output files generated by COBRAS is delivered together with the main program file. The final output file saved in the *.mat format contains the information on impact pressure, flow velocity and layer thickness for each

node and each time step. For each time step the model calculates the infiltration and saturation water front (Eqs. 5.37 or 5.41) and the resulting volumetric water content in the soil according to a linear distribution along the vertical infiltration path.

5.3.1.2 Grass and clay erosion

The erosion of the grass cover (breaching Phase 1) is calculated for all numerical nodes of the seaside slope. In the first step, the soil cohesion is calculated as a function of the water content. Applying Eq. 5.46 the root volume ratio is then calculated. Based on this information the erodibility coefficient for impact pressures is calculated (Tab. 4.3 and Eqs. 5.45) and the erosion depth for each node and each time step is calculated (Eq. 4.1). Simultaneously, for each node, the erosion depth due to flow of wave run-up and run-down is calculated by applying Eqs. 5.48 - 5.49 and 5.54 - 5.55, where the erodibility coefficient is obtained using Eq. 5.50. For each time step the total erosion depth is calculated and the condition of critical erosion depth is controlled. The assumed critical depth is reached, when the root percentage in the soil volume becomes negligible, i.e. $RVR < 0.44\%$. If this condition is fulfilled, the breach is initiated. As a result, the numerical and graphical information on the erosion progress history, development of the dike profile and associated time are stored in an .xls file.

At the next time step breaching Phase 2 (clay erosion) begins. The local clay cover erosion is calculated for all sections of the seaside slope. The erodibility coefficient due to impact pressures is calculated as a function of water content and soil type (Eq. 5.44). The depth of erosion resulting from a single wave impact is calculated using Eq. 5.43. Simultaneously, the depth of erosion induced by the wave run-up and run-down flow is calculated by using Eqs. 5.48 - 5.49 and the erodibility coefficient is determined by applying Eqs. 5.50 - 5.52. For each time step also the soil cohesion is calculated and the limit state equation for the shear failure in water filled cracks is solved (Eq. 4.9). If a shear failure occurs, the dike profile is updated. For each time step the total erosion depth is calculated and the condition of critical erosion depth ($d > d_c$) is controlled. If this condition is fulfilled for at least one node, the information on the erosion progress history, updated dike profile and time associated with this phase are stored. At the next time step the transition phase between clay and sand erosion begins.

5.3.2 Sand core erosion - beach profile formation and transition phase

Compared to the preliminary model, an additional phase between clay and sand core erosion is introduced, based on the results of the laboratory experiments performed at the LWI. This transition phase starts when the clay erosion phase ended, and ends when the dimensions of the scour hole have grown up to the point, when the plunge point is located on the uncovered sand core. At that moment, the core erosion starts and ends when the overflow occurs, i.e. when the dike crest is below the mean water level.

5.3.2.1 Flow simulation

During the transition phase the flow parameters are obtained exactly like in the case of cover erosion, i.e. using the information provided by the COBRAS model.
After the end of the transition phase for each time step the condition for wave overtopping is controlled by comparing the wave run-up limit (Eq. 5.22) and the highest node of the dike.

Depending on whether overtopping occurs or not two alternative cases may occur for each time step:

- **No overtopping occurs** - only the flow on the outer slope is simulated. The energy flux is calculated by using Eqs. 5.8-5.14, then the wave height is given by Eqs. 5.17 - 5.20 and finally the wave energy dissipation along the outer slope is obtained from Eq. 5.21;
- **Overtopping occurs** - the flow on the crest and on the inner slope is also simulated. In this case the flow on the outer slope is calculated with Eqs. 5.23 - 5.24, on the crest with Eqs. 5.25 - 5.26 and on the inner slope with Eqs. 5.27 - 5.29. The flow parameters within a wave cycle are then calculated according to Eq. 5.31.

5.3.2.2 Simulation of the sand core erosion

All essential calculations regarding clay erosion during the simulation of the transition phase between clay and core are performed as in the previous breaching phase. Simultaneously, the progress of sand core erosion in the direction of waves is calculated applying the model of Larson et al. (2004) given by Eq. 3.27. As the progress of sand erosion is significantly faster than that of the clay cover, undermining of the clay revetment occurs. The collapse condition is controlled by the limit state equation (Eq. 5.56). If a bending failure occurs, the dike profile is updated and it is assumed that the collapsed block of clay is removed instantaneously by wave action. The transition phase ends, when the dimensions of the scour hole have grown up to the point, when the plunge point is located on the uncovered sand core. In the next time step, the numerical and graphical outputs are stored and the next phase, i.e the sand core erosion starts.

When no overtopping occurs, Eqs. 5.57 - 5.60 are used to describe the sediment transport rate and bed profile change on the outer slope. If overtopping occurs, the erosion along the dike profile is calculated using Eqs. 5.48 - 5.53 for the erosion of the clay revetment and Eqs. 3.30 - 3.35 for the erosion of the sand core. For each time step the condition of overflow is controlled (see Fig. 3.8), and if the latter occurs, the outputs are stored, and the last phase, i.e. dike core wash-out begins. The sand core wash-out is calculated with the volume-averaged approach (Eqs. 3.58 - 3.63), but energetic approach can be alternatively selected. Although the results provided by the volume-averaged approach are comparable with those given by the 1D Exner equation, the selection of the former is recommended since the related computational effort is one order of magnitude smaller when compared to the latter.

5.3.3 Example application, results and discussion

The detailed model was applied for the breaching simulation of a typical prototype dike in order to explore the main differences between the preliminary model and the detailed model. The simulation of a historical dike damage and a historical dike breach are performed. The results are compared with the results of the preliminary model and the verification against the measurements is made.

5.3.3.1 Breaching of a typical North Sea dike

As a first example simulation, the model was applied for the breaching simulation of a typical North Sea dike considered in the preliminary model (Section 3.5.1.1). The same main parameters as in the case of preliminary model were used, while the parameters that are used only

either in the preliminary or in the detailed model were so adjusted, that they represent the grass and clay of the same quality (c.f Table 5.10).

INPUT PARAMETER	SYMBOL	Value	UNIT
Significant wave height	H_s	1.4	$[m]$
Peak period	T_p	4.7	$[s]$
Mean water level	mwl	6	$[m]$
Dike height	H_D	10	$[m]$
Dike crest	B_D	2	$[m]$
Outer slope	m	6	$[-]$
Inner slope	n	3	$[-]$
Thickness of the clay layer	d_c	1	$[m]$
Polder area	A_p	1000000	$[m^2]$
Root volume ratio	RVR	$2.67 \cdot 0.75^{(d-2)}$	$[\%]$
Grass cover factor	C_f	0.75	$[-]$
Damping coefficient	w	2	$[-]$
Initial infiltration front	z_{inf}	0.25	$[m]$
Initial water content	θ_i	0.2	$[m^3/m^3]$
Saturated water content	θ_s	0.42	$[m^3/m^3]$
Clay content	$c\%$	30	$[\%]$
Mean depth of cracks	$d_{c,mean}$	0.4	$[m]$
Sediment size	D_{50}	0.2	$[mm]$
Internal friction angle	ϕ	32	$[deg]$
Porosity of the sand	p	0.4	$[-]$

Table 5.10: Input parameters for the simulation of breaching

The main outcomes from both models and the relative differences are given in Table 5.11.

Parameter	Symbol	Unit	PM	DM	ε
Grass erosion time	t_g	h	16.03	18.98	-18%
Clay erosion time - cracks	$t_{c,c}$	h	-	5.33	-
Clay erosion time - transition phase	$t_{c,tr}$	h	-	9.22	-
Total time of clay erosion	t_c	h	14.15	14.55	-3%
Cover failure time	$t_{c,t}$	h	30.18	33.53	-11%
Time of core erosion and wash-out	t_s	h	5.57	12.87	-42%
Total time of breaching	t_t	h	35.75	45.35	-28.1%
Peak outflow discharge	Q_p	m^3/s	1367	1248	+8.7%
Final breach width	$B_{b,max}$	m	93.26	86.22	+7.5%
Difference between PM and DM: $\varepsilon = 100 \cdot (PM - DM)/PM$					

Table 5.11: Main outputs of the simulation and comparison with the preliminary model

The progress of the grass and clay erosion calculated by the preliminary and detailed model and the indications on the most important points of the erosion course are comparatively shown in Fig. 5.15.

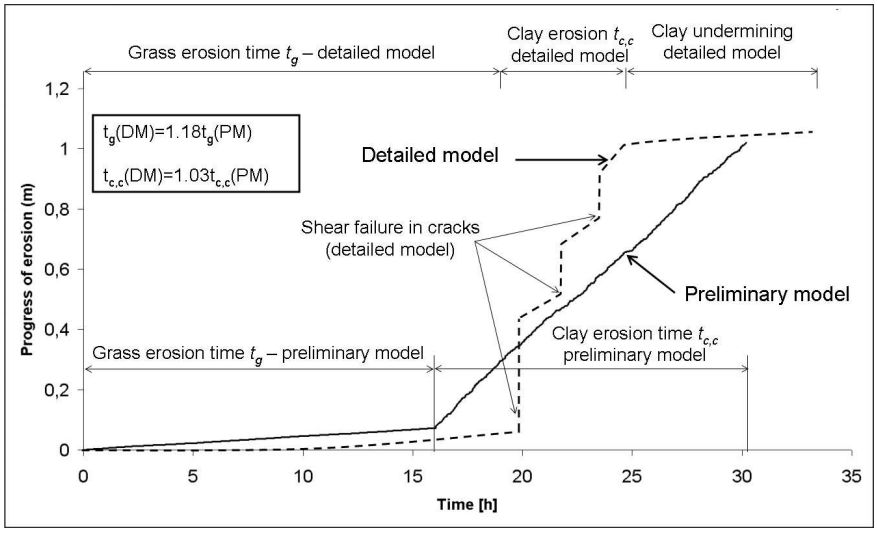

Figure 5.15: Progress of the cover erosion - comparison of the preliminary and detailed model

The comparative analysis of the results indicates the following aspects related to the erosion of grass and clay (Tab. 5.11 and Fig. 5.15):

- ***time of grass erosion*** (t_g) calculated by the detailed model is 18% higher than in the preliminary model, due to the completely different method to simulate the erosion process. In the preliminary model the modified equations for the estimation of the residual strength of grass cover were applied. In those formulae, possible weaker points were accounted for in the safety coefficients, resulting in faster erosion.
  The detailed model is based on the results of the laboratory experiments on the reinforcement grass properties, and the variations in the grass properties are already directly included as material properties and in the simulation. Due to the higher concentration of the roots directly under the surface of the slope, almost no damage is observed in the first 10 hours, which relatively corresponds to the observations in large-scale tests on grass erosion in a wave flume (Smith et al, 1994);
- ***time of clay erosion*** ($t_{c,c}$) calculated by the detailed model is almost the same (3% higher) as in the case of the preliminary model. Similarly to the grass erosion, an additional safety coefficient was also included in the preliminary model. However, no influence of cracks was taken into account in the preliminary model.
  In the detailed model the cracks in the clay layer that result in faster erosion were included, but on the other hand the safety coefficients are not included anymore. The clay erosion phase is divided into two parts, with two different courses of erosion. During the first part, the rapid progress of erosion after the shear failure (Fig. 5.15) clearly dominates, confirming the observations made by Führböter (1966) on the crucial importance of cracks for the stability of clay revetments. Nevertheless, the distribution, the number, location and depth of the cracks on the slope, which are purely random, can strongly influence this part resulting either in shorter or longer time of erosion. In the second part of this phase, the clay erosion decelerates as the sand core erosion and consequently the clay undermining occurs (Fig. 5.15). Till the end of this part the clay layer is stable and the collapse of the undermined clay cover is considered to be the end of the clay erosion phase;
- ***warning time*** (t_w) which is equal the cover failure time ($t_{c,t}$) is slightly (11%) higher for the detailed model than for the preliminary one, which is a logical consequence of the higher grass and clay erosion times.

The time of front-face core erosion (t_s) is significantly (42%) higher for the detailed model. The main reason of this difference is the protective function of the remaining parts of the clay cover that is accounted for in the detailed model. In the preliminary model the clay cover was assumed to fail instantaneously as soon as at least one point of the clay cover failed. This assumption was however a simplification and the latter was removed in the detailed model, based on the results of the new laboratory experiments performed at the LWI.

The total breaching time (t_t) is 28% higher than in the case of the preliminary model, and the highest time increase was contributed by the core erosion time. The increase of the total breaching time results from the removal of the simplifying assumptions made in the preliminary model. Those simplifications, especially assumptions on instantaneous failure of grass and clay cover were always on the safe side, decreasing the time of breaching. Consequently, the preliminary model provides results on the conservative side as intended.

The final breach shape obtained from the detailed model is similar to the one obtained from the preliminary model (Figure 5.16). The largest differences can be noted on the crest and on the landside, where the breach calculated by the detailed model is wider. This difference is due to the fact, that in the detailed model also the simulation of the inner slope erosion resulting from wave overtopping is included. Therefore, different initial conditions for the simulation of the overflow are provided. This results also in an 8% difference in the ***peak outflow discharges***

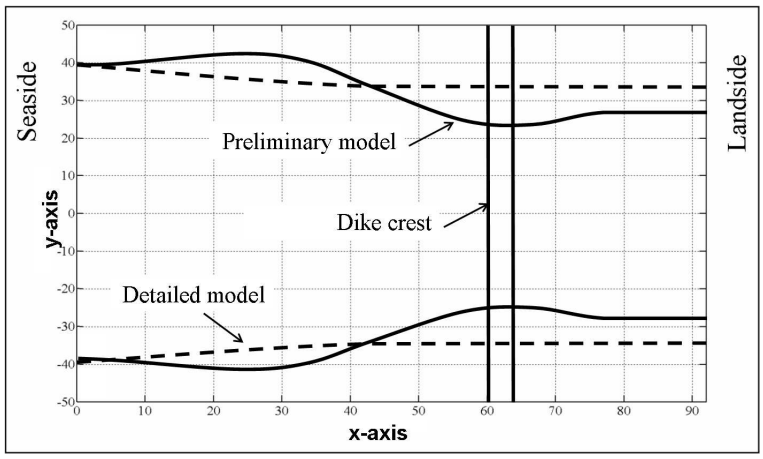

Figure 5.16: Final breach shape - comparison of the preliminary and detailed model

5.3.3.2 Historical dike damage

The data on the damage of a dike (Fig. 5.17) caused by breaking wave impact on the outer slope was used to test the prediction capability of the detailed model to simulate the first breaching phase, which is crucial for the entire breaching process. The obtained results are compared with the predictions given by the preliminary model and with the measured dimensions of the scour hole. Unfortunately, very limited information on this damage is available, and it is only possible to compare the dimensions of the scour hole. In this case the results given by the detailed model are almost identical to those given by the preliminary one and to the observed values. No information on the time needed for this damage to occur is available. The time of storm duration needed for this damage to occur given by the detailed model is 33% higher than the time given by the preliminary model. The source of this difference is the same as in the case of dike breach simulation given in Section 3.5.1

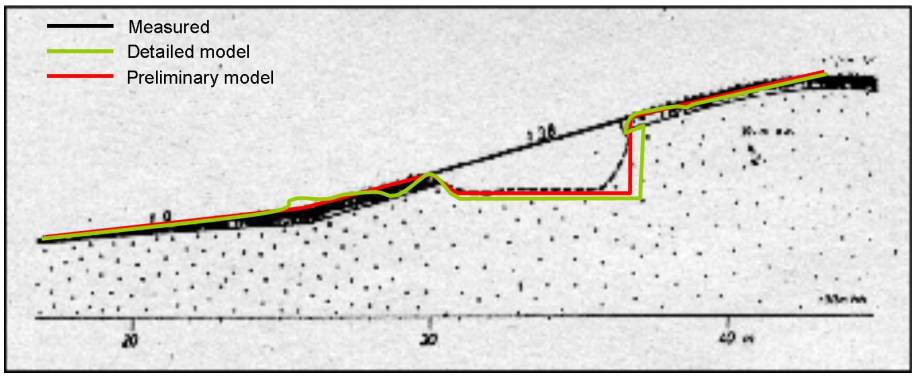

Figure 5.17: Damage of the dike (after Forschungs- und Vorarbeitenstelle Neuwerk) and comparison with the results from preliminary and detailed model

Parameter	Measured	Preliminary model	Detailed model
Diameter of the hole	6.0*	6.0	6.0
Depth of the hole	2.0*	2.11	2.25
Storm surge duration needed for this damage to occur	unknown	13.52	18.06
* Fuhrböter et al (1976)			

Table 5.12: Main outputs of the simulation and comparison with the preliminary model

5.3.3.3 Historical dike breach

The available information on the dike breach in Ülversbüller Koog (Wohlenberg,1963) was compared with the results provided by the preliminary and detailed model (Table 5.13).

Parameter	Observed	Preliminary model	Detailed model
Total time of breaching $[h]$	≈23*	27.07	31.64
Core wash-out time $[h]$	≈2**	3.33	3.85
Final breach width (min) $[m]$	≈35**	37.6	62.16
Final breach width (max) $[m]$	≈80**	88.2	88.10
* Landesamt für Wasserwirtschaft - SH (1962); ** Wohlenberg (1963)			

Table 5.13: Main outputs of the simulation and comparison with the preliminary model

In the investigated case, the preliminary model seems to provide better results concerning the time of breaching, while the detailed model overestimates the temporal parameters and minimal breach width. Nevertheless, the results given by both models are only indicative, due to the lack of information on the actual prototype parameters which are essential for the proper breaching simulation. The description of breaching time, progress of erosion as well as the breach widening and deepening rate were reported by accidental eye witnesses and therefore are roughly estimated, not measured. Although some pictures of the full breach are available, the shape and final breach dimensions are also roughly estimated and the detailed measurements are lacking. For the purposes of this example application, the grass cover quality, clay layer thickness and the mean grain size D_{50} were arbitrary assumed so that the moderate erosion resistance is accounted for.

Generally, the detailed information on the historical dike breaching initiated from the seaside which would allow for a better model validation is lacking.

6 Uncertainties, sensitivity and reliability analyses

Both preliminary and detailed models are based on a deterministic formulation. However, as input parameters are stochastic, the model outcomes should include an assessment of the uncertainties. This chapter provides a brief analysis of uncertainties and their influence on the model outputs. The uncertainties of the model system are defined, Section 6.1. The information on the influence of single parameters on the model outcomes are provided in Section 6.2. Finally, the influence of the input parameters on the probability density function of the model outputs is analysed in Section 6.3 .

6.1 Uncertainties

The uncertainty of the simulation results is due to two types of uncertainties: **input parameter uncertainties** and **model parameter uncertainties**. The uncertainties of the input parameters result from the natural variations in the sea state and soil properties as well as from the imperfections during the dike construction. The uncertainties in the model parameters may result from (i) the limitations of the empirical formulation, which are always based on a limited number of laboratory tests, and (ii) the simplifications made in the mathematical/numerical simulation of the processes involved. The input parameters are described with a gaussian probability density function that is characterised by the following parameters:

- **mean value**:

$$\mu_x = \frac{1}{N}\sum_{i=1}^{N} X_i \tag{6.1}$$

- **standard deviation**

$$\sigma_x = \sqrt{\frac{1}{N-1}\sum_{i=1}^{N}(X_i - \mu_x)^2} \tag{6.2}$$

- **Coefficient of variation**

$$\sigma'_x = \frac{\sigma_x}{\mu_x} \tag{6.3}$$

where X denotes the investigated parameter and N the number of samples.

6.1.1 Main uncertainties in the preliminary model

Among all input parameters, the most important and also the most uncertain refer to the sea parameters - wave height (H or H_s), wave period (T or T_p), mean water level (MWL) as well as to the grass erosion coefficient $E_{g,max}$ or clay erosion coefficient $E_{c,max}$. Furthermore, the critical depth of grass erosion depends on the grass properties, grass condition and even on the seasons of the year. Furthermore, since Phase 3 and Phase 4 of breaching simulation are based only on two parameters, i.e. on the sediment density (ρ_s) and sediment size (D_{50}), they both should be also investigated. Model uncertainties refer essentially to the parameters that describe the impact pressures (Eqs. 3.2 - 3.9) and to the initial breach channel dimensions (Fig. 3.14).

6.1.2 Main uncertainties in the detailed model

The parameters describing the root volume ratio (RVR) in Eq. 4.14 are the most important and the most uncertain input parameter in the grass erosion simulation. This parameter depends on the grass type, soil type, maintenance and even season of the year. The same concerns also the grass cover factor C_f (Eq. 5.54) and total Manning roughness (Eq. 5.55). The input parameters for the clay erosion simulation due to impact pressures are calculated based on the definition of three clay types: weak, moderate and strong. Those definitions cover however a wide range of soil types and are therefore subject to large uncertainties. Some of the parameters (k_d in Eq. 5.44, for instance) are a function of water content, that depends on the assumed initial water content and applied infiltration model, which are both subject to large uncertainties. The leading parameters of the core erosion process (D_{50} and n) should have controlled values of the construction materials and are subject to relatively well known uncertainties. More information on the identified uncertainties and their range is provided in Table 6.1.

INPUT PARAMETER	SYMBOL AND UNIT	μ	σ	σ'
Significant wave height	$H_s[m]$	2.50	0.325	0.13
Peak period	$T_p[s]$	8.00	1.6	0.20
Mean water level	$MWL[m]$	7.00	1.05	0.15
Dike height	$H_d[m]$	10.00	0.10	0.01
Crest width	$B_d[m]$	2.00	0.10	0.05
Outer slope	$m[-]$	6.00	0.30	0.05
Inner slope	$n[-]$	3.00	0.15	0.05
Grass cover thickness	$d_g[m]$	0.08	0.02	0.25
Initial saturated water front	$z_{inf}[m]$	0.25	0.005	0.20
Hydraulic permeability - grass	$k_{inf,g}[m/s]$	$1.30 \cdot 10^{-7}$	$2.60 \cdot 10^{-8}$	0.20
Hydraulic permeability - clay	$k_{inf,c}[m/s]$	$5.50 \cdot 10^{-8}$	$1.10 \cdot 10^{-8}$	0.20
Number of cracks on the slope	$n_{cracks}[-]$	40	10	0.25
Mean depth of the cracks	$a_{mean}[m]$	0.3	0.06	0.20

Table 6.1: Uncertainties related to the input parameters for the hydrodynamic module (partially taken from D'Eliso, 2007 and Kortenhaus, 2003)

6.2 Sensitivity analysis

The variability of the input parameters influences the results given by the model. In order to investigate this influence, three types of sensitivity analysis may be applied:

- Level I analysis - only one parameter varies, while the other are kept constant. The tests are performed five times, and if necessary, i.e. if the outputs of variations are significant, the number of tests is increased. On the basis of the Level I analysis results, the sets of parameters for the Level II analysis are selected.
- Level II analysis - a set of parameters varies, according to their assumed distribution, while, as in the case of Level I analysis, all other parameters are kept constant.
- Level III analysis - all parameters vary in the simulation and all possible combinations are taken into account. Due to the significant computational effort, this type of analysis will not be applied for the model system.

For the purposes of the present study only Level I analysis is performed, since the influence of variation of all parameters will be investigated during the reliability analysis (Section 6.3). During the analysis the influence of the variations of a single parameter on the variations in the model outputs is investigated. The leading parameters for each phase together with the related phases and investigated range of variation are listed in Table 6.2. For each parameter given in Table 6.2 five tests are performed. The considered parameter varies in the given range, while all the other parameters are kept constant.

Description	Symbol	Unit	μ	σ	Phase
Root Volume Ratio	A	$[-]$	2.65	0.265	GE
Grass cover factor	Cf	$[-]$	0.75	0.1	GE
Damping coefficient	w	$[-]$	2.5	0.5	GE
Initial infiltration front	z_{inf}	$[m]$	0.25	0.05	GE
Initial water content	θ_i	$[m^3/m^3]$	0.2	0.05	GE,CE
Saturated water content	θ_s	$[m^3/m^3]$	0.42	0.02	GE,CE
Clay percentage	$c\%$	$[-]$	30	7.5	GE,CE
Minimal depth of cracks	$d_{c,min}$	$[m]$	0.15	0.05	CE
Maximal depth of cracks	$d_{c,max}$	$[m]$	0.4	0.1	CE
Sediment size	D_{50}	$[mm]$	0.2	0.02	SE
Sand density	ρ_s	$[kg/m^3]$	1800	60	SE
Internal friction angle	ϕ_s	$[^0]$	30	2	SE
Breach growth ratio	Kvl	$[-]$	0.03	0.006	SE
GE - grass erosion, CE - clay erosion, SE - sand erosion					

Table 6.2: Input parameters for the Level I analysis

6.2.1 Grass erosion time

In the preliminary model the grass erosion coefficient E_g is the leading parameter, while in the detailed model four key parameters were identified: Root Volume Ratio (RVR), damping coefficient w, grass cover factor C_f and saturated water content θ_s.

6.2.1.1 Preliminary model

Only one key parameter, i.e. grass erosion coefficient E_g is identified during the grass erosion phase simulated by the preliminary model (Fig. 6.1).
In the typical range ($E_g = 1.5 \cdot 10^{-6} - 2.2 \cdot 10^{-6}$) the grass erosion time t_g increases linearly as the erosion coefficient E_g decreases and this increase rate becomes larger when E_g becomes smaller than $1.2 \cdot 10^{-6}$.

6.2.1.2 Detailed model

Time of grass erosion t_g is influenced by the parameters of clay and reinforcement properties of the grass cover. Figures 6.2 - 6.8 show the effect of the key parameters on the grass erosion time. The root volume ratio RVR and the damping coefficient w are the leading parameters that describe the grass erosion due to impact pressures . Already a small increase of the root network density can significantly increase the time of grass erosion (Fig. 6.2) and a similar increase can also be observed during the analysis of the influence of the changes of the damping coefficient w on the model outputs (Fig. 6.3).

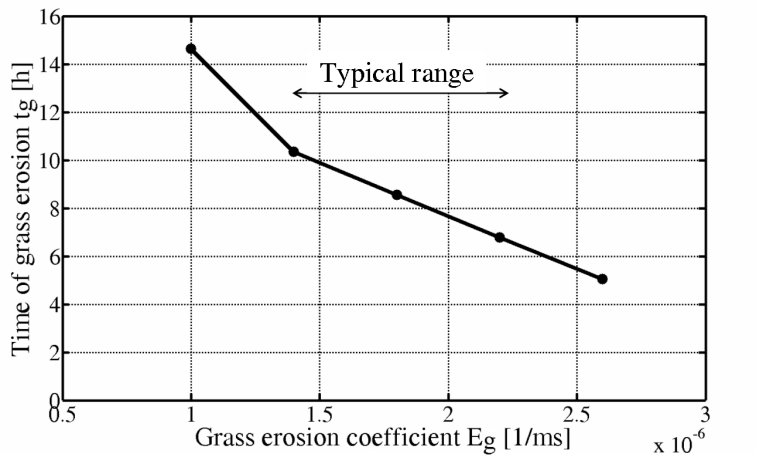

Figure 6.1: Influence of the grass erosion coefficient E_g on the time of grass erosion

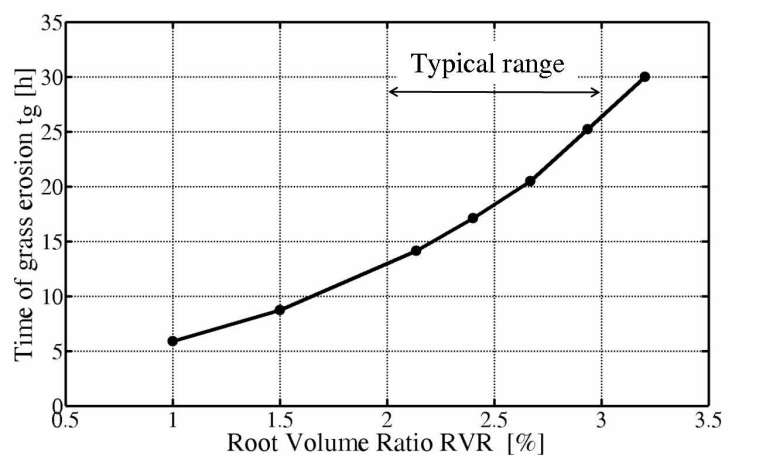

Figure 6.2: Influence of the root volume ratio RVR on the grass erosion time

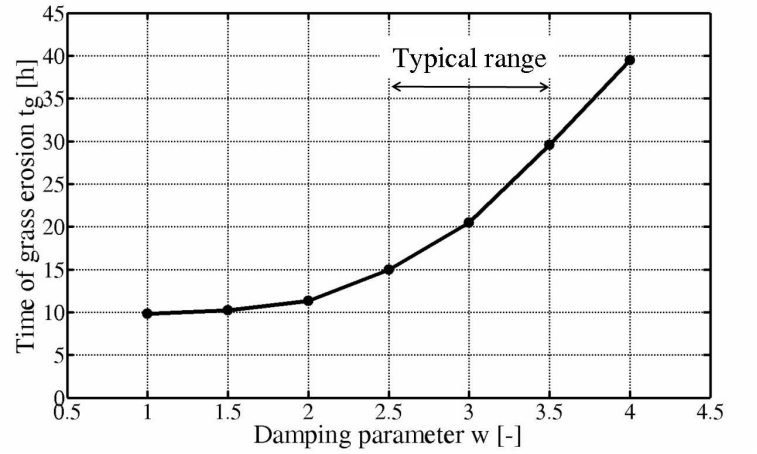

Figure 6.3: Influence of the damping coefficient w on the grass erosion time

Typically, the root volume ratio RVR is in the range $RVR = 2 \div 3\%$, the damping coefficient w takes the value $w = 2.5 \div 3.5[-]$, the C_f factor is typically equal $C_f = 0.7 \div 0.9[-]$ and the clay content in the subsoil typically varies in the range $c\% = 20 \div 40[\%]$
The grass cover factor C_f and the clay content in the subsoil are identified as the key parame-

ters describing the erosion due to the wave run-up and run-down flow. The influence of the C_f on the grass erosion time is given in Fig.6.4. The grass erosion time increases together with the increase of the grass cover factor C_f, but this increase is rather linear, especially when compared to the exponential increase of the RVR as given in Fig. 6.2. This confirms that the erosion due to the impact pressures dominates the grass erosion phase. The influence of the clay content on the subsoil seems to be negligibly small (Fig. 6.5).

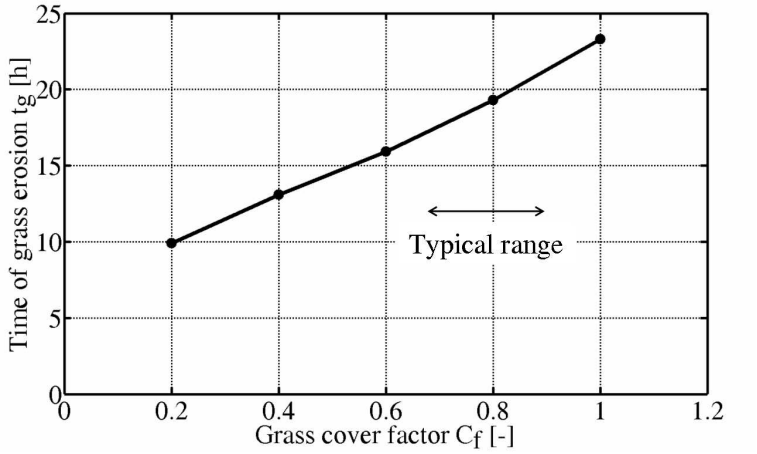

Figure 6.4: Influence of the grass cover factor C_f on the grass failure time

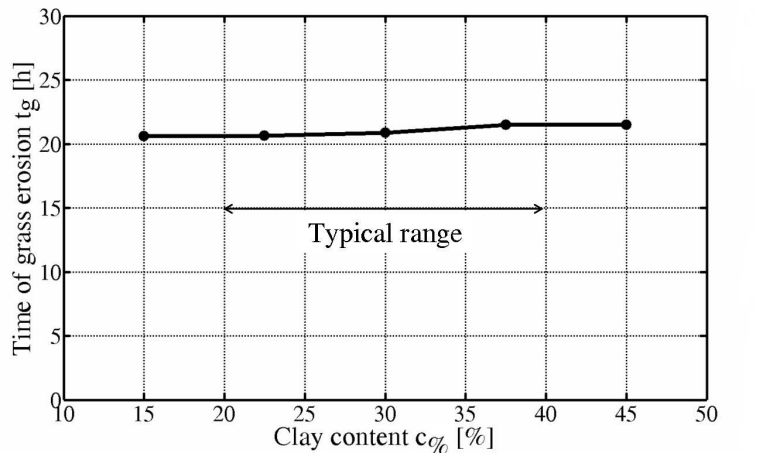

Figure 6.5: Influence of the clay percentage in the substrate soil $c\%$ on the grass erosion time

Furthermore, the performed analysis the parameters describing water conditions in the soil, and thus also the erosion properties of the subsoil were considered. The effect of the initial infiltration front z_{inf} (Fig. 6.6) and that of the initial volumetric water content θ_i (Fig. 6.7) are relatively small. Theses negligibly small effects are mainly due to the high infiltration rate of the vegetated cover. The water content in the grass cover rapidly increases, and reaches in very short time the saturated state resulting in a very high effect of the saturated water content θ_s (Fig. 6.8).

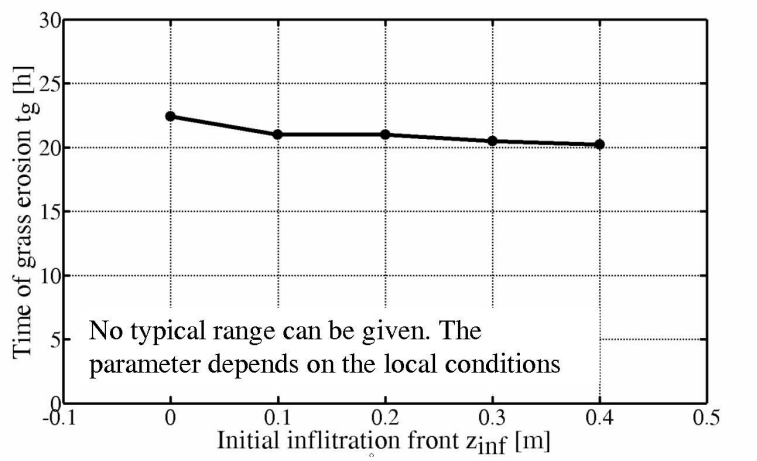

Figure 6.6: Influence of the initial infiltration front z_{inf} on the grass erosion time

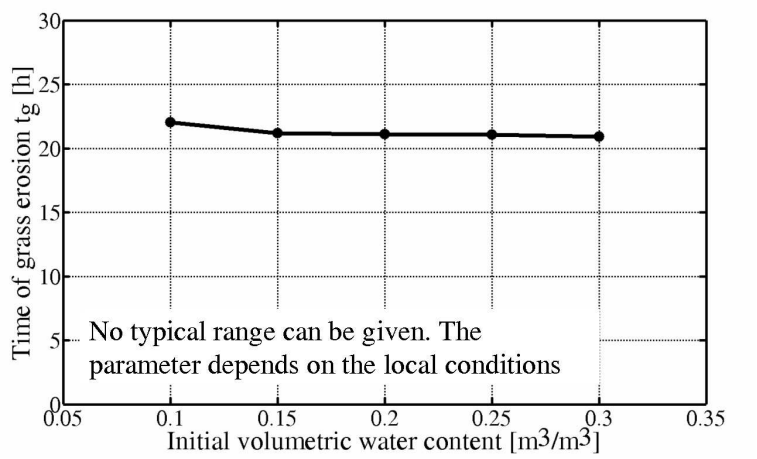

Figure 6.7: Influence of the initial volumetric water content θ_i on the grass erosion time

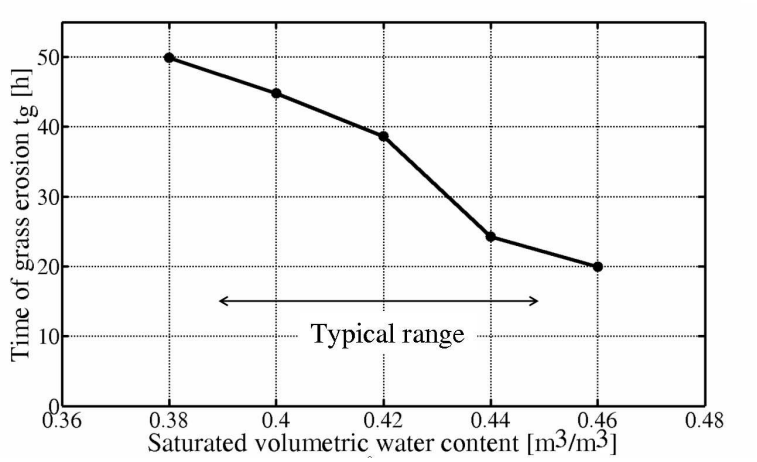

Figure 6.8: Influence of the saturated volumetric water content θ_s on the grass erosion time

6.2.2 Clay erosion time

During the simulation of clay erosion with the preliminary model only one key parameter, i.e. clay erosion coefficient E_c, was identified. In the detailed model, the results are affected by the following key parameters: clay percentage in the soil ($c\%$), initial infiltration front (z_{inf}), initial (θ_i) and saturated (θ_s) water content as well as dimensions of cracks in the clay layer. For the purposes of the sensitivity analysis, the random cracks are generated within a range that is defined by the minimal and maximal allowable crack depth.

6.2.2.1 Preliminary model

The clay erosion phase is governed by only one parameter, i.e. clay erosion coefficient E_c. The observed relationship between the clay erosion time and E_c is almost linear (Fig. 6.9).

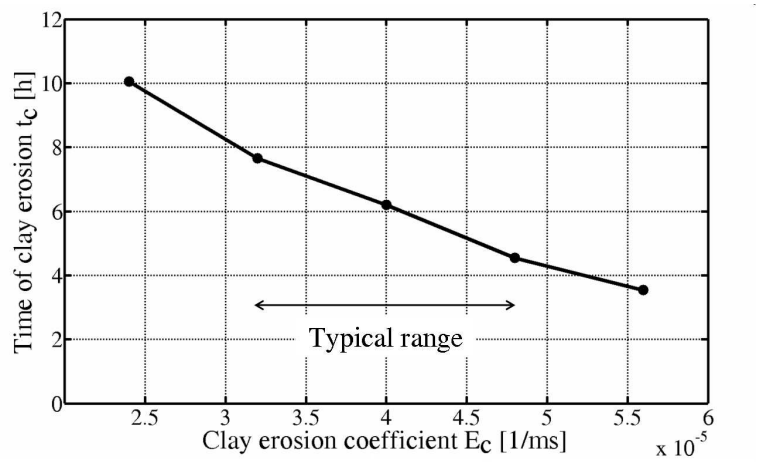

Figure 6.9: Influence of the clay erosion coefficient E_c on the clay erosion time

6.2.2.2 Detailed model

The tests were performed five times for each of the parameters listed in Table 6.2. During all tests, one of the selected parameters varies in the given range, while all others take their mean value and are kept constant. The results of the simulations are presented in Figs. 6.10 - 6.15.

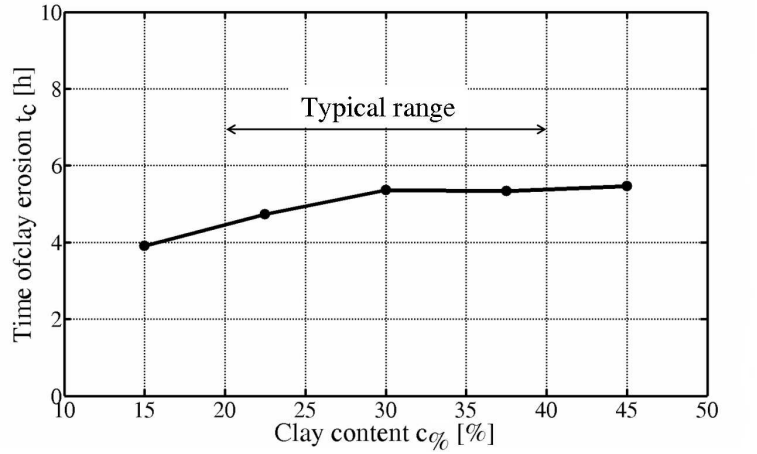

Figure 6.10: Influence of the clay percentage in the substrate soil $c\%$ on the clay erosion time

The influence of clay percentage $c\%$ in the soil and the initial infiltration front on the erosion time (Figure 6.10 and Figure 6.11, respectively) is relatively small. The time of clay erosion is however very sensitive to the changes in both the initial (Fig.6.12) and saturated (Fig.6.13) volumetric water content. This results from the fact, that the erodibility coefficient of the clay depends nonlinearly on the changes on the water content w_c in the soil (Eq. 5.44) and even small changes in the water content w_c may cause significant increase or decrease in the soil erosion resistance. Furthermore, since soil cohesion is an exponential function of the water content, possible cracks in the clay layer are more susceptible to be subject to shear failure together with the increase of water content.

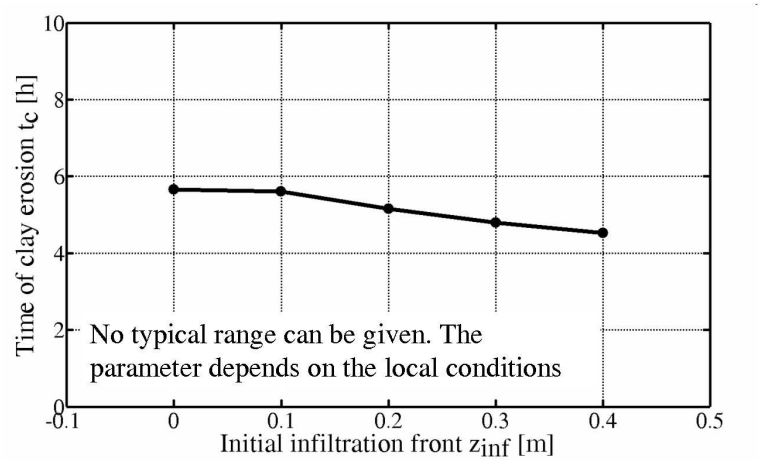

Figure 6.11: Influence of the initial infiltration front z_{inf} on the clay erosion time

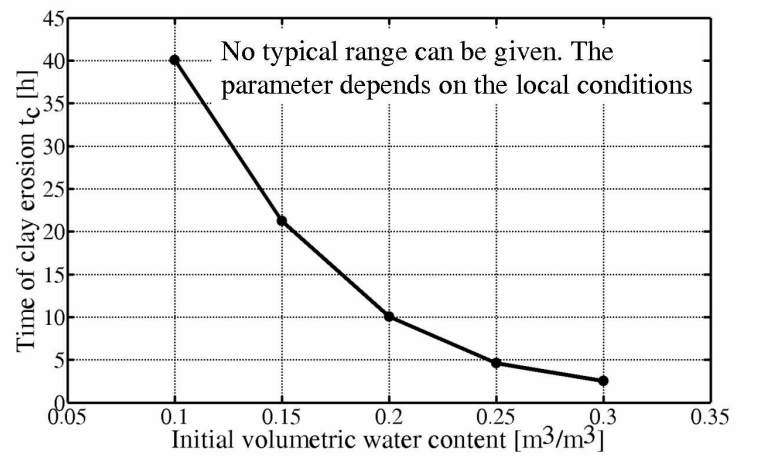

Figure 6.12: Influence of the initial volumetric water content θ_i on the clay erosion time

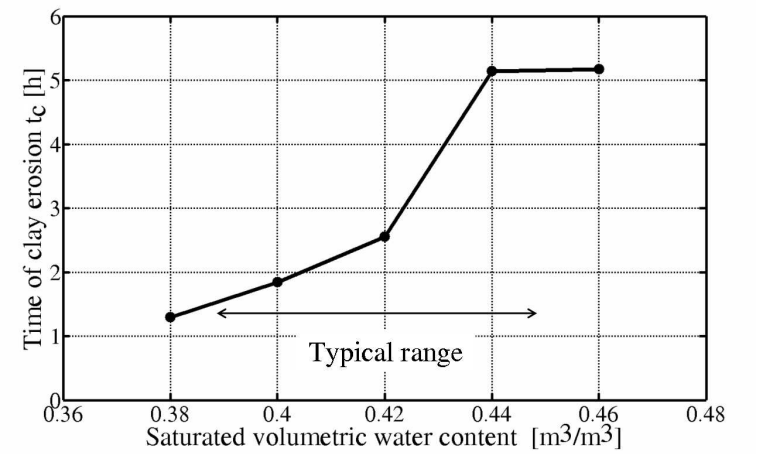

Figure 6.13: Influence of the saturated volumetric water content θ_s on the clay erosion time

The variation in the depth of the cracks, especially the minimal crack depth (Fig. 6.14) influences significantly the clay cover failure time since the presence of cracks in the clay layer strongly increase the soil permeability which leads to the increase of the water content. This will decrease the clay erodibility coefficient, and thus the clay erosion time.

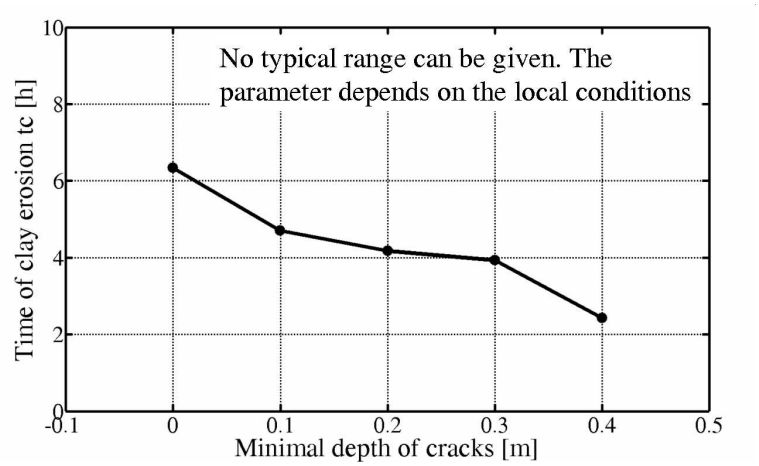

Figure 6.14: Influence of the minimal depth of cracks on the clay erosion time

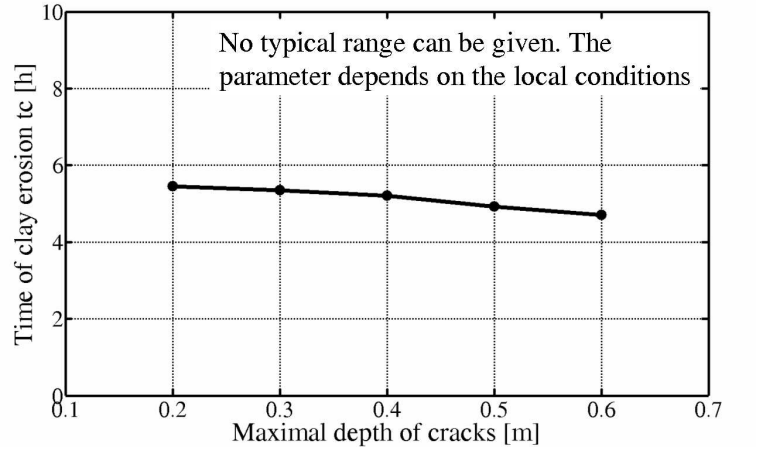

Figure 6.15: Influence of the maximal depth of crack on the clay erosion time

Furthermore, a rapid local erosion may occur, when a water-filled crack is subject to impact pressure and since the condition for the shear failure in cracks to occur is a function of the

crack depth (Eq. 4.9), the clay erosion time decreases as the crack depth increases (Fig. 6.14 and Fig. 6.15). This effect is especially observed in the case of the minimal depth of crack.

6.2.3 Core erosion and wash-out time

The key parameters during the erosion and wash-out of the sand core in both the preliminary and the detailed models are the median grain size D_{50} and the breach growth ratio Kvl. The influence of those parameters on the peak outflow discharge and time of sand core erosion was investigated.

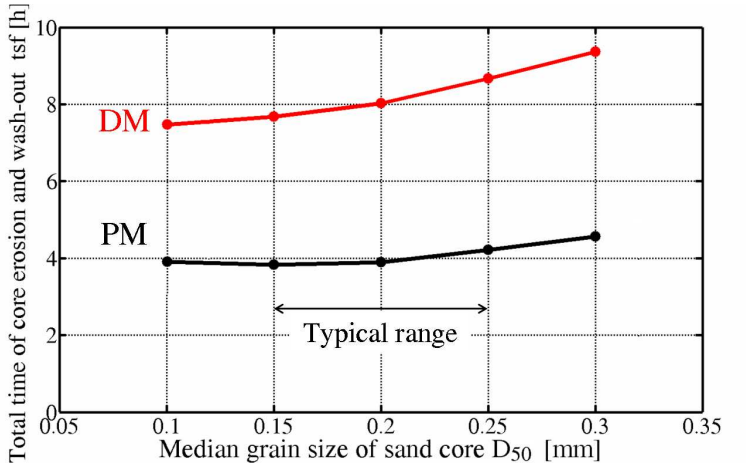

Figure 6.16: Influence of the grain size on the sand core erosion time

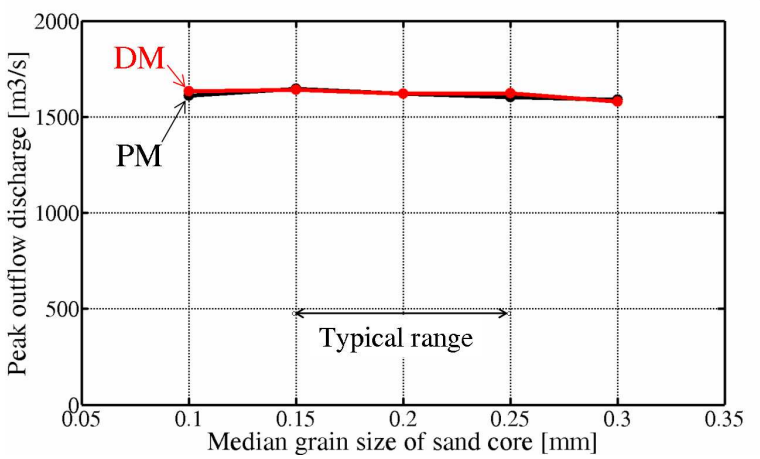

Figure 6.17: Influence of the grain size on the peak outflow discharge

The performed tests show that the influence of the grain size D_{50} on both core erosion time (Fig. 6.16) and peak outflow discharge (Fig. 6.17) is relatively small. Higher grain sizes result in both longer time of sand core erosion and smaller peak outflow discharge. It has to emphasized that although the same flow and sediment transport models were applied in the preliminary and detailed models, due to different definition of the sand erosion phases and additional transition phases between (i) clay and sand core erosion and (ii) between erosion of the front-face of the sand core and erosion due to the overflow, the times provided by the preliminary and detailed model cannot be directly compared. However, almost no differences in the peak outflow discharges predicted by the preliminary and detailed models were observed.

The effect of the breach growth ratio Kvl on the results provided by the detailed model was also investigated (Figs. 6.18 - 6.20).

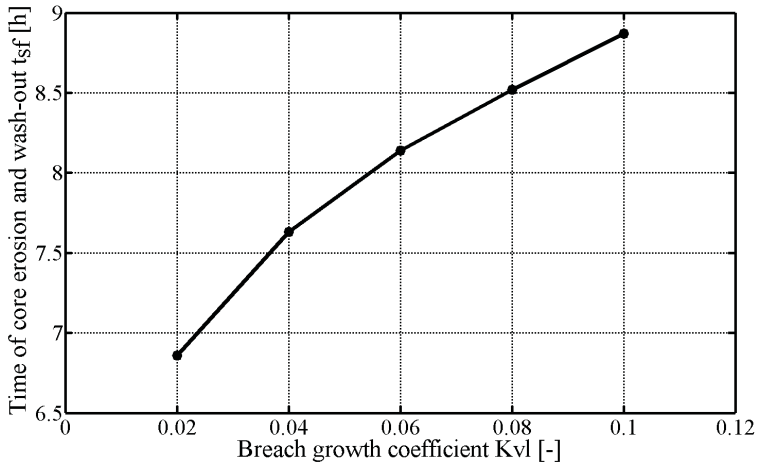

Figure 6.18: Influence of the breach growth coefficient on the core erosion and wash-out time

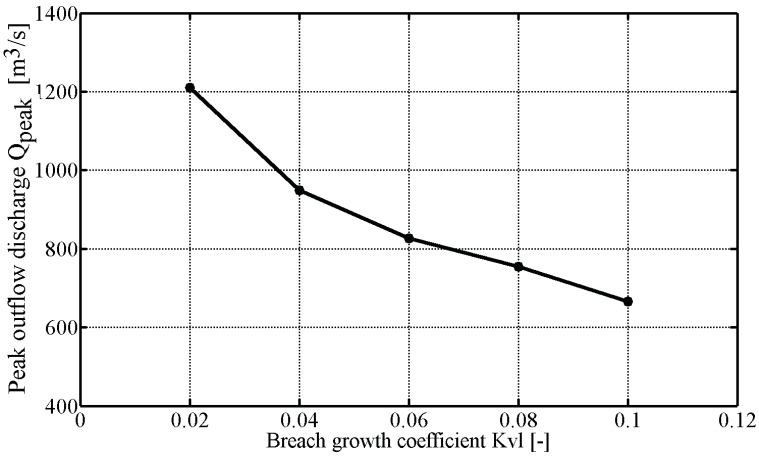

Figure 6.19: Influence of the breach growth coefficient on the peak outflow discharge

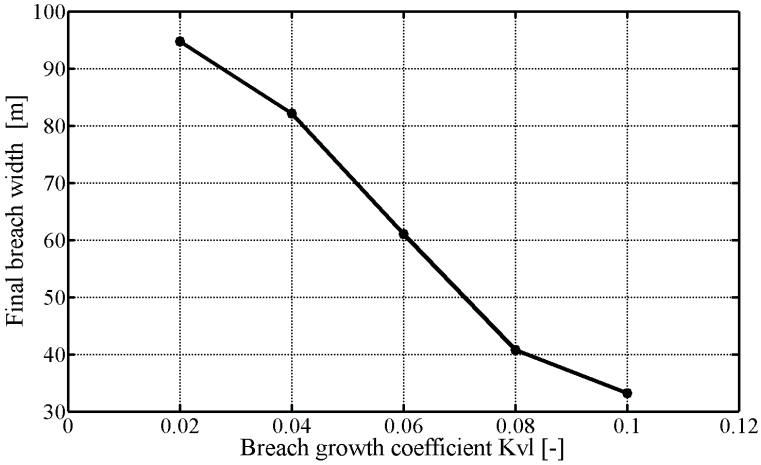

Figure 6.20: Influence of the breach growth coefficient on the final breach width

It can be observed that the the breach growth coefficient strongly influences all the investigated model outputs. This effect, together with very limited information on the measured values of the Kvl - coefficient ephasises the need for further researches on this topic.

6.3 Reliability analysis

The **system reliability** describes the ability of this system to operate without failure in a given period of time. Generally, the reliability of a system is calculated as a function of the probability of failure which in turn is the outcome of the reliability analysis. Similarly as in the case of the sensitivity analysis, three levels of reliability analysis can be distinguished (see also D'Eliso, 2007):

- Level I analysis - deterministic model outcomes are multiplied by a safety factor
- Level II analysis - the influence of the uncertain parameters on the model output is given by indices
- Level III analysis - full probability density function of the model outcomes is obtained either by numerical solutions or by means of sampling techniques.

Level III reliability analysis provides the best results, and since it is very time consuming sampling techniques are used. The Monte Carlo method is one of the most common sampling method, where (i) the most uncertain input parameters together with the respective probability density functions are identified, (ii) the number of realisations (N) is selected and (iii) the model is run N times, each time with the input parameters randomly extracted according to their probability density functions. The results given by each realisation are stored and after all realisations are performed the histograms are plotted. For the simulation of dike breaching the following key outputs are selected:

- time of grass erosion t_g;
- time of clay erosion t_c;
- total time of breaching t_b;
- final breach width B_b;
- peak outflow discharge Q_p;

The simulation is performed for both preliminary and detailed model. The most uncertain parameters together with their mean values and standard deviations are given in Table 6.3.
All the parameters are assumed to be normally distributed. For each model N=10000 realisations are performed.

6.3.1 Results of the analysis

Although the input parameters are assumed normally distributed, due to the nonlinearity of equations implemented in both preliminary and detailed model, the probability density functions of all outcomes are asymmetric with clearly wider right tail. Generally, the preliminary model provides more conservative results, as intended. Table 6.4 provides the mean values (μ), standard deviations (σ) and coefficients of variation (σ') provided by the preliminary and detailed model. It should be however emphasized, that the times of clay failure given by the preliminary and detailed model cannot be compared directly, as the models are differently sub-divided, with two additional transition phases included in the detailed model.

INPUT PARAMETER	SYMBOL AND UNIT	MEAN	σ	σ'
Mean root volume ratio	$RVR[-]$	0.55	0.41	0.74
Root reinforcement coefficient	$b[-]$	5.00	1.20	0.24
Grass cover factor	$C_f[-]$	0.75	0.1	0.13
Critical grass erosion depth	$d_{crit}[m]$	0.08	0.02	0.25
Damping coefficient	$w[-]$	2.5	0.5	0.20
Saturated water content	$\theta_s[m^3/m^3]$	0.42	0.06	0.15
Clay percentage	$c\%[-]$	30.00	7.50	0.25
Internal friction angle	$\phi[^0]$	32.00	3.20	0.10
Sediment size	$D_{50}[mm]$	0.20	0.02	0.1
Internal friction angle	$\phi[^0]$	32.00	3.20	0.10
Soil porosity	$n[-]$	0.40	0.112	0.28
Initial breach channel width	$B_{ini}[n \cdot r_h]$	2.00	0.5	0.25
Breach growth coefficient	$Kvl[-]$	0.03	0.006	0.2
SBeach coefficient	$K[m^4/N]$	$1.4{\cdot}10^4$	$0.4 \cdot 10^4$	0.28

Table 6.3: Uncertainties related to the input parameters for the morphodynamic module (partially after D'Eliso, 2007 and Kortenhaus, 2003)

Outcome	Preliminary model			Detailed model		
	μ	σ	σ'	μ	σ	σ'
Grass erosion time $[h]$	13.61	10.08	0.74	28.57	20.68	0.72
Clay erosion time $[h]$	11.06	9.04	0.81	4.12	1.55	0.37
Core failure time $[h]$	11.96	11.67	0.98	5.87	0.82	0.14
Total breaching time $[h]$	36.54	21.60	0.59	38.53	21.68	0.56
Peak outflow discharge $[m^3/s]$	1287	378	0.29	1241	179	0.15
Final breach width $[m]$	81.22	21.4	0.26	63.19	12.49	0.20

Table 6.4: Main outcomes from the Monte Carlo simulation

The mean **time of grass erosion** (Fig. 6.21) - is much longer in the detailed model ($\mu = 28.57h$) when compared to the results given by the preliminary model ($\mu = 13.61h$). This difference occurred most probably due to a new model for the calculation of the grass root reinforcement and grass erosion resistance that was applied in the detailed model.

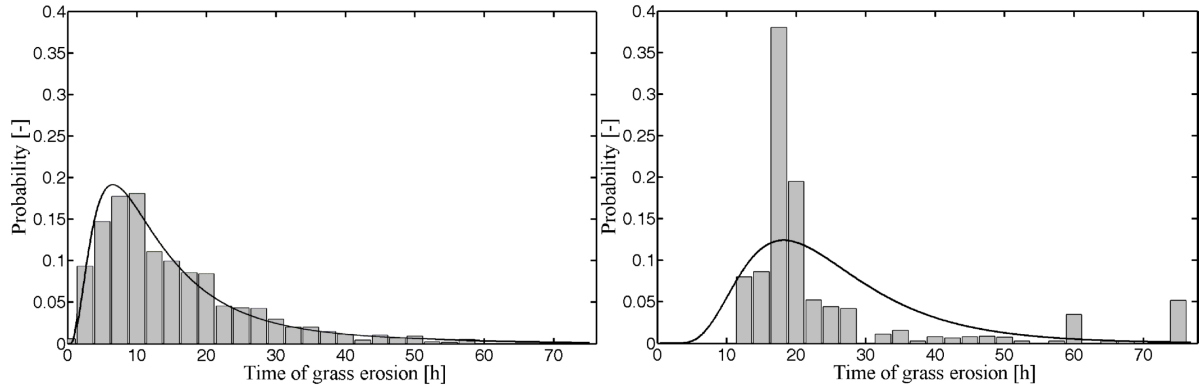

a) preliminary model b)detailed model

Figure 6.21: Monte Carlo simulation results for the time of grass erosion

The coefficients of variation are however very similar ($\sigma' = 0.74$ for the preliminary model and $\sigma' = 0.72$ for the detailed one) indicating a similar relative level of the uncertainties of model outputs.The uncertainties of the outputs given by the detailed model however are related rather to the input parameters than to the model parameters and the detailed model itself is considered to be more reliable. The mean values of the **clay erosion time** (Fig. 6.22) - obtained from the preliminary and the detailed model cannot be directly compared, as a different phase subdivision is used. In the detailed model the transition phases between (i) grass and clay and (ii) clay and sand erosion are included. However, even assuming that the transition phases between clay and sand erosion are included in the clay erosion time, in the detailed model ($\mu = 4.12h$) it is still significantly shorter than in the preliminary model ($\mu = 11.06h$). The most probable reason might be the cracks in the clay layer. In the preliminary model they were fully neglected, while their presence and the calculation of possible shear failure due to impact pressures are implemented in the detailed model. In fact, the dominant role of the cracks on the clay erosion was already observed during the laboratory tests described in Section 4.2. Moreover, the prediction of the clay cover erosion time given by the detailed model is subject to relatively smaller uncertainties ($\sigma' = 0.37$ as compared with $\sigma' = 0.81$ for the preliminary model).

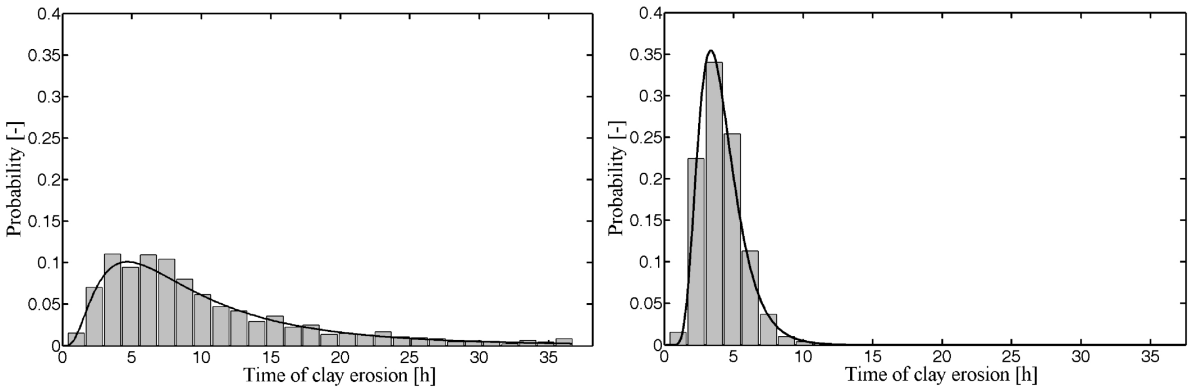

a) preliminary model b)detailed model

Figure 6.22: Monte Carlo simulation results for the time of clay erosion

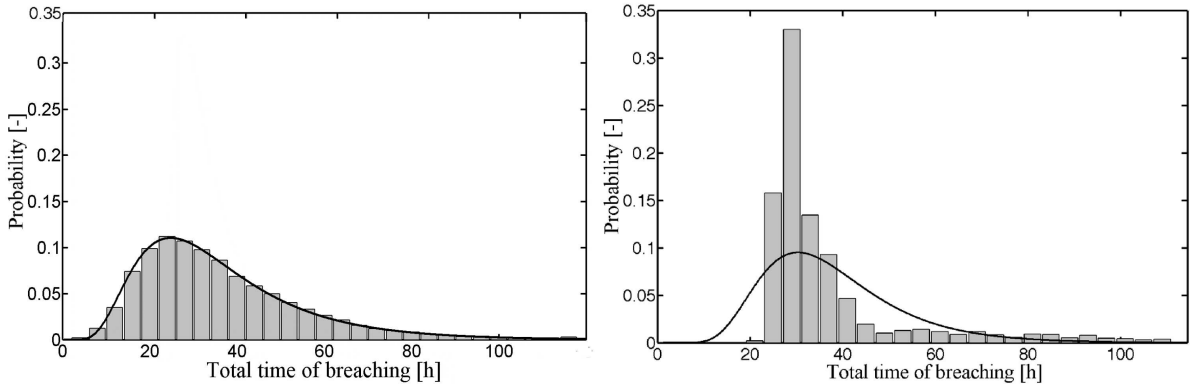

a) preliminary model b)detailed model

Figure 6.23: Monte Carlo simulation results for the time of the full breaching

The mean **total breaching times** (Fig. 6.23) obtained from the preliminary and detailed model are comparable ($\mu = 36.54h$ for the preliminary model and $\mu = 38.53h$ for the detailed model). The standard deviation and consequently the coefficient of variation that are observed in the case of the detailed model ($\sigma' = 0.56$) indicate that it is subject to slightly smaller

uncertainties, compared with $\sigma' = 0.59$ for the preliminary model. However, the levels of the uncertainties indicated by both models are similar, which suggest that rather the variations in the input parameters, than the model formulation have the most important effect on the overall model performance.

The application of the alternative volume-averaged approach for the calculation of the growth of the breach channel results in the reduction of the uncertainties related to the **final breach width** (Fig. 6.24) and **peak outflow discharge** (Fig. 6.25). The following differences are observed: reduction of the coefficient of variation σ' for the final breach width from $\sigma' = 0.26$ obtained from the preliminary model to $\sigma' = 0.20$ from the detailed model. In the case of the peak outflow discharge the coefficient of variation is reduced from $\sigma' = 0.29$ to $\sigma' = 0.15$. The second reason of this improvement is the better prediction of the boundary conditions for the overflow simulation. In the preliminary model they were assumed (with a given range of variation), while in the detailed model they are directly calculated, including the changes of the inner slope profile due to the erosion which results from wave overtopping.

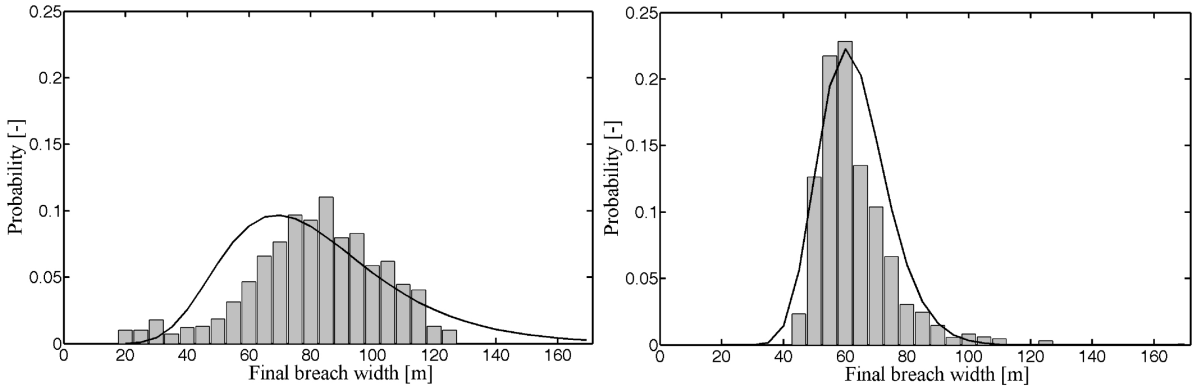

a) preliminary model b) detailed model

Figure 6.24: Monte Carlo simulation results for the final breach width

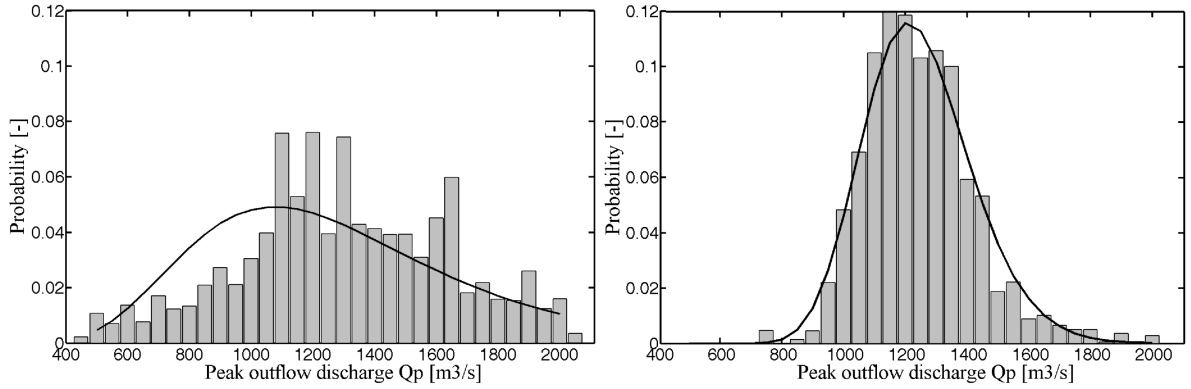

a) preliminary model b)detailed model

Figure 6.25: Monte Carlo simulation results for the peak outflow discharge

The following can be stated from the results of the uncertainty analysis for both preliminary and detailed model using Monte Carlo simulation (Table 6.4):

- Although the predicted time of grass erosion is significantly shorter in the preliminary model, the uncertainties are in fact the same for both preliminary and detailed model

and occur rather due to the values of the input parameters and related uncertainties than due to the model formulation;

- a sustainable reduction of the coefficient of variation σ' related to the clay erosion time was achieved in the detailed model. The transition phase between clay and sand erosion is driven not only by relatively uncertain clay properties, but also by quite certain properties of the sand, which results in the overall reduction of the input parameter uncertainties for this phase;

- the application of the volume-averaged approach for the calculation of the breach channel growth resulted in a reduction of coefficient of variation σ' which is observed in the case of peak outflow discharge and final breach width

The model outcomes given by both preliminary and detailed model are affected mostly by the uncertainties related to the material properties of the dike revetment, i.e. grass and clay covers. Therefore, a significant reduction of the uncertainties related to the dike breaching model can be achieved only if more specific information on the properties of grass and clay is available.

7 Summary, conclusions and recommendations

In this study the process of dike breaching initiated from the seaside by breaking wave impact was investigated both experimentally and theoretically. The main objective was to develop a model system that applies to a typical sea dike made of sandy core that is protected by clay cover with grass.

7.1 Summary of key results

A tiered and modular approach was pursued. The complete computational model system contains of a preliminary simplified model and more process-oriented detailed model. Figure 7.1 provides an overview of the performed research tasks.

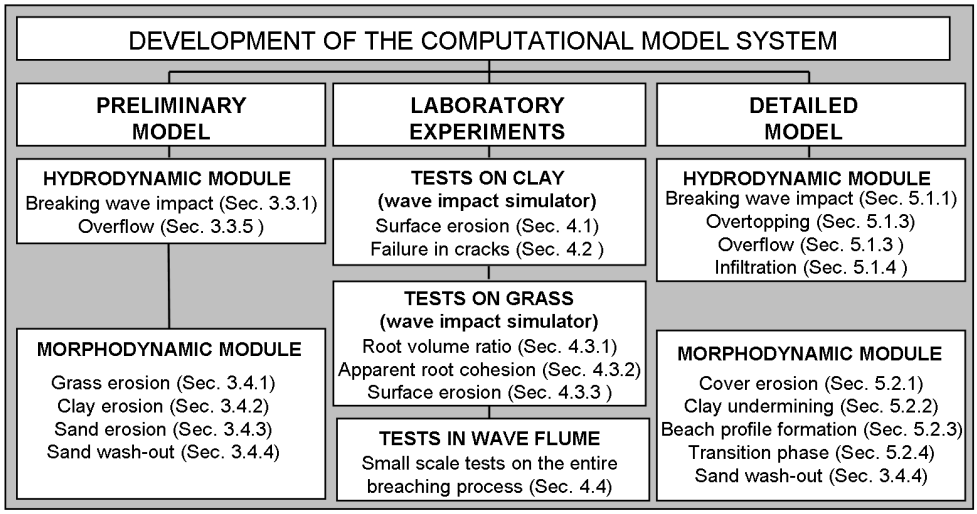

Figure 7.1: Overview of the undertaken work

The **preliminary model** is essentially based on a combination of existing models for the calculation of breaking wave induced loads and further models for the residual strength of the dike cover. Since all the existing models are only capable to simulate the cover failure, empirical models for dune erosion, including erosion due to overflow, were adopted in order to develop the complete preliminary model. The development of the preliminary model revealed knowledge gaps for the physical processes related to surface erosion of clay and to the reinforcement properties of a grass cover, so that a series of **laboratory experiments** were performed to close those gaps. The erosion resistance of a clay cover with and without vegetation as well as the shear failure in water-filled cracks in clay cover were investigated using a wave impact simulator. Furthermore, the models for the root distribution underneath the soil surface and for the estimation of the influence of the grass roots on the soil erosion resistance and shear strength were proposed.

The results of the performed laboratory investigations together with a numerical model for the simulation of breaking wave impact on the slope form the basis of the **detailed model**. The

detailed model includes also processes that were neglected in the preliminary model, especially concerning the water infiltration into the dike, and the revetment stability. Furthermore, based on the observations made during the small-scale tests in the wave flume, an additional transition phase was included and the erosion of the inner slope due to wave overtopping and combined flow was accounted for. Table 7.2 provides an overview on the processes included in the available models for dike breaching initiated by the breaking wave impact and in the developed preliminary and detailed models.

PROCESS	AM	PM	DM	ACHIEVEMENTS
Breaking wave impact main cause of breaching	Y	Y	Y	Empirical (PM) and numerical (DM) approach
Combined flow determines inner slope erosion	N	N	**I**	Simple wave-averaged models adopted
Overflow determines breach channel erosion	N	**I**	**I**	Steady nonuniform flow through the breach channel
Infiltration influences soil erosion resistance	N	N	**I**	Simplified infiltration models adopted
Grass erosion determines breach initiation	Y	Y	Y	Simplified models for the residual strength adopted (PM), new models developed (DM)
Clay erosion determines breach formation	Y	Y	Y	Simplified models for the residual strength adopted (PM), new models developed (DM)
Shear failure in cracks influences breach formation	N	N	**I**	Existing model experimentally verified and improved
Root reinforcement model improves of the soil strength	N	N	**I**	Existing model experimentally verified and enhanced
Sand core erosion breach development	Y	Y	Y	Empirical model for dunes (PM) or numerical model for beaches (DM) adopted
Inner slope erosion induced by combined flow	N	N	**I**	Excess shear approach
Breach widening and deepening induced by overflow	N	**I**	**I**	Equilibrium sediment transport simple morphodynamic model
AM - available models , PM - preliminary model, DM - detailed model N - neglected, Y - included **I** - neglected in available models, but represents and innovation of the models developed in this study				

Table 7.1: Summary of processes included in the model system

Final model validation requires specific data that contains not only information of the times associated with breaching but also detailed data on the outflow discharge and breaching progress. Generally, the detailed information on the historical dike breaching initiated from the seaside which would allow for the model validation is not available. The description of breaching time, progress of erosion as well as the breach widening and deepening rate are usually not only very rare, but also reported by accidental eye witnesses and therefore rather very roughly estimated than measured. Although some pictures of the full breaches are avail-

able, the shape and final breach dimensions are also estimated and the detailed measurements are lacking. Nevertheless, the application of the model to reproduce experienced dike failures shows satisfactory results, especially concerning the times associated with breaching.

OUTCOME	AM		PM		DM	
	μ	σ'	μ	σ'	μ	σ'
Grass erosion time t_g $[h]$	≈ 17	NA	13.61	0.74	28.57	0.72
Clay erosion time t_c $[h]$	≈ 16	NA	11.06	0.81	4.12	0.37
Sand core erosion time t_s $[h]$	NA	NA	11.96	0.98	5.84	0.45
Total breaching time t_t $[h]$	NA	NA	36.54	0.59	38.53	0.56
Peak outflow discharge Q_{peak} $[m^3/s]$	NA	NA	1287	0.29	1241	0.15
Final breach width B_b [m]	NA	NA	81.22	0.26	63.19	0.20
NA - not available or, available but not comparable						

Table 7.2: Summary of processes included in the model system

Probability density functions of both models obtained using Monte Carlo simulation are subject to significant uncertainties, especially in the case of the preliminary model. Generally, the uncertainties related to the final breach width ($\sigma' = 0.26$ for the preliminary model and $\sigma' = 0.15$ for the detailed model) and peak outflow discharge ($\sigma' = 0.29$ and $\sigma' = 0.20$ for the preliminary and detailed model, respectively) are smaller than the uncertainties related to the calculated times of particular breaching phases. The latter are in the range from $\sigma' = 0.37$ that was obtained from the detailed model for the clay erosion time up to $\sigma' = 0.98$ in the case of sand core erosion time calculated by the preliminary model. It has to be stressed, that the uncertainty analysis applied to the model system suggests that rather the material properties than the model parameters influence the uncertainties of the model outcomes so that further improvements of the model should be concentrated on the more reliable estimation of the input material parameters.

7.2 Applicability of the results and future research

The developed model system may be used either in the engineering practice or as a basis for a future research work. In **engineering practice**, the model system can be applied to provide the initial conditions at the breach that are needed to simulate the flood wave propagation. Furthermore, the warning time t_w is an important input parameter for the emergency management and damage mitigation in the flood-prone area. For this purpose the model system can also be applied for preliminary calculations of the breaching time. It should be however emphasized, that due to the lack of a final model validation a practical application should be always performed with caution and the uncertainties have to be necessarily quantified. The model outcomes, especially concerning the uncertainty analysis may provide further indications on the direction of **further detailed investigation**. Among the identified problems and issues related to further research, the most important can be summarized as follows:

- **Understanding of physical processes:**

  Although a number of laboratory experiments were performed in this study to understand the processes associated with breach initiation, only limited types of clay and grass

were tested. More detailed experimental investigations with different types of grass and soil are therefore needed to better understand the interaction between grass and subsoil. The cracks and fissures in the clay cover were identified as crucial points on the slope, so a reliable prediction of their occurrence, location and dimensions is also required. The processes of sediment transport under breaching conditions have also to be better understood. Among the most urgent problems that have to be solved is a three-dimensional description of all relevant processes or, alternatively the understanding of relationship between vertical and lateral erosion that would allow one to reduce the entire morphodynamic to a two-dimensional problem. Although some small-scale experiments in a wave-flume have been recently performed (Tuan, 2007, Hunt et al, 2005) their results are not clear enough to be used in the model for sea dike breaching.

- **Improvements toward a fully process-oriented model**

  The proposed model system can be considered as the basis for future developments towards a completely process-oriented model. The suggested improvements should refer to:

  - three-dimensional modeling of wave impact on the slope and flow through the breach channel, possibly with a VOF model,
  - FEM for the simulation of water infiltration,
  - detailed description of clay erosion, reinforcement properties of grass roots and interaction between grass and subsoil,
  - detailed description of the relationship between breach widening and deepening and the changes of this relationship dependant on the time

  Such a model system should be combined with other models for dike breaching due to other reasons, including wave overtopping (D'Eliso, 2007) or seepage.

- **Final model validation**

  Detailed field tests and laboratory experiments, if possible at or near prototype scale are needed in order to provide appropriate data for the final validation of the model system. The provided data should necessarily include loading parameters, times associated with the various breaching phases, definition of transition between phases, outflow hydrograph and final breach dimensions.

Bibliography

[1] Bailard, J.A. (1981): An energetics total load sediment transport model for plane sloping beach. Journal of Geophysical Research, Vol.86

[2] Battjes, J.A. (1974): Computation of set-up, longshore currents, run-up and overtopping due to wind-generated waves, Ph.D. Thesis, Delft University of Technology, Civil Engineering Department, Delft, The Netherlands, 244 pp

[3] Bleck, M.; Oumeraci, H.; Schüttrumpf, H. (2000): Combined Wave Overtopping and Overflow of Dikes and Seawalls. 27th International Conference on Coastal Engineering 16 - 21 July 2000 Sydney, Australia

[4] Berkenbrink, C.(2006): Laboruntersuchungen zur spannungsoptischen Darstellung der Wellenschlagwirkung auf Seedeiche. Diploma Thesis, TU Braunschweig, 150pp.

[5] Bosboom. J., S.G.J. Aarninkhof, A.J.H.M. Reniers, J.A. Roelvink, and D.J.R. Walstra (2000), Unibest-TC 2.0x, Overview of model formulations. WL | Delft Hydraulics report H2305.42.

[6] Bölke, S., Relotius P.C. (1974): Über die wellenerzeugten Druckschlagbelastungen von Seedeichen im Böschungsbereich zwischen 1:4 und 1:6. Mitteilungen Leichtweiss-Institut für Wasserbau der Technischen Universität Braunschweig Heft 42: pp. 358-388.

[7] Brooks, R.H, Coorey, A.J. (1964): Hydraulic properties of porous media. Hydrol. Paper 3. Colorado State University, Fort Collins, CO, USA

[8] Caan, C.P. (1996) Breach growth; an experimental investigation of the development of the scour hole. Master Thesis, Hydraulic Engineering Division, Delft University of Technology, Delft, The Netherlands

[9] Carsel, R.F., Parrish, R.S. (1988): Developing joint probability distributions of soil water retention characteristics. Water Resource Research, Vol.24, pp 755-769

[10] Coleman, S. E., D. P. Andrews, et al. (2002). "Overtopping breaching of noncohesive homogenous embankments." Journal of Hydraulic Engineering vol. 128(no. 9): pp. 829-838.

[11] Dean, R. G. (1977). Equilibrium beach profiles: U.S. Atlantic and Gulf coasts. Technical Report. No. 12.

[12] Delft Hydraulics (1992): Reststerkte van dijkbekledingen. Granulaire filters. Verslag modelonderzoek in Scheldebal. Rapport H195 deel II.

[13] Delft Hydraulics (1982), Computational model for the estimation of dune erosion during storm surge. (Rekenmodel voor de verwachting van duinafslag tijdens stormvloed.) WL | Delft Hydraulics report M1263 part 4 (in Dutch).

[14] D'Eliso, C. (2007): Breaching of sea dikes initiated by wave overtopping. A tiered and modular modelling approach. Ph.D-Thesis, TU Braunschweig

[15] Doorn, N., Van Gent, M. R. A. (2000). Numerical model investigations on coastal structures with shallow foreshores. Delft Hydraulics Laboratory. H. Delft, The Netherlands.

[16] Fischenich, C. (2001): Stability thresholds for stream restoration materials. Technical Note: ERDC TN-EMRRP-SR-29. US Army Corps of Engineers Research and Development Center. Vicksburg, Mississippi, USA. 10p.

[17] Fisher, J.S. and M.F. Overton (1984), Numerical model for dune erosion due to wave uprush. Proceedings of the 19th ICCE. ASCE, pp. 1553 – 1558.

[18] Führböter, A.(1966): Der Druckschlag durch Brecher auf Deichböschungen, Mitteilungen des Franzius-Instituts für Grund- und Wasserbau der Technischen Universität Hannover, Heft 31

[19] Führböter, A. ; Dette, H.-H.; Grüne, J. (1976): Response of seadykes due to wave impacts, Proceedings 15th International Conference Coastal Engineering (ICCE), Honolulu, Hawaii,pp. 2604-2622

[20] Führböter, A.; Sparboom, U. (1988): Shock pressure interaction on prototype sea dikes caused by breaking waves, Proceedings of the International Symposium on Modelling Soil- Water- Structure Interactions, Rotterdam, The Netherlands,pp. 243-252

[21] Führböter, A.; Sparboom, U.(1988a): Full-scale attack on uniformly sloping sea dikes. Proceedings of the 21st ICCE, pp 2174-2188

[22] Geisenhainer, P. and A. Kortenhaus (2006). Hydraulic model tests on breaching with and without waves - description of experiments performed at LWI. FLOODsite - Integrated Flood Risk Assessment and Management Methodologies. Braunschweig, Germany: 75 pp.

[23] Gencarelli, R.; Johnson, B.; Kobayashi, N.; Tomasicchio, G.R. (2007): Dune erosion and breaching. Proceedings of the International Conference Coastal Structures; Venice, Italy.

[24] González-Escrivá, J. A. and J. R. Medina (1999). Wave and wind tunnel testing for analysis of runup and overtopping. Proceedings Coastal Structures'99, Santander, Spain, Balkema Publishers.

[25] Hassan, M.A.A.M, (2002): Embankment breach formation and modelling methods. Ph.D. thesis. The Open University, HR Wallingford (UK)

[26] Holtan, H.N. (1961): A concept for infiltration estimates in watershed engineering. USDA Agricultural Resource Service Pubblications (ARS), pp. 41-51.

[27] Hunt, S.L.; Hanson, G.J.; Cook, K.R.; Kadavy, K.C. (2005): Breach widening observations from earthen embankment tests. Transactions of the ASAE, vol 48(3), pp.1115-1120.

[28] Husrin, S. (2007) Laboratory Experiments on the Erosion of Clay Revetment of Sea Dike due to Breaking Wave Impacts. MSc Thesis WSE-HE-CEPD-07.03, UNESCO, Institute for Water Education

[29] IGBFM - Institut für Grundbau und Bodenmechanik, Felsmechanik und Tunnelbau (2001): Belastung der Seedeichbinnenböschungen durch Wellenüberlauf. Abschlussbericht, University of Essen

[30] IMPACT (2004). Breach formation, Investigation of Extreme Flood Processes and Uncertainty (IMPACT): 12 pp.

[31] Koster (2004), Adaptation of computational model for dune erosion. (Aanpassing rekenmethode voor duinafslag.) Koster Engineering, June 2004 (in Dutch).

[32] Kothe, D.B., Mjolsness, R.C., and Torrey, M.D. (1991): RIPPLE: A computer program for incompressible flows with free surfaces. Los Alamos National Laboratory, LA-12007-MS

[33] Kortenhaus, A. (2003): Probabilistische Methoden für Nordseedeiche, Ph.D-Thesis, TU Braunschweig

[34] Landesamt für Wasserwirtschaft - Schleswig-Holstein (1962): Die Sturmflut vom 16./17. Februar 1962 an der Schleswig-Holsteinischen Westküste

[35] Larson, M.; Erikson, L.; Hanson, H. (2004) : An analytical model to predict dune erosion due to wave impact, Coastal Engineering, vol. 51, pp. 675-696

[36] Larson, M. and Kraus, N.C., (1989): SBEACH: Numerical modeling for simulating storm-induced beach change. Report 1 : empirical foundation and model development. Technical Report,CERC-89– 9, U.S.Army Engineer Waterways Experiment Station, Coastal Engineering Research Center, Vicksburg, Mississippi.

[37] Larson, M., Capobianco, M., et al. (1999): Modelling cross-shore sediment transport at different scales using equilibrium beach profile theory. Proceedings 4th International Symposium on Coastal Sediments, New York, USA, ASCE

[38] Laustrup, Chr.; Toxvig Madsen, H; Jensen, J.; Poulsen, L. (1990): Dike failure calculation model based on in situ tests. Proceedings of the International Conference on Coastal Engineering, pp.2671-2681

[39] Liu, P.L.F.; Lin, P.(1997): A numerical model for breaking waves: The Volume of Fluid method. Research report no. CACR-97-02. Center for Applied Coastal Research, Newark, Delaware

[40] Meyer, L.D. (1964): Mechanics of soil erosion by rainfall and runoff as influenced by slope length, slope steepness, and particle size. Ph.D. thesis, Purdue University Library, W. Lafayette, IN

[41] Neelamani, S. (2003). "Subareal wave pressures, layer thicknesses, run-up and run-down velocity on plane sea walls." Ocean Engineering: 13pp.

[42] Overton, M.F., Pratikto, W.A., Lu, J.C., Fisher, J.S., (1994) : Laboratory investigation of dune erosion as a function of sand grain size and dune density. Coastal Engineering 23, pp. 151- 165.

[43] Overton, M.F., Fisher, J.S. and K. Hwang (1994b), Development of a dune erosion model using SUPERTANK data. Proceedings of the 24th Coastal Engineering Conference. ASCE, pp. 2488– 2502.

[44] Oumeraci, H.; Kortenhaus, A. (2002): Risk-based design of coastal flood defences: a suggestion for a conceptual framework. Proceedings 28th International Conference Coastal Engineering (ICCE), ASCE, Volume 2, Cardiff, U.K., pp. 2399-2411.

[45] Pilarczyk, K. W. (1998): Dikes and revetments. Rotterdam/Brookfield, A.A. Balkema: 522 pp.; 2 Appendices.

[46] Pilarczyk, K. W. (2003): Design of low-crested (submerged) structures: an overview. Proceedings 6th International Conference on Coastal and Port Engineering in Developing Countries (COPEDEC), Colombo, Sri Lanka.

[47] Pugh, C. A. (1985). Hydraulic model studies of fuse plug embankments. United States Department of the Interior, Bureau of Reclamation, Engineering and Research Center. Denver, CO, USA. no. REC-ERC-85-7: 33 pp.

[48] Richards, L.A. (1931): Capillary conduction of liquid through porous medium. Journal of physics, Vol. 1, pp. 318-333

[49] Richwien, W. (2002). Ansatz zur Bemessung der Außenböschung von Seedeichen. BAW-Kolloquium, Karlsruhe, Germany.

[50] Rijkswaterstaat (1961) : Verslag over de stormvloed van 1953. Ministry of Transport, Public Works and Water Management. s'Gravenhage, The Netherlands, Staatsdrukkerij: 714 pp.

[51] Rozov, A. L. (2003). "Modeling of washout of dams." Journal of Hydraulic Research vol. 41(no. 6): pp. 565-577.

[52] Schüttrumpf, H.(2001): Wellenüberlaufströmung bei Seedeichen - Experimentelle und theoretische Untersuchungen. Mitteilungen aus dem Leichtweiß-Institut für Wasserbau der Technischen Universität Braunschweig, Heft 149, 2001

[53] Schüttrumpf, H.; Oumeraci, H. (2005): Layer thicknesses and velocities of wave overtopping flow at seadikes. Coastal Engineering vol. 52(no. 6): pp. 473-495

[54] Smith, G.M., Seijffert, J.W.W., van der Meer, J.W. (1994): Erosion and overtopping of a grass dike. Large scale model tests. Proceedings 24th International Conference Coastal Engineering (ICCE). Kobe, Japan, pp. 2639-2652.

[55] Sprangers, J.T.C.M.(1999):Vegetation dynamics and erosion resistance of seadyke grassland, Ph.D.-Thesis, Wageningen Agricultural University, Wageningen.

[56] Stanczak, G., Oumeraci, H., and Kortenhaus, A. (2007a): Laboratory tests on the erosion of clay revetment of sea dike with and without a grass cover induced by breaking wave impact, LWI-Bericht Nr 935

[57] Stanczak, G., Oumeraci, H., and Kortenhaus, A. (2007b): Breaching of sea dikes initiated from the seaside by breaking wave impacts. Detailed computational model. LWI-Bericht Nr 951.

[58] Stanczak, G., Oumeraci, H., Kortenhaus, A. (2007c): Effect of Wave Impacts on the Cover Layer of Sea Dikes. Proceedings of the International Conference Coastal Structures; Venice, Italy.

[59] Stanczak, G., Oumeraci, H., and Kortenhaus, A. (2007d): Breaching of sea dikes initiated from the seaside. State of the art report. LWI-Bericht Nr 952.

[60] Steetzel, H,J, (1993), Cross-shore transport during storm surges. Ph.D. Thesis Delft University of Technology, ISBN 9090063455.

[61] Stephan, H.-J. (1981): Über Schäden an Seedeichen durch Wellen- und Druckschlagbelastungen; Mitteilungen - Issue 70; Leichtweiß-Institut für Wasserbau der Technischen Universität Braunschweig; Braunschweig

[62] Stive, R.J.H. (1983): Internal note, Delft Hydraulics (quoted by TAW, 1990)

[63] TAW (1996): Clay for dikes. Technical Advisory Committee on Water Retaining Structures. Delft, The Netherlands: 58 pp.

[64] TAW (1999a). Water retaining earth structures. Technische Adviescommissie voor de Waterkeringen (TAW). Delft, The Netherlands: 105 pp.

[65] Temple, D. M., J. Wibowo, et al. (2003). Erosion of earth spillways. Proceedings USSD Reducing Risk from Extreme Events.

[66] Temple, D.M.; Robinson, K.M.; Ahring, R.M.; Davis, A.G. (1987): Stability design of grass-lined open channels. USDA Agricultural Handbook. No. 667.

[67] Temple, D.M.; Hanson, G.J. (1994): Headcut development in vegetated earth spillways. Applied Engineering in Agriculture, 10, pp. 677-682

[68] Thao, N.D.; Shibayama, T. (2006): Numerical simulation of 3-D wave breaking on breakwater, Proceedings of the 30th International Conference on Coastal Engineering; San Diego, California, pp. 261-273

[69] Troch, P., T. Li, et al. (2003). Wave interaction with a sea dike using a VOF finite-volume method. Proceedings of the International Offshore and Polar Engineering Conference (ISOPE), Honolulu, Hawaii, USA, ISOPE.

[70] Tuan, T.Q. (2007): Seasonal breaching of coastal barriers. PhD-thesis, TU Delft, 179pp

[71] Wang, Q.; Horton, R.; Shao, M. (2003): Algebraic model for one-dimensional infiltration and soil water distribution. Soil Science, Williams and Wilkins Vol. 168, No. 10, pp. 671-676.

[72] Wang, Z. (2000): Seepage erosion and surface erosion. Interner Bericht ProDeich, Vorläufiger Bericht 3, Essen, Germany, 15 pp.

[73] Weißmann, R. (2003): Die Widerstandsfähigkeit von Seedeichbinnenböschungen gegenüber ablaufendem Wasser. Ph.D. thesis, Universität Duisburg-Essen, Fachgebiet Grundbau und Bodenmechanik, Essen, Deutschland, 147 pp.

[74] Wohlenberg, E. (1963): Der Deichbruch des Ülversbüller Kooges in der Februar-Sturmflut 1962. Die Küste, Issue 11, pp.52-90

[75] Woolhiser DA, Smith R.E., Goodrich D.C. (1990): KINEROS, a Kinematic Runoff and Erosion Model: Documentation and User Manual. USDA-Agricultural Research Service, ARS-77. US Department of Agriculture: Washington, DC.

[76] Wu, T.H., McKinnell, W.P., Swanston, D.N. (1979): Strength of tree roots and landslides on Prince of Wales Island, Alaska. Canadian Geotechnical Journal, Vol. 114, No.12, pp 19-33

[77] van Genuchten, M.T. (1980): A close-form equation for predicting the hydraulic properties of unsaturated soils. Soil Scienc Society of American Journal, No.44, pp.892-899

[78] Vellinga, P., (1986), Beach and dune erosion during storm surges. Ph.D. Thesis, Delft University of Technology;

[79] Verheij, H. J. (2003). Time-dependent breach development in cohesive material. Delft Hydraulics. Delft, The Netherlands: 6 pp.

[80] Visser, P. J. (1998). "Breach growth in sand-dikes." Communications on Hydraulic and Geotechnical Engineering vol. 98(nr. 1): 172 pp.

[81] Young,M.J. (2005): Wave Overtopping and Grass Cover Layer Failure on the Inner Slope of Dikes,MSc Thesis WSE-CEPD-05.03,UNESCO,Institute for Water Education

[82] Zitscher, F.-F. (1962): Analyse zur Bemessung von Außenböschungen scharliegender Seedeiche gegen Wellenbeanspruchung, Wasser und Boden, Issue 10, pp.337-349

[83] Zhong, H., (1985): Theoretische und experimentelle Untersuchungen ober den Druckschlag bei Wellenangriff auf einen 1:4 geneigten Seedeich. Mitteilungen des Leichtweiß- Institut für Wasserbau, TU Braunschweig, pp.401-453

[84] Zhu, Y. (2007): Breach growth in clay dikes. PhD-thesis, TU Delft, 231pp